A CLUTTER SUPPRESSION SCHEME FOR HIGH FREQUENCY (HF) RADAR

MARTIN WAI YEE POON, B.Eng.

A Clutter Suppression Scheme for High Frequency (HF) Radar

By

©Martin Wai Yee Poon, B. Eng.

A thesis submitted to the School of Graduate Studies in partial fulfillment of the requirements for the degree of Master of Engineering

Faculty of Engineering and Applied Science
Memorial University of Newfoundland

December, 1991

St. John's Newfoundland Canada

ISBN 0-315-73332-2

Abstract

A clutter suppression scheme for high frequency (HF) radar is presented in this thesis. The HF radar has been developed for coastal surveillance and the remote sensing of the ocean. When the HF electromagnetic waves propagate over the ocean, the backscatter from the ocean surface has well defined frequencies, known as "Bragg" frequencies, shifted from the radar frequency. One of the characteristics of the HF backscatter is the high level of ocean clutter which hampers target detection. It is desirable to suppress the ocean clutter before target detection operation. The proposed scheme is developed based on the recognition of the time-varying behaviour of the ocean clutter that can be simply characterized by two narrowband frequency-modulated sinusoidal signals with their centre frequencies equal to the "Bragg" frequencies. The scheme consists of two parts. First, a time-varying technique referred to as Hankel rank reduction method is used to estimate the instantaneous frequencies of the clutter signals. The method states that a Hankel matrix of a time series data consisting of a finite number of sinusoids can be approximated to, via Singular Value Decomposition (SVD), a lower rank matrix defined by the finite number of the principal singular values, even if the frequencies of the sinusoids are varying slowly with time. The instantaneous frequencies are estimated from those principal singular values. The use of SVD is to decompose the Hankel matrix into a signal and a noise vector subspace. The signal subspace is identified by the largest singular values. Second, a process in which the frequency component of the clutter signals is removed from the reduced rank Hankel matrix instantaneously is developed to suppress the ocean clutter. Subsequently, another reduced rank Hankel matrix is constructed from which the target signal can be extracted.

The performance of the scheme has been evaluated on computer-synthesized

data and on some real data collected from a recently developed HF radar. The results from both cases showed that the instantaneous frequencies of the ocean clutter signals and the target signal were properly tracked by the Hankel rank reduction method and that a substantial level of the ocean clutter, in the range of 20 to 50 dB, could be suppressed by the scheme proposed.

Acknowledgements

I would like to express my deep gratitude to my two supervisors, Dr. R. H. Khan and Dr. S. LeNgoc, for all their guidance, advices and assistance during the course of my graduate studies and the writing up of the thesis.

I am thankful to Northern Radar Systems Ltd. for their permission to use their HF data for the tests.

The financial assistance received from the School of Graduate Studies, the Faculty of Engineering and C-CORE (Centre for Cold Ocean Resource Engineering) is gratefully acknowledged.

Last, but not least, the completion of the thesis cannot be done without the support from my wife, Vivian.

Contents

List of Figures

List of Tables

List of Principal Symbols

a_i	Coefficients of the autoregressive (AR) process
$A(z)$	Characteristic polynomial of $H(z)$
c	Speed of light
c_i	Amplitude of ith complex sinusoid
D	Diagonal matrix containing the eigenvalues of R_k
$\epsilon(k)$	Output of the prediction error filter (PEF)
$E[\epsilon^2(k)]$	Mean-square error
f_{i1}, f_{i2}	Instantaneous frequencies of the ocean clutter signals
f_{oc}	"Bragg" frequency of the ocean clutter signal
f_r	Carrier frequency of the radar signal
f_t	Doppler freqency of a target
F	State feedback matrix
h	State matrix
H	Hankel data matrix
$Hnew$	Reduced rank Hankel matrix
$H(z)$	z-domain transfer function of the AR process
g	Acceleration due to the gravity
L	Order of the AR process
N	Total number of data samples
Q	Orthegonal matrix containing eigenveciors of R_k
$Q_x(\omega)$	Modified power spectrum of PEF
R	Covariance data matrix
R_k	Time-varying estimate of kth covariance data matrix
ΔR	Range resolution of the HF radar
$s_1(t), s_2(t)$	Simulated ocean clutter signals

S	Diagonal matrix containing the singular values of a matrix
$S_x(\omega)$	Power spectrum of PEF
U	Unitary matrix
v	Velocity of the ocean wave
$v(k)$	State input vector
V	Unitary matrix
V_t	Radial velocity of a target
W	Bandwidth of the FMCW waveform
$y(k)$	Data samples
X	State vector matrix
Y_f	Data matrix formed from a forward linear prediction
Y_b	Data matrix formed from a backward linear prediction
λ	eigenvalues of a matrix
λ_o	Ocean wavelength
λ_r	Wavelength of the radar signal
Θ	Observability matrix
Θnew	New observability matrix
ω_i	Angular frequency of ith complex sinusoid
σ_i	Singular values of the Hankel matrix, $H(z)$
ϕ_i	Phase of ith sinusoidal signal
α	Memory factor
μ	Scalar porportionality constant

Chapter 1

Introduction

1.1 Problem Statement

High frequency (HF) radar systems have been developed for coastal surveillance and the remote sensing of the ocean, e.g. detection of ships and monitoring the sea conditions. The HF electromagnetic waves in the frequency band of 3-30 MHz propagate over the ocean surface in groundwave mode. The high conductivity of the sea water results in low propagation loss of the groundwave and hence allows long-range (over the horizon) target detection. Echoes from the sea surface and for any surface targets are received by the radar system. One of the characteristics of the sea echo, known as the ocean clutter, is its high level energy. Although these ocean clutter signals have been realized to be a good source of information on the ocean conditions, such as wave height, wind direction and etc., they become the unwanted signals as far as target detection is concerned because they will obscure the required target signals, particularly when the target's Doppler frequency (a frequency shifted from the transmitted frequency of the radar) falls close to the clutter's Doppler frequency. Doppler frequency discrimination to separate the target from the ocean clutter will not be possible except by additional signal processing. Thus, it is desirable to suppress the clutter as much as possible before the target detection operation. The objective of this thesis is to develop a clutter

suppression scheme for HF radar.

1.2 Brief Background Review

In order to suppress the ocean clutter in the HF radar, it is important to understand the behaviour of the clutter signal first and then specific signal processing technique can be developed based on the clutter's characteristics. In 1955, Crombie [1] first observed that the two dominant peaks displayed by the ocean clutter in the Doppler spectrum were due to the scattering from two sets of ocean waves whose wavelength equals half the radar wavelength approaching and receding from the radar. The scattering from these two sets of waves is similar to that from a diffraction grating which is sometimes described as the Bragg-scatter, by analogy to the Bragg-scatter mode for the X-ray diffraction by crystals [2]. Thus, the Doppler frequencies of this ocean clutter are also known as the "Bragg" frequencies. In addition to those two dominant first-order peaks, there are some smaller and more complex high-order components. The theoretical expressions of the ocean clutter were derived by others in more recent years [3, 4, 5, 6]. An average Doppler spectrum of the first- and second-order scattering can be determined from the theoretical expressions. Recent work by Khan [7] has demonstrated that the ocean clutter has a time-varying behaviour that can be modelled by two narrowband time-varying signals and tracked by time-varying signal processing techniques. This time-varying model treats the ocean clutter as two moving targets in addition to any other potential targets during target detection. Thus, that poses a problem in suppressing two moving targets among the other targets. The traditional way of suppressing radar clutter, referred to as the moving target indicator (MTI) filter, is not applicable to this problem because the ocean clutter has nonzero Doppler frequency while the MTI assumes that the clutter is stationary and has zero Doppler frequency [8].

As the radar clutter in reality is rather non-stationary, adaptive filter theory provides a popular way of dealing with the problem. Gibson and Haykin [9] proposed an adaptive clutter suppression technique in 1983. The technique is based on the use of an adaptive autoregressive (AR) modelling of the radar clutter along with the Least Mean Square (LMS) adaptation algorithm. It is assumed that the clutter signals can be modelled quite closely by a relatively low order AR process. That means the clutter signal is modelled as the output of an all-pole filter having a white noise source to its input. The technique also assumes that the target and the clutter have generally different Doppler spectra where the clutter's spectrum tends to be diffused as compared to that of the target. This technique worked well when dealing with the clutter such as weather, ground and ice pellet encountered by air traffic surveillance radar. All these clutter phenomena appear to have a wide spread Doppler spectrum. However, the ocean clutter in HF radar is observed to have a similar Doppler spectrum as that of the target, i.e. of narrow spectral widths. In this case, the clutter components are not likely to be suppressed.

A similar approach has been used by Hou [10] in 1984. In this clutter suppression technique, Maximum Entropy Method (MEM) which is a spectral analysis method of the AR process is used to model the clutter of interest. A predetermined model of the clutter is assumed to be available and adaptively updated to obtain an optimum estimate of the clutter. The updating process of the clutter stops when a target is detected. The model of the clutter is then subtracted from the received signal.

Another type of clutter suppression scheme was presented by Zhang and Haykin [11] in the same year. This scheme makes use of the idea of noise cancellers in which the data samples from two adjacent range cells are used as references when the data samples from the range cell of interest is processed. Here, it is assumed that no target is present in those two adjacent cells except clutter. The suppression of

the radar clutter is achieved by subtracting the data of the two adjacent cells from the one being processed.

A common point is observed among the method presented by Zhang and Haykin [11] and the AR modelling clutter suppression methods. They assume that a predetermined clutter model can be obtained from the range cell which has nothing but only the clutter, and then the model is adaptively updated. However, the ocean clutter is not stationary. The characteristic of the ocean clutter may vary from one range cell to another. It will be difficult to have a predetermined ocean clutter model to begin with. Therefore, an ultimate solution to the clutter suppression problem would utilize models for the clutter and the target in each range cell simultaneously and then identify the clutter by its properties. The clutter is suppressed by subtracting effects attributed to clutter by the model from the received signal. Since the ocean clutter is found to have time-varying frequencies, the clutter suppression scheme proposed in this thesis is based on the use of a time-varying frequency tracking technique to track the frequencies of the ocean clutter as well as those of any other targets. The ocean clutter is then suppressed by removing its corresponding frequency components from the received signal.

1.3 Scope of the thesis

A new technique, based on the use of a time-varying frequency tracking method referred to as the Hankel rank reduction method, to selectively remove the ocean clutter components from the radar data is proposed in this thesis. The method [12] shows that a Hankel matrix of time series data containing a finite number of narrowband time-varying sinusoids can be approximated by a matrix whose rank is equal to the finite number of the principal singular values given by the Singular Value Decomposition (SVD). The frequencies of the sinusoids are estimated from

those principal singular values. This attribute linked with the time-varying ocean clutter model suggests that for an ocean range cell containing a single target, the Hankel matrix would contain only three principal singular values - one corresponding to the target signal and the other two corresponding to the well known "Bragg" clutter signals. This assumption is valid for ocean range cells with dimensions under one kilometer. (There is a common practice that the ships usually keep a certain distance away from each other on the sea.) For larger range cells, one just needs to increase the number of the singular values without affecting the analysis or significantly increasing the computational burden. The reason why the Hankel matrix is utilized in the method is that the linear prediction porperty is found in the structure of the matrix. Each entry of the matrix can be expressed as the sum of a weighted linear combination of the rest of the data along the row of the matrix. The linear prediction is a basis for the frequency estimation of the sinusoidal signal. How the linear prediction is used to estimate the sinusoidal frequency is discussed in Chapter 4. The SVD is used to decompose the Hankel matrix into a signal and a noise vector subspace. The signal subspace is associated with the finite number of the dominant singular values. By approximating the Hankel matrix to a matrix defined by the signal subspace, the effect of noise can be substantially reduced.

By use of the Hankel rank reduction method, the frequencies of the clutter signals can be tracked or the signal parameters of the ocean clutter signals can be estimated. A process is then developed to suppress the clutter signals by removing their estimated frequency components from the received data. The performance of the proposed scheme is tested on both the computer-synthesized and the real HF data which is collected from a recently developed HF groundwave radar located at Cape Race, Newfoundland, Canada. It should be pointed out that the above evaluation is an off-line testing.

1.4 Organization of the Thesis

The thesis is organized in the following way:

- *Chapter* 2 presents a brief description of the background of HF radar and the time-domain model of the ocean clutter signals.
- *Chapter* 3 reviews some techniques of tracking time-varying frequencies of the sinusoids.
- *Chapter* 4 is a background review of the frequency estimation of stationary sine waves because it forms the basis of the method to deal with non-stationary (time-varying) sine waves.
- *Chapter* 5 describes details on the proposed clutter suppression method in this thesis including the method used to estimate the instantaneous frequencies of the ocean clutter signals and the procedures to remove the ocean clutter from the received signal.
- *Chapter* 6 presents the results obtained by using both the computer-synthesized and the real HF radar data.
- *Chapter* 7 contains conclusions and some recommendations for future work.

Chapter 2

Introduction to High Frequency (HF) Radar

High frequency (HF) radar, using the groundwave mode of propagation, has been established as a remote sensing methodology for the ocean environment [13, 14, 15]. The high conductivity of sea-water accounts for the low propagation loss of the ground wave mode and allows long ranges (over the horizon) to be achieved with modest transmitter power. The detection of targets such as ships, icebergs and sea-ice, and ocean environmental monitoring of waves, currents and winds are some of the applications for the HF groundwave radar. Moreover, this technology can fill some gaps in the radar coverage presently available with microwave radars. For example, surface based microwave radar is limited to line-of-sight detection and cannot detect targets over the horizon. Also, due to the multipath reflection effects, detection of low altitude targets is very difficult with microwave radar. In the following sections, other aspects of HF radar are discussed. The discussion includes: a brief review of the operating theory of HF radar; an overview of some HF radar systems; the ocean clutter in HF radar and the time-domain model of ocean clutter signals.

2.1 Brief Review of Operating Theory of HF Radar

In the backscatter HF radar system, the transmitter and the receiver can either be at the same site (monostatic) or separated by some small distances (bistatic). Generally, a vertically polarized antenna is utilized to radiate electromagnetic waves of frequencies in the band of 3-30 MHz that propagates over the sea surface. If a target lies along the path, a reflected signal will be captured by the receiver via the same path taken by the transmitted signal. The backscatter from the target has a frequency shift proportional to its radial velocity. Such frequency shift, known as the Doppler frequency, provides a means for target discrimination and is given by

$$f_t = \frac{2V_t}{\lambda_r} \tag{2.1}$$

where f_t is the Doppler frequency; V_t is the radial velocity of the target; and λ_r is the wavelength of the transmitted signal. The derivation of Eq. (2.1) is shown in Appendix A. In addition to the detection of a target, the backscatter HF radar can also provide information on the target's range from the time delay between the transmitted and the received signals.

For an HF groundwave radar, long-range target detection requires maximum duty cycle of the transmitter waveform [16]. Thus, the frequency modulated continuous wave (FMCW) waveform is commonly used in HF radar. In an FMCW radar, a continuous frequency-swept signal with a bandwidth, W, is transmitted. This sweep bandwidth determines the desired range resolution as $\Delta R = c/(2W)$. The target range is measured as the instantaneous frequency difference between the transmitted and received waveforms. The FMCW has a 100 percent duty cycle and it is ideal for the bistatic configuration but not for the monostatic operation. One problem with the FMCW waveform in the monstatic operation is the difficulty in isolating the receiver from the transmitter. The receiver suffers from

the transmitter induced noise. Thus, an interrupted FMCW waveform, namely FMICW, is implemented in order to overcome the problem. The FMCW waveform is simply gated on and off with a well defined sequence. The sequence disables the transmission while the receiver is on.

2.2 Overview of Some HF Radar Systems

In recognizing the unique advantages of HF radar as compared to the microwave radar, countries like the United States, the United Kingdom and Canada have been doing extensive work on HF radar, using both groundwave and skywave propagation, for the past 30 years. In the United States, research and development of HF radar began in the early 1940s. Naval Research Laboratory (NRL) was one of the pioneer institutions to design and conduct experiments with HF radar. MADRE was an experimental HF skywave radar designed by NRL and was first put into operation in 1961 [14]. It had a target-detection capability up to 4000 km. Its antenna had a dimension of 98 meters (m) wide by 43 m high and consisted of twenty corner reflector elements arranged in two rows of ten elements each. The radar generally operated with an average power from 5 to 50 KW. In 1970, the Office of Naval Research/SRI International developed another HF skywave over the horizon (OTH) radar, namely the Wide Aperture Research Facility (WARF), for detecting and tracking ships at ranges of 2000 km or more at sea [17]. WARF employed a linear frequency-modulated continuous-wave (FMCW) waveform and transmitted 1 MW average effective radiation power. Reflection signals from the ocean were received by a 2.55 km broadside array of vertical monopole element pairs. The said systems have a considerably huge physical size and high cost. A small transportable system with a broad beam scanning characteristic, called CODAR (Coastal Ocean Dynamic Applications Radar), was developed later in

the 70's. The concepts of CODAR were originated from the National Oceanic and Atmospheric Adminstration's (NOAA) Wave Propagation Laboratory for the measurement of ocean surface currents from the coast or the offshore platforms.

In the United Kingdom, the University of Birmingham in association with other organizations have also done significant work on HF OTH radar. An experimental HF groundwave radar was designed to transmit 1 KW peak power frequency-modulated interrupted continuous-wave (FMICW) signal via a 6-30 MHz vertically polarized logarithmic periodic dipole array. The receiving antenna consists of two nested broadside arrays with 15 vertical loop elements each [18]. The system has been used for remote sensing of ocean waves and currents.

In Canada, the CODAR system has been used as remote sensor for the northern oceans where exploration and transportation activities take place [19]. Icebergs are considered as a significant hazard to the ships and construction such as offshore platforms in those areas. The ability of long range (over the horizon) detection demonstrated by HF radar would reduce the chance of possible collisions between the icebergs and the ships or any other constructions at sea.

Recently, an FMICW groundwave radar system has been built at Cape Race, Newfoundland, by Northern Radar Systems Ltd. in association with the Centre for Cold Ocean Resource Engineering (C-CORE), Memorial University of Newfoundland, for the purpose of ocean surveillance including the detection and the tracking of vessels and icebergs, plus the measurement of sea-state and currents [13]. The radar operates at a centre frequency of 6.75 MHz along with a sweep bandwidth of 375 kHz and is designed to detect and track ships at a distance up to 400 km, with a range resolution of 400 m. The transmitter and the receiver are located at the same site (a monostatic configuration). The transmit antenna is an off-the-shelf log periodic array with an average transmit power of 2.5 KW and covers over a 120 degree sector of the ocean with an average nominal beamwidth of 3.5 degree.

The receiving antenna consists of an array of 40 quarter wavelength height broadband elements which are equally spaced a distance of half wavelength. The total distance taken by the receiving antenna is about 880 m. The clutter suppression scheme proposed in this thesis will be tested using the data collected from this radar.

2.3 Ocean Clutter in HF Radar

In HF radar, the backscatter from the ocean surface, namely the ocean clutter, appears at well defined frequencies shifted from the transmitted frequency of the radar. Crombie [1] first observed this effect and attributed the dominant component of the return energy to the back-scattering from the ocean waves having a wavelength half the radar wavelength. Two sets of such ocean waves, moving radially to and away from the radar site, behave as diffraction gratings and cause constructive interference of the scattering returns. As shown in Fig. 2.1, these "Bragg" scattering returns exhibit two distinct Doppler frequencies corresponding to the characteristic velocity of propagation of the two sets of ocean waves. These frequencies are given by

$$f_{oc} = \pm\sqrt{\frac{g f_r}{\pi c}} \tag{2.2}$$

where f_{oc} are the Doppler frequencies of the ocean clutter signals; f_r is the radar carrier frequency; g is the acceleration due to the gravity and c is the speed of light. Equation (2.2) is derived from Eq. (2.1) with the velocity of the ocean wave, $v = (g\lambda_o/2\pi)^{1/2}$, where the ocean wavelength, λ_o, equals half the radar wavelength, λ_r, i.e. $\lambda_o = \lambda_r/2$. The Doppler spectrum of the ocean clutter in Fig. 2.1 is observed by an HF groundwave radar operating at a frequency of 25.4 MHz. In addition to the dominant "Bragg" scattering returns, a smaller and more complicated feature of the HF radar spectrum is referred to as the "second-order"

scattering. As the name implies, this portion of the Doppler spectrum has been modelled as double scattering from two ocean wave components, which match half the radar wavelength after vector addition along the radar beam direction [20, 21]. Also, part of this second-order comes from a single scatter from second-order ocean waves produced by nonlinear wave-wave interaction.

The Doppler spectrum of the ocean clutter can qualitatively show some properties of the ocean waves. If the wind blows towards the shore, the dominant peak at the plus side of the Doppler spectrum will exhibit a noticeable higher magnitude level than the one at the minus side. Opposite scenario will be seen if the wind blows away from the coast. In general, the direction of the wind can be deduced from the ratio of the amplitude of the dominant peaks. As the speed of the wind increases, the energy in the ocean wave spectrum increases. The peak in the spectrum moves to the lower frequencies, then the amplitude of the second-order Doppler spectrum increases which results in a close frequency separation between the first- and the second-order scattering [15].

Barrick [3, 4] first derived theoretical expressions for the first- and the second-order HF scattering from the ocean surface using Rice's [22] perturbation technique which has been used to study the problems of scattering from random and slightly rough surface. The ocean surface is modelled as a three dimensional random surface governed by a Fourier series expansion over time as well as space. The surface Fourier coefficients are treated as random variables [3]. Average first- and second-order backscattered Doppler spectra could then be derived from Barrick's theoretical model of HF sea echo. Crombie's experimental observation was confirmed by Barrick's theoretical model for the first-order scattering.

Another theoretical analysis of HF scattering from an ocean surface was carried out by Srivastava [5] using an alternate approach based on Walsh's [21] general formulation for the scattering from a time invariant rough surface described by a

set of two vector integral equations in a two-dimensional spatial Fourier transform domain. Srivastava has also derived average first- and second-order backscattered Doppler spectra of the ocean clutter. Both Barrick's and Srivastava's derivations had the same result in the first-order scattering but differed in the second-order where the first author's result contained only one term while the latter contained three. The first term, interpreted as the occurrence of a double ocean wave interaction with the radar wave, is almost the same in both cases [5]. The two additional second-order terms which are significant for iceberg detection when the radar is used on the ship or platform may be neglected if the radar is located on the coast [19]. Both findings established a fundamental model of ocean clutter and the model of the second-order scattering enables information on the ocean, such as wave height, to be extracted.

2.3.1 Time-Domain Model for Ocean Clutter Signals

Knowing the average first- and second-order Doppler spectra of the ocean clutter may not be sufficient to distinguish the ocean clutter from the potential targets. This is because Doppler frequency discrimination may become ineffective when the target exhibits a Doppler frequency close to the "Bragg" frequencies. Also, target detection is a continuous process where it is preferable to know the instantaneous behaviour of the ocean clutter. Therefore, the time domain characteristic of the ocean clutter would possibly provide a means which could be used to separate the ocean clutter from the targets. The spectrum of Fig. 2.1 suggests that fairly broadband processes are responsible for the ocean clutter. However, Khan [7] has shown that the ocean clutter can be simply modelled by two narrowband signals, with time-varying frequencies, centered about the two "Bragg" frequencies described in Eq. (2.2). The time variation of the two narrowband clutter signals, as shown in Fig. 2.2, can be interpreted as two independent angle modulated

components. It is noticed that the instantaneous frequencies of the clutter signals fluctuate around the centre frequencies of ± 0.51 Hz as obtained from Eq. (2.2). It is demonstrated that the spectrum of such an angle modulated signals agrees closely with the spectrum of HF radar data and accounts for the characteristics corresponding to both the well known first- and second-order scattering peaks.

Thus, pre-processing operations on HF radar data, before target detection, can simply be specified as the estimation of the parameters of the two narrowband "Bragg" signals centered about their average frequencies given by Eq. (2.2). The clutter signals can be subsequently suppressed so that the capability to detect a target is enhanced.

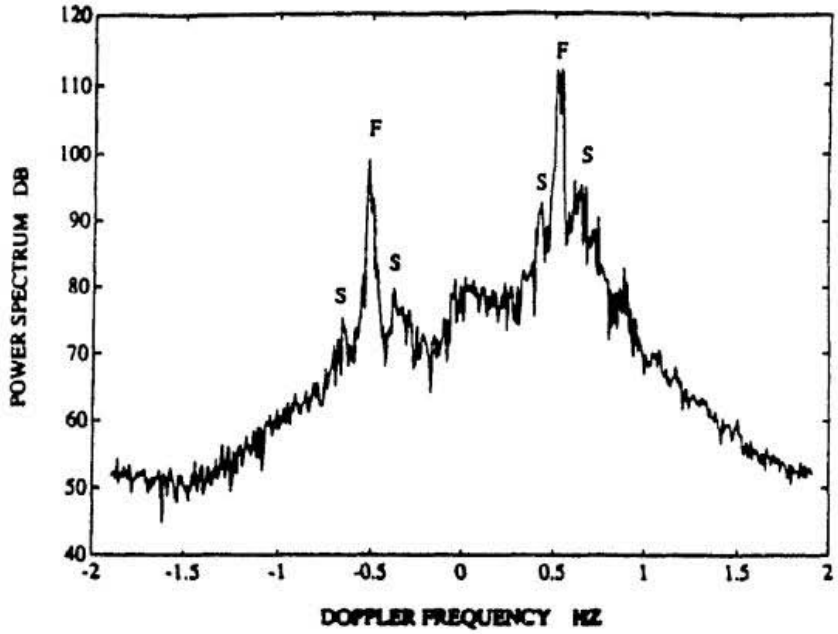

Figure 2.1: Typical HF radar power spectrum showing the characteristics of first-(F) and second-order(S) scattering peaks (From Ref. [7])

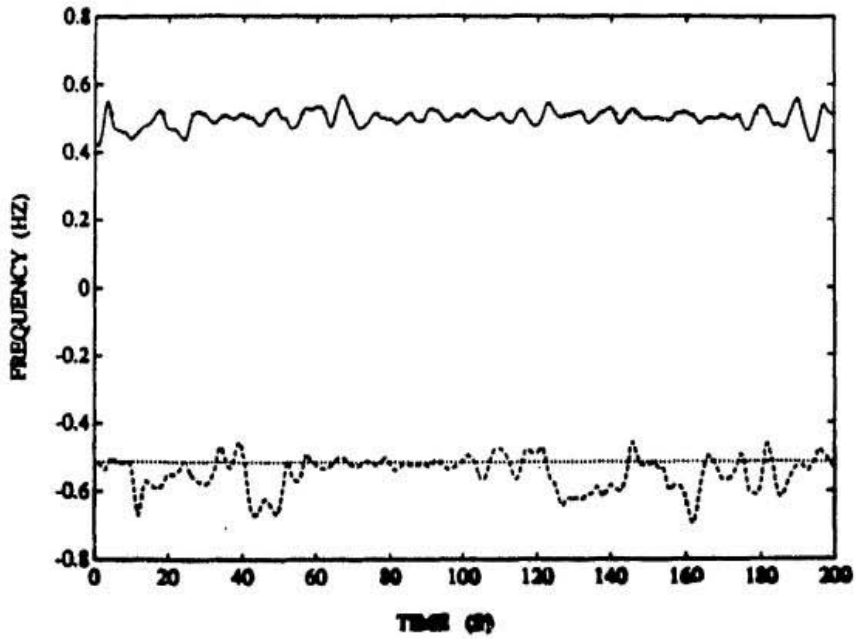

Figure 2.2: Time-varying behavior of the two dominant narrowband frequency components in HF radar ocean clutter (From Ref. [7])

Chapter 3

Some Time-varying Frequency Tracking Techniques

It has been shown in Chapter 2 that the ocean clutter has a time-varying characteristic and can be modelled as two narrowband frequency-modulated sinusoidal signals which can be tracked by time-varying signal processing techniques. The proposed clutter suppression scheme in this thesis is based on the use of a time-varying frequency tracking technique. Thus, in the following sections, a general review of some time-varying frequency tracking methods is presented. One of them is selected to be the basis of the clutter suppression scheme presented in this thesis. The decision is made based on the analytical comparison of the methods rather than the actual experimental results.

3.1 Adaptive Linear Prediction Filter

In 1975, Griffiths [23] presented an adaptive technique to track the instantaneous frequencies of a signal which has a narrow-band, time-varying spectrum. The method makes use of a linear prediction-error filter (PEF) derived from the property of linear prediction. It is used to estimate the instantaneous frequencies of the signal by computing the power spectrum from the filter coefficients which are updated continuously by the Least Mean Square (LMS) gradient adaptation algo-

rithm when a new data sample is obtained.

In the process of linear prediction-error filtering, a predicted value, $\tilde{x}(k)$, of the input at time k is given as a linear combination of the previous values.

$$\tilde{x}(k) = \sum_{i=1}^{L} g_i x(k-i) \tag{3.1}$$

where g_i are the Lth order prediction filter coefficients. An output error sequence, $\epsilon(k)$, of the filter is produced by subtracting the predicted value from the actual input.

$$\epsilon(k) = x(k) - \tilde{x}(k) \tag{3.2}$$

A minimum mean-square error, $E[\epsilon^2(k)]$, is produced by a set of optimum filter coefficients, $g_1^*, g_2^*, \cdots, g_L^*$. The power spectrum of the PEF for a stationary process is given by

$$S_x(\omega) = \frac{E[\epsilon^2(k)]_{min}}{|1 - \sum_{i=1}^{L} g_i^* \exp(-j\omega_i)|^2} \tag{3.3}$$

For a perfectly predictable input signal, $S_x(\omega)$ in Eq. (3.3) will be equal to 0 for $\omega \neq \omega_i$ and 0/0 when $\omega = \omega_i$. A modified power spectrum of PEF is defined by Griffiths to locate the frequency of narrowband input signals,

$$Q_x(\omega) = \frac{1}{|1 - \sum_{i=1}^{L} g_i^* \exp(-j\omega_i)|^2} \tag{3.4}$$

$Q_x(\omega)$ and $S_x(\omega)$ differ by a numerator scale factor. The advantage of having $Q_x(\omega)$ over $S_x(\omega)$ is to replace the 0/0 indeterminacy inherent with narrowband spectra by the computationally tractable limit of 1/0. If the signal is time-varying, the instantaneous power spectrum estimate will be given by

$$Q_x(\omega, k) = \frac{1}{|1 - \sum_{i=0}^{L-1} g_i^*(k) \exp[-j\omega_{(i+1)}]|^2} \tag{3.5}$$

The PEF coefficients are determined directly from the data sample by the following relationship that is derived from the LMS algorithm,

$$G(k+1) = G(k) + \mu[x(k)X(k-1) - X(k-1)X^T(k-1)G(k)] \tag{3.6}$$

where μ is a scalar proportionality constant which regulates the iteration step size, and

$$G(k) = \begin{bmatrix} g_1(k) \\ g_2(k) \\ \vdots \\ g_L(k) \end{bmatrix} \tag{3.7}$$

$$X(k-1) = \begin{bmatrix} x(k-1) \\ x(k-2) \\ \vdots \\ x(k-L) \end{bmatrix} \tag{3.8}$$

The above technique is basically a parametric estimation method in which the signal parameters, the prediction filter coefficients, are estimated instantaneously and then used to compute the instantaneous power spectrum. Unlike other techniques, the data samples are directly used in this technique to calculate the filter coefficients and no autocorrelation function is involved.

3.2 Eigenstructure Updating Method

In 1988, DeGroat and Roberts [24] presented another technique to track time-varying frequencies of narrow-band signals, based on the use of weighted linear prediction along with rank-one updating of the eigenvalue decomposition (EVD) of an estimated data covariance matrix. The idea behind this method is that the eigenvalue decomposition of an estimated covariance matrix is to identify signal and noise subspaces in the data vector space. Each subspace is characterized by a set of eigenvector/eigenvalue pairs. In the case of high SNR, the signal subspace is distinguished by the larger eigenvalues as compared to those associated with the noise subspace. However, as the SNR decreases, the signal subspace becomes perturbed. The eigenvalues of the signal subspace do not appear to be quite distinguishable from the noise subspace. A signal subspace pre-processing is introduced. The noise in the signal is identified and suppressed by zeroing its corresponding eigenvalues before the tracking of the frequencies is done. This pre-processing technique can also reduce the computational load by means of rank reduction of the covariance matrix. The method by DeGroat and Roberts is briefly discussed below.

If the signal is stationary, the covariance matrix of a data sequence $x(n)$ which is composed of r sinusoidal components plus white noise, based on an L-by-L Toeplitz matrix, can be written as

$$R = \frac{1}{L}\sum_{i=1}^{L} x_i x_i^T \tag{3.9}$$

where $x_i = [x(i)\ x(i+1)\cdots x(i+L-1)]^T$ and T denotes the transpose of a matrix.

In the case of a non-stationary process, a time-varying estimate of the kth covariance matrix is given as

$$R_k = (1-\alpha)\sum_{i=1}^{k} \alpha^{k-i} x_i x_i^T \tag{3.10}$$

where α is a memory factor, $0 \leq \alpha \leq 1$, and it is used to de-emphasize old data as new data is received. The estimated covariance matrix is recursively updated as

$$R_{k+1} = \alpha R_k - (1-\alpha) x_{k+1} x_{k+1}^T \tag{3.11}$$

with the recursion initialized as $R_1 = x_1 x_1^T$. The EVD is used to reduce the rank of R_k and to suppress noise as well. EVD of R_k is given by

$$R_k = Q D Q^T \tag{3.12}$$

where $D = diag[\lambda_1, \lambda_2, \cdots, \lambda_L]$ contains the eigenvalues of R_k in the order of $\lambda_1 \geq \lambda_2 \geq \cdots, \lambda_L$; and Q is an orthogonal matrix containing the corresponding eigenvectors. However, a new $\tilde{R}_k$ can be approximated by setting the eigenvalues λ_{r+1} through λ_L to zero in D. This noise suppression process is done each time when the covariance matrix is updated.

With each updated covariance matrix, the instantaneous frequencies are estimated using weighted linear prediction (LP) filter. The weighted LP equations at the kth update in the matrix form is given below.

$$g_k^T R_k \approx -r_k^T \tag{3.13}$$

or

$$g_k^T = -r_k^T R_k^{\sharp} \tag{3.14}$$

where g_k^T is a 1-by-L column vector of LP coefficients; R_k is the kth estimated covariance matrix; r_k^T is the estimated covariance vector; and $R_k^{\sharp}$ is the pseudo-inverse of R_k. The instantaneous frequency is then obtained from the angular locations of the zeros (on the unit circle on the z plane) of the denominator polynomial in the transfer function of the LP filter, that is form the roots of

$$G(z) = 1 + \sum_{i=1}^{L} g_k(i) z^{-i} = 0 \tag{3.15}$$

The eigenstructure updating method is also a parametric estimation technique with a signal pre-processing which can reduce a certain level of noise. The instantaneous frequencies of the sinusoids are estimated from the LP coefficients.

3.3 Hankel Rank Reduction Method

DiMonte and Arun [12] presented another technique to track the instantaneous frequencies of superimposed harmonics, referred to as the Hankel rank reduction method. The technique utilizes the property that a Hankel matrix (data matrix) constructed directly from a time series data containing a finite number of sinusoids can be approximated by the Singular Value Decomposition (SVD) to a matrix of rank equal to the number of principal singular values, even when the frequencies of the sinusoids are slowly varying with time; and then the instantaneous frequencies of the sinusoids can be estimated from those principal singular values. The frequency estimation is associated with the property of linear prediction which is observed in the characteristic of the Hankel matrix. The data in the matrix can simply be expressed as the sum of a weighted linear combination of the other data along the row of the matrix. The weighted coefficients are used to estimate the signal's frequency. The discussion on how the signal's frequency is estimated from the weighted coefficients is detailed in Chapter 4. The SVD plays here a similar role as the EVD. It decomposes the Hankel matrix into a signal and a noise vector subspace. Then the Hankel matrix is approximated by the signal subspace defined by the dominant singular values. This method is implemented in the clutter suppression scheme proposed in this thesis after the following consideration. (The derivation of the method is described in Chapter 5).

The eigenstructure updating method by DeGroat and Roberts works quite similarly to the adaptive linear prediction method by Griffiths - both of them using linear prediction-error filtering as the basis to estimate the sinusoids' frequencies, except that in the latter the eigenstructure updating method involves a signal pre-processing which identifies the signal and noise subspaces before the actual frequency estimation is performed. The advantage of having the pre-processing

is that certain level of noise suppression can be achieved. Therefore, the eigenstructure updating method will perform better than the adaptive linear prediction method in the case of low signal-to-noise ratio (SNR).

Both the eigenstructure updating method and the Hankel rank reduction method have a signal pre-processing step to suppress the effect of noise in a different fashion. The SVD in the latter method decomposes the Hankel matrix of entire data record into the signal and the noise subspaces at one time. That gives better noise suppression than the way of having multiple EVD's of the localized covariance matrices which are updated at every instant through [12]. The methodology seems to be robust if the process involves one single SVD rather than many EVD's. Also, it is more computationally advantageous to have a single SVD operation than multiple EVD's. With regard to simplicity, the Hankel rank reduction method involves less mathematical steps. Finally, the selection of appropriate memory factor, α, in the eigenstructure updating method imposes a trade-off between temporal resolution and noise suppression [12]. Therefore, the Hankel rank reduction method is selected to be used in the proposed clutter suppression scheme to estimate the instantaneous frequencies of the ocean clutter signals from which the clutter components can be identified and suppressed.

Chapter 4

Frequency Estimation of Stationary Sine Waves

Based on the inherent time-varying characteristic of the ocean clutter in HF radar, the Hankel rank reduction method which is a time-varying signal processing technique, is utilized in the clutter suppression scheme proposed in this thesis to track the clutter signal's frequencies and then to suppress them. Before discussing the time-varying frequency tracking technique, it is worthwhile to review the background of the frequency estimation of the stationary sine waves since it forms the basis for the method to deal with the non-stationary (time-varying) process. In this chapter, the main focus is on the procedure methodology for estimating the frequencies of the sine waves by parametric modelling. In other words, it is possible to fit a model to the process and then to determine the parameters of the model from which the sinusoidal frequencies can be obtained [25]. The method is referred to as the autoregressive (AR) or linear prediction modelling. In addition to the common transfer-function representation approach used for the model-based spectral estimation method, the state-variable representation approach is also described here as it was used in the Hankel rank reduction method. It is found that both approaches yield the same result. The estimation of the sinusoidal frequencies in both noiseless and noisy cases will be discussed.

4.1 Noiseless Case

A sampled signal, $y(k)$, composed of M complex sinusoids with no noise present is represented by the following equation,

$$y(k) = \sum_{i=1}^{M} c_i \exp(j\omega_i k), \quad k = 1, 2, \cdots, N \tag{4.1}$$

where c_i is the amplitude; ω_i is the angular frequency of the ith complex sinusoid and N is the number of data samples. The angular frequencies of the complex sinusoids are assumed to be invariant with time and they can be estimated by the autoregressive (AR) process (modelling) or linear prediction method in which $y(k)$ is given by a linear combination of its past values and an additive white noise signal, $w(k)$, with zero mean.

$$y(k) = -\sum_{i=1}^{L} a_i y(k-i) + w(k) \tag{4.2}$$

where $a_i, i = 1, 2, \cdots, L$, are known as the AR coefficients and L is the order of the AR process. That means the signal, $y(k)$, is modelled as the output of an AR process whose input is a white noise source. The z-domain transfer function of the AR process is

$$H(z) = \frac{1}{A(z)} \tag{4.3}$$

where

$$A(z) = 1 + \sum_{i=1}^{L} a_i z^{-i} \tag{4.4}$$

The AR process is closely related to the linear prediction-error filtering when operating on the frequency estimation of the stationary sine waves. Their relationship is depicted in Fig. 4.1. The prediction-error filter is an all-zero filter with an impulse response of a finite duration whereas the inverse filter in the AR model is an all-pole filter with an impulse response of an infinite duration [26]. The zeros of the transfer function of the prediction-error filter are located at exactly the same

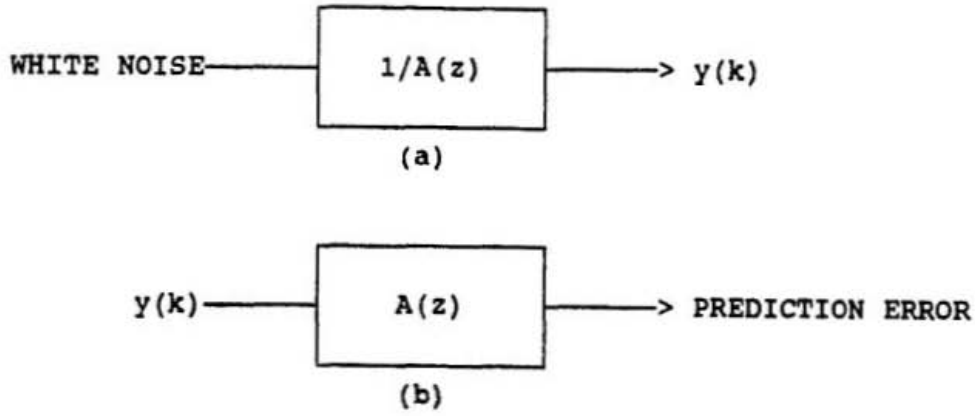

Figure 4.1: (a) an AR process, (b) a linear prediction-error filter

positions (inside the unit circle on the z plane) as the poles of the transfer function of the inverse filter of the AR model. This assures the stability of the filters because in the s domain ($s = \sigma + j\omega$), $H(s)$ is considered stable if the poles are located in the left hand side of the s plane and, for $z = e^s$, the left half s plane is mapped into the unit circle. $H(s)$ is considered marginally stable if the poles are on the imaginary axis of the s plane where $\sigma = 0$.

It was first shown in the Prony's method described by Hilderbrand [27] that in a noiseless condition, the angular frequencies of the complex sinusoids can be obtained from the angular locations of the roots of an Mth order polynomial $A(z)$ on the unit circle on the z plane. The roots lying on the unit circle are mapped onto the imaginary axis of the s plane ($s = j\omega$) where the system is marginally stable. However, in the practical situation, L can be greater than or equal to M. Tufts and Kumaresan [28, 29] have demonstrated that under the inequality, $M \leq L \leq (N - M/2)$, the polynomial $A(z)$ has M roots on the unit circle on the z plane with their angular locations corresponding to the angular frequencies of the M sinusoids in the signal, and the $(L - M)$ extraneous roots are uniformly

distributed along the circumference inside the unit circle. The property that the roots of the polynomial $A(z)$ on the unit circle ($|z| = 1$) determine the angular frequencies of the sinusoids can be shown by the following observations.

Consider a system of prediction equations in matrix form used to determine the coefficients, $a_i, i = 1, 2, ..., L$

$$\begin{bmatrix} y(L) & y(L+1) & \cdots & y(1) \\ y(L+1) & y(L) & \cdots & y(2) \\ \cdot & \cdot & & \cdot \\ \cdot & \cdot & & \cdot \\ y(N-1) & y(N-2) & \cdots & y(N-L) \end{bmatrix} \begin{bmatrix} a_1 \\ a_2 \\ \cdot \\ \cdot \\ a_L \end{bmatrix} = - \begin{bmatrix} y(L+1) \\ y(L+2) \\ \cdot \\ \cdot \\ y(N) \end{bmatrix} \tag{4.5}$$

or

$$Y_f a = b_f \tag{4.6}$$

Rearrange Eq. (4.6)

$$Y_f' = [b_f | Y_f] \tag{4.7}$$

and

$$a' = [1, a_1, a_2, \cdots, a_L]^T \tag{4.8}$$

Therefore,

$$Y_f' a' = 0 \tag{4.9}$$

Y_f' is a $(N-L)$-by-$(L+1)$ Toeplitz matrix formed from a forward linear prediction, i.e. $y(k) = -\sum_{i=1}^{L} a_i y(k-i), i = 1, 2, \cdots, M$, and it has a rank of M. (The rank of a matrix is defined as the number of rows or columns which are linearly independent.) To see this, an M-by-1 sinusoidal column vector is defined as follows:

$$f_i = [1, e^{-j\omega_i}, e^{-2j\omega_i}, \cdots, e^{-Lj\omega_i}]^T, \quad i = 1, 2, \cdots, M \tag{4.10}$$

It is observed that any row of Y_f' can be written as a linear combination of the M independent vectors in f_i. Thus, the rank of Y_f' is M as long as Y_f' has at least M rows. The null space of Y_f' has a dimension of $L + 1 - M$. Since a' lies in the null

space of Y_f', the inner product of f_i and a' is zero [29]. That is,

$$1 + a_1 e^{-j\omega_i} + a_2 e^{-2j\omega_i} + \cdots + a_L e^{-Lj\omega_i} = 0, \quad i = 1, 2, \cdots, M \tag{4.11}$$

and this equation is recognized as the transfer function of the prediction-error filter and evaluated on the unit circle at $z = e^{j\omega_i}, i = 1, 2, \cdots, M$. Then the polynomial $A(z)$ has roots, on the unit circle, that determine the sinusoidal frequencies [28].

Not only can the signal, $y(k)$, be predicted from forward linear prediction, but it can also be predicted from backward linear prediction. A system of prediction equations from backward linear prediction is obtained to determine the coefficients, $a_i, i = 1, 2, \cdots, L$, as below:

$$\begin{bmatrix} y^*(2) & y^*(3) & \cdots & y^*(L+1) \\ y^*(3) & y^*(4) & \cdots & y^*(L+2) \\ . & . & & . \\ . & . & & . \\ y^*(N-L+1) & y^*(N-L+2) & \cdots & y^*(N) \end{bmatrix} \begin{bmatrix} a_1 \\ a_2 \\ . \\ . \\ a_L \end{bmatrix} = - \begin{bmatrix} y^*(1) \\ y^*(2) \\ . \\ . \\ y^*(N-L) \end{bmatrix} \tag{4.12}$$

or

$$Y_b a = b_b \tag{4.13}$$

Rearrange Eq. (4.12) to

$$Y_b' a' = 0 \tag{4.14}$$

where

$$Y_b' = [b_b | Y_b] \tag{4.15}$$

Y_b' is a $(N-L)$-by-$(L+1)$ Hankel matrix in which the N data samples, $y(k)$, are complex conjugated because $y(k)$ is complex valued. ($*$ denotes complex conjugate). Y_b' also has a rank of M which can be seen from the previous observation in Y_f'. Similarly, the polynomial $A(z)$ has roots of $e^{j\omega_i}, i = 1, 2, \cdots, M$.

Transfer-function representation has been widely used in model-based spectral estimation methods. This approach as used above demonstrated that the parameters or coefficients of an AR model could be utilized to determine the sinusoidal

frequencies. The state variable representation however is an alternative approach to analyze a linear system [30]. It will be shown that this approach can also be used to describe the AR model, and then the AR parameters are determined to give the sinusoidal frequencies. In general, a discrete-time system is represented by a set of state variable equations:

$$x(k+1) = Ax(k) + Bv(k) \tag{4.16}$$

$$y(k) = Cx(k) + Dv(k) \tag{4.17}$$

where $x(k)$ is the state vector describing the system at the kth instant; $y(k)$ is the output vector; $v(k)$ is the input vector; A, B, C and D are the matrices determined from the constants of the system [31]. Consider a second order AR process,

$$y(k) = -a_1 y(k-1) - a_2 y(k-2) + w(k) \tag{4.18}$$

Define the first state variable

$$x_2(k) = -a_1 y(k-1) - a_2 y(k-2) \tag{4.19}$$

Combine Eq. (4.18) and Eq. (4.19) to get

$$y(k) = x_2(k) + w(k) \tag{4.20}$$

From Eq. (4.19), increasing k by 1 gives

$$x_2(k+1) = -a_1 y(k) - a_2 y(k-1) \tag{4.21}$$

Select a second state variable

$$x_1(k) = -a_2 y(k-1) \tag{4.22}$$

Substitute Eq. (4.22) into Eq. (4.21), it can be written as

$$\begin{aligned} x_2(k+1) &= x_1(k) - a_1 y(k) \\ &= x_1(k) - a_1(x_2(k) + w(k)) \\ &= x_1(k) - a_1 x_2(k) - a_1 w(k) \end{aligned} \tag{4.23}$$

From Eq. (4.22), increasing k by 1 gives

$$\begin{aligned} x_1(k+1) &= -a_2 y(k) \\ &= -a_2(x_2(k) + w(k)) \\ &= -a_2 x_2(k) - a_2 w(k) \end{aligned} \tag{4.24}$$

Equation (4.23) and Eq. (4.24) may be combined in matrix form as

$$\begin{bmatrix} x_1(k+1) \\ x_2(k+1) \end{bmatrix} = \begin{bmatrix} 0 & -a_2 \\ 1 & -a_1 \end{bmatrix} \begin{bmatrix} x_1(k) \\ x_2(k) \end{bmatrix} + \begin{bmatrix} -a_2 \\ -a_1 \end{bmatrix} w(k) \tag{4.25}$$

From Eq. (4.20) and Eq. (4.25), the AR process is now represented by the following state variable equations:

$$x(k+1) = Ax(k) + Bw(k) \tag{4.26}$$

$$y(k) = Cx(k) + Dw(k) \tag{4.27}$$

where

$$A = \begin{bmatrix} 0 & -a_2 \\ 1 & -a_1 \end{bmatrix}, B = \begin{bmatrix} -a_2 \\ -a_1 \end{bmatrix}, C = [0, 1], D = [1] \tag{4.28}$$

The derivation of a simple second order AR process in terms of state variable representation can also be extended to a general L order AR process where the matrices A, B, C and D are as follows.

$$A = \begin{bmatrix} 0 & 0 & 0 & \dots & 0 & 0 & -a_L \\ 1 & 0 & 0 & \dots & 0 & 0 & -a_{L-1} \\ 0 & 1 & 0 & \dots & 0 & 0 & -a_{L-2} \\ . & . & . & & . & . & . \\ . & . & . & & . & . & . \\ 0 & 0 & 0 & \dots & 1 & 0 & -a_2 \\ 0 & 0 & 0 & \dots & 0 & 1 & -a_1 \end{bmatrix}, B = \begin{bmatrix} -a_L \\ -a_{L-1} \\ -a_{L-2} \\ . \\ . \\ -a_2 \\ -a_1 \end{bmatrix} \tag{4.29}$$

and

$$C = \begin{bmatrix} 0 & 0 & 0 & \dots & 0 & 1 \end{bmatrix}, D = [1] \tag{4.30}$$

where A, B, and C are the constant matrices with the size of L-by-L, L-by-1 and 1-by-L, respectively.

Consider the sampled signal, $y(k)$, in Eq. (4.1) again. Without the presence of noise, the signal is exactly predictable as a linear combination of its past samples and the prediction error is zero. Consequently, $y(k)$ can be adequately modelled as the output of an AR process of the order $L = M$ with zero input, i.e. $w(k) = 0$, or simply as the output of an oscillator [30]

$$y(k) = -\sum_{i=1}^{M} a_i y(k-i) \tag{4.31}$$

In the state variable representation, the signal, $y(k)$, is described by the following set of equations:

$$x(k+1) = Fx(k) \tag{4.32}$$

$$y(k) = hx(k) \tag{4.33}$$

where $x(k)$ is an M-by-1 state vector. F and h are the M-by-M and 1-by-M state matrices in the form of A and C given in Eq. (4.29) and Eq. (4.30), respectively. It will be shown that the eigenvalues of F are exactly the same as the roots of the M order polynomial $A(z)$. (The eigenvalues and the eigenvectors of a matrix are discussed in Appendix B). The angles of the eigenvalues will give the frequencies of the sinusoids. If F can be estimated, then the sinusoidal frequencies will be determined from the angles of the eigenvalues of F.

Now consider an $(N-L+1)$-by-L Hankel matrix constructed directly from the sampled signal, $y(k)$, where $L > M$ and $N \gg L$.

$$H = \begin{bmatrix} y(1) & y(2) & \cdots & y(L) \\ y(2) & y(3) & \cdots & y(L+1) \\ \cdot & \cdot & & \cdot \\ \cdot & \cdot & & \cdot \\ y(N-L+1) & y(N-L+2) & \cdots & y(N) \end{bmatrix} \tag{4.34}$$

In terms of state variables, H can be written in the following form using Eq. (4.32) and Eq. (4.33).

$$
\begin{aligned}
H &= \begin{bmatrix} hx(1) & hx(2) & \cdots & hx(L) \\ hx(2) & hx(3) & \cdots & hx(L+1) \\ hx(3) & hx(4) & \cdots & hx(L+2) \\ \cdot & \cdot & & \cdot \\ \cdot & \cdot & & \cdot \\ hx(N-L+1) & hx(N-L+2) & \cdots & hx(N) \end{bmatrix} \\
&= \begin{bmatrix} hx(1) & hx(2) & \cdots & hx(L) \\ hFx(1) & hFx(2) & \cdots & hFx(L) \\ hF^2x(1) & hF^2x(2) & \cdots & hF^2x(L) \\ \cdot & \cdot & & \cdot \\ \cdot & \cdot & & \cdot \\ hF^{N-L}x(1) & hF^{N-L}x(2) & \cdots & hF^{N-L}x(L) \end{bmatrix}
\end{aligned} \tag{4.35}
$$

H can be factorized as

$$
\begin{aligned}
H &= \begin{bmatrix} h \\ hF \\ hF^2 \\ \cdot \\ \cdot \\ hF^{N-L} \end{bmatrix} \begin{bmatrix} x(1), & x(2), & x(3), & \cdots, & x(L) \end{bmatrix} \\
&= \Theta X
\end{aligned} \tag{4.36}
$$

The matrix Θ is known as the observability matrix and X is the state vector matrix. It is noticed that matrix Θ has only M columns and X has only M rows. It means that the rank of H cannot be greater than M. If there are M distinct sinusoidal frequencies, H will have a rank of M even though the size of H is greater than M-by-M.

F can be determined from Θ. If Θ is partitioned into two matrices, Θ_1 having rows from the first one to the second last and Θ_2 having rows from the second one to the last one, then a relationship between F, Θ_1 and Θ_2 will be observed. That is,

$$\Theta_1 F = \Theta_2 \tag{4.37}$$

where

$$\Theta_1 = \begin{bmatrix} h \\ hF \\ hF^2 \\ \cdot \\ \cdot \\ hF^{N-L-1} \end{bmatrix}, \Theta_2 = \begin{bmatrix} hF \\ hF^2 \\ hF^3 \\ \cdot \\ \cdot \\ hF^{N-L} \end{bmatrix} \tag{4.38}$$

Since Eq. (4.37) is overdetermined, F can be solved by the least square method as

$$F = \Theta_1^{\sharp}\Theta_2 \tag{4.39}$$

where $\Theta_1^{\sharp} = (\Theta_1^T\Theta_1)^{-1}\Theta_1^T$. Θ_1^T is the transpose of Θ_1 and $(\Theta_1^T\Theta_1)^{-1}$ is the inverse of $(\Theta_1^T\Theta_1)$. The eigenvalues of F are determined by (see Appendix B for the computation of the eigenvalues of a matrix)

$$\det \begin{vmatrix} -\lambda & 0 & 0 & \dots & 0 & 0 & -a_M \\ 1 & -\lambda & 0 & \dots & 0 & 0 & -a_{M-1} \\ 0 & 1 & -\lambda & \dots & 0 & 0 & -a_{M-2} \\ \cdot & \cdot & \cdot & & \cdot & \cdot & \cdot \\ \cdot & \cdot & \cdot & & \cdot & \cdot & \cdot \\ 0 & 0 & 0 & \dots & 1 & -\lambda & -a_2 \\ 0 & 0 & 0 & \dots & 0 & 1 & -a_1 - \lambda \end{vmatrix} = 0 \tag{4.40}$$

where λ is a scalar parameter. The resultant equation of Eq. (4.40) is simplified in the following form.

$$\lambda^M + a_1\lambda^{M-1} + a_2\lambda^{M-2} + \cdots + a_M = 0 \tag{4.41}$$

This equation is called the characteristic equation of the matrix F, and its roots are the eigenvalues of matrix F. Recall the characteristic polynomial in the transfer function of the M order AR process,

$$A(z) = 1 + \sum_{i=1}^{M} a_i z^{-i} = 0 \tag{4.42}$$

$A(z) = 0$ can be rewritten in the following form:

$$z^M + a_1 z^{M-1} + a_2 z^{M-2} + \cdots + a_M = 0 \tag{4.43}$$

With reference to Eq. (4.41) and Eq. (4.43), it is shown that the eigenvalues of F are exactly the same as the roots of the polynomial $A(z)$. Hence, the angular frequencies of the complex sinusoids can be determined from the angles of the eigenvalues of F which are in the form of $(e^{j\omega_1}, e^{j\omega_2}, \cdots, e^{j\omega_M})$ on the unit circle on the z plane.

4.2 Noisy Case

It has been shown in the noiseless case that the Hankel matrix H exhibits a low rank property, and the rank is equal to the number of complex sinusoids in the signal. However, in the practical situation, the signal is always corrupted by noise. Therefore, the low rank property of H will no longer hold. In fact, H tends to have a full rank.

The Singular Value Decomposition (SVD) has been recognized as a numerical tool for displaying closeness to low rank of a matrix [30] (see Appendix B), and its structure and numerical detail can be utilized to suppress noise as well. The SVD of any rectangular matrix, such as the Hankel matrix H in Eq. (4.34), takes the following form,

$$\begin{aligned} H &= USV^T \\ &= \sum_{i=1}^{L} \sigma_i u_i v_i^T \end{aligned} \tag{4.44}$$

where S is a L-by-L diagonal matrix. Its diagonal elements, known as the singular values of H, are arranged as $\sigma_1 \geq \sigma_2 \geq \cdots \geq \sigma_M \geq \sigma_{M+1} \geq \cdots \geq \sigma_L \geq 0$; u_i and v_i are the corresponding left and right singular vectors which are the eigenvectors of the matrices HH^T and H^TH, respectively. Similarly, the singular values are the square roots of the eigenvalues of the matrices HH^T or H^TH (see Appendix B for the definition of the SVD of a matrix). It can be shown that above a certain signal-to-noise (SNR) threshold, a data matrix H is decomposed into two vector subspaces. One is the signal subspace spanned by the left and the right singular vectors associated with the M largest singular values, and the other is the noise subspace spanned by the remaining $(L - M)$ singular values. Thus H can be rearranged as

$$H = \begin{pmatrix} U_1, & U_2 \end{pmatrix} \begin{pmatrix} S_1 & 0 \\ 0 & S_2 \end{pmatrix} \begin{pmatrix} V_1 \\ V_2 \end{pmatrix}^T \tag{4.45}$$

where S_1 is an M-by-M diagonal matrix containing the M principal singular values; U_1 and V_1 contain the corresponding left and right singular vectors. S_2 has the remaining $(L-M)$ smaller singular values associated with the left and the right singular vectors in U_2 and V_2. If there is no noise, the $(L-M)$ singular values will be zero. Thus the rank of H is determined by the M principal singular values. A significant break will be observed beween the singular values, σ_M and σ_{M+1}, when the SNR is above a certain threshold level. Then H can be approximated by the M principal components as

$$\begin{aligned} H &\simeq U_1 S_1 V_1^T \\ &= \sum_{i=1}^{M} \sigma_i u_i v_i^T \end{aligned} \tag{4.46}$$

Rearrange Eq. (4.46)

$$H = U_1 S_1^{1/2} S_1^{1/2} V_1^T \tag{4.47}$$

Comparing Eq. (4.47) and Eq. (4.36), the observability martix Θ can be identified as $U_1 S_1^{1/2}$ [30]. Using the relationship between F and Θ derived as in Eq. (4.37), F can be determined and the angular frequencies of the complex sinusoids can be estimated from the angles of the eigenvalues of F.

The SVD can be used to decompose a Hankel matrix (data matrix) of a signal containing a finite number of sinusoids plus noise into a signal and a noise vector subspaces provided that the noise level is not very high. The Hankel matrix is then approximated as detailed above, by a reduced order Hankel matrix conforming to the signal subspace defined by the finite dominant singular values. This lower rank Hankel matrix gives estimate for the frequencies of the sinusoids contained in the state matrix F.

A procedure, based on the SVD, was developed by Eckart and Young in 1936 to find the best lower rank approximation to a given matrix [32, 33]. First of all, let the rank of H be L, and let $y(M)$ be the set of all $(N-L+1)$-by-L matrices

of rank $M < L$. Then for all matrices G in $y(M)$,

$$\|H - \tilde{H}\| \leq \|H - G\| \tag{4.48}$$

where $\tilde{H} = U\tilde{S}V^T$ and $\tilde{S}$ is obtained from the matrix S by setting all except the M largest singular values to zero. The matrix norm of Eq. (4.48) is the Frobenius form,

$$\|H - G\|^2 = trace[(H - G)^*(H - G)] \tag{4.49}$$

where the *trace* of a matrix is defined as the sum of the matrix's diagonal elements and the asterisk, $*$, stands for complex conjugate transpose of a matrix. Thus $\tilde{H}$ will be the best approximation of H if the condition of Eq. (4.48) is satisfied.

The frequencies of stationary sine waves can be estimated by the parametric modelling. The parametric modelling can be realized by both the transfer-function representation and the state-variable representation. Although the estimation of the sinusoidal frequencies obtained from the model parameters are presented by the two representations in a different way, i.e. the zeros of the denominator polynomial of the transfer function for the AR model and the eigenvalues of the state matrix F, the results are the same. Moreover, the SVD can serve to reduce the data space to a dimensionally smaller signal space and the effect of noise can be substantailly suppressed.

Chapter 5

The Clutter Suppression Scheme

As mentioned in Chapter 2, ocean clutter in HF radar can be viewed as two narrowband frequency-modulated sinusoidal signals, with their centre frequencies given by Eq. (2.2). Based on this time-varying model of the ocean clutter presented in Khan's recent work [7], a clutter suppression scheme is developed to selectively suppress the clutter components from the received radar signal. The instantaneous frequencies of the clutter signals can be tracked by a time-varying signal processing technique, namely Hankel rank reduction method, and the clutter signals can then be identified from their centre frequencies which almost agree with the average values of their instantaneous frequencies. The clutter suppression scheme proposed in this thesis involves two steps. The first one is to estimate the instantaneous frequencies of the ocean clutter signals by applying the Hankel rank reduction method, and the other one is to remove the signal power associated with the clutter signals from the time series data so that the resultant data samples will be clutter free. The derivation of the Hankel rank reduction method and the procedures to suppress the clutter signals will be discussed in detail in this chapter.

5.1 Hankel Rank Reduction Method

The Hankel rank reduction method presented by DiMonte and Arun [12] utilizes the property that a Hankel matrix constructed directly from a time series containing a finite number of sinusoids can be approximated by a lower rank matrix characterized by the principal singular values obtained from the Singular Value Decomposition (SVD), even if the sinusoidal frequencies are varying slowly with time. The instantaneous frequencies are then estimated from those principal singular values. The derivation of the method is shown in the following sections.

Given a sampled signal, $y(k)$, composed of r superimposed real-valued sinusoids whose frequencies are assumed to be varying slowly with time,

$$y(k) = A_1 \cos(\phi_1(k)) + A_2 \cos(\phi_2(k)) + \cdots + A_r \cos(\phi_r(k)), k = 1, 2, 3, \cdots, N \quad (5.1)$$

where N is the total number of data samples. $A_i, i = 1, 2, \cdots, r$, are the amplitudes of the sinusoids. The instantaneous frequency of each sinusoid is defined as

$$\omega_i(k) \equiv [\phi_i(k) - \phi_i(k-1)], \quad i = 1, 2, \cdots, r \quad (5.2)$$

where the sampling period is assumed to be unity. A Hankel matrix constructed directly from the data samples has a size of $(N - L + 1)$-by-L, where L is of the order of $3r$ [12]; and $N \gg L$.

$$H = \begin{bmatrix} y(1) & y(2) & \cdots & y(L) \\ y(2) & y(3) & \cdots & y(L+1) \\ \cdot & \cdot & & \cdot \\ \cdot & \cdot & & \cdot \\ y(N-L+1) & y(N-L+2) & \cdots & y(N) \end{bmatrix} \quad (5.3)$$

In the previous chapter, it has been proved that H has a rank of $2r$ (note that $\cos(\phi(k)) = 1/2(e^{j\phi(k)} + e^{-j\phi(k)})$) when the sinusoidal frequencies are invariant with time and the data sequence is noiseless. However, if the frequencies are changing with time, H will be of full rank. DiMonte and Arun [12] have demonstrated

that if the frequencies of the signals change sufficiently slowly over a period of L data samples, the rank of H will be close to $2r$. This claim can be shown by the related approach used for the stationary sine waves in Chapter 4. The sampled signal, $y(k)$, can also be modelled as the output of the special AR process with zero input, or simply as the output of an oscillator. The model is governed by the following two state variable equations,

$$x(k+1) = F(k)x(k) \tag{5.4}$$

$$y(k) = hx(k) \tag{5.5}$$

where $x(k)$ is a $2r$-by-1 state vector; $F(k)$ is known as the instantaneous state feedback matrix with a size of $2r$-by-$2r$. The F matrix is now no longer constant. Since F is a frequency dependent matrix, it will change with time as the sinusoidal frequencies are time-varying. h is the 1-by-$2r$ output vector. The instantaneous frequencies of the sinusoids will be given by the angles of the eigenvalues of $F(k)$. The eigenvalues of $F(k)$ are in the form of $e^{\pm j\omega_i(k+1)}, i = 1, 2, \cdots, r$. The relationship to the signal parameters can be explicitly shown in the diagonal canonical representation of the system where

$$F(k) = diag[e^{j\omega_1(k+1)}, e^{-j\omega_1(k+1)}, e^{j\omega_2(k+1)}, e^{-j\omega_2(k+1)}, \cdots, e^{j\omega_r(k+1)}, e^{-j\omega_r(k+1)}] \tag{5.6}$$

$$h = [A_1, A_1, A_2, A_2, \cdots, A_r, A_r] \tag{5.7}$$

$$x(0) = [e^{j\phi_1(0)}, e^{-j\phi_1(0)}, e^{j\phi_2(0)}, e^{-j\phi_2(0)}, \cdots, e^{j\phi_r(0)}, e^{-j\phi_r(0)}]^T \tag{5.8}$$

From Eq. (5.4) and Eq. (5.5) , H in Eq. (5.3) can be rewritten as

$$H = \begin{bmatrix} hx(1) & hx(2) & \cdots & hx(L) \\ hx(2) & hx(3) & \cdots & hx(L) \\ \cdot & \cdot & & \cdot \\ \cdot & \cdot & & \cdot \\ hx(N-L+1) & hx(N-L+2) & \cdots & hx(N) \end{bmatrix}$$

$$= \begin{bmatrix} hx(1) & hx(2) & \cdots & hx(L) \\ hF(1)x(1) & hF(2)x(2) & \cdots & hF(L)x(L) \\ hF(1)F(2)x(1) & hF(2)F(3)x(2) & \cdots & hF(L)F(L+1)x(L) \\ \cdot & \cdot & & \cdot \\ \cdot & \cdot & & \cdot \end{bmatrix} \quad (5.9)$$

If the frequencies are changing significantly slowly with time, the state feedback matrix $F(k)$ can be considered approximately constant over the period of L time instants. Such being the case, along each row of H, the sinusoidal frequencies are assumed to be invariant with time. As a result, the feedback matrices $F(k+1)$, $F(k+2), \cdots, F(k+L)$, $k = 0, 1, 2, \cdots$ can be approximated by its mean value in the L time instants, that is $F(k+d), d = (L+1)/2$. Then H will be close to the following form.

$$\begin{aligned} H &\simeq \begin{bmatrix} hx(1) & hx(2) & \cdots & hx(L) \\ hF(d)x(1) & hF(d)x(2) & \cdots & hF(d)x(L) \\ hF(d)F(d+1)x(1) & hF(d)F(d+1)x(2) & \cdots & hF(d)F(d+1)x(L) \\ \cdot & \cdot & & \cdot \\ \cdot & \cdot & & \cdot \end{bmatrix} \\ &= \begin{bmatrix} h \\ hF(d) \\ hF(d)F(d+1) \\ \cdot \\ \cdot \end{bmatrix} \begin{bmatrix} x(1), & x(2), & x(3), \cdots, & x(L) \end{bmatrix} \\ &= \Theta X \end{aligned} \quad (5.10)$$

Because Θ has only $2r$ columns and X has only $2r$ rows, the rank of H will not be greater than $2r$. It can be shown that if the r instantaneous frequencies are different for at least $2r$ time instants, the factors Θ and X are full rank, and hence H has rank of $2r$ [12]. However, the global change in the frequencies in the data can affect the approximation of matrix H to the lower rank matrix.

In the case of stationary sine waves, their frequencies can be estimated from the angles of the eigenvalues of F. Similarly, for non-stationary sine waves, their instantaneous frequencies can also be determined from the eigenvalues of $F(k)$. When the sinusoidal frequencies are time-varying, the Hankel matrix H is full

rank. The Singular Value Decomposition (SVD) is used to obtain a low rank approximation of H from which an estimate of the observability matrix Θ in (5.10) can be identified. Hence, it is possible to determine $F(k)$ from Θ. The SVD of the Hankel matrix H is expressed as

$$\begin{aligned} H &= USV^T \\ &= \sum_{i=1}^{L} \sigma_i u_i v_i^T \end{aligned} \tag{5.11}$$

where $S = diag[\sigma_1, \sigma_2, \cdots, \sigma_L]$ and $\sigma_1 \geq \sigma_2 \geq \cdots \sigma_{2r} \geq \sigma_{2r+1} \cdots \sigma_L \geq 0$ are known as the singular values of H. u_i and v_i are the corresponding left and right singular vectors. It can be shown that if the sinusoidal frequencies are changing slowly with time and the noise level is not very high, then there will be $2r$ principal singular values which represent most power of the signal and the rest of the $(L-2r)$ singular values will be small and close to zero. Thus H can be rewritten as

$$H = \begin{pmatrix} U_1, & U_2 \end{pmatrix} \begin{pmatrix} S_1 & 0 \\ 0 & S_2 \end{pmatrix} \begin{pmatrix} V_1 \\ V_2 \end{pmatrix}^T \tag{5.12}$$

where $S_1 = diag[\sigma_1, \sigma_2, \cdots, \sigma_{2r}]$ and $S_2 = diag[\sigma_{2r+1}, \sigma_{2r+2}, \cdots, \sigma_L]$. U_1 and V_1 contain the left and the right singular vectors corresponding to the $2r$ principal singular values whereas U_2 and V_2 consist of the left and the right singular vectors associated with the remaining $(L-2r)$ singular values. If $\sigma_{2r} \gg \sigma_{2r+1}$, then it will lead to a good approximation of H defined by the $2r$ dominant singular values, i.e.

$$\begin{aligned} H &\simeq U_1 S_1 V_1^T \\ &= \sum_{i=1}^{2r} \sigma_i u_i v_i^T \end{aligned} \tag{5.13}$$

Rearranging Eq. (5.13) gives

$$H = U_1 S_1^{1/2} S_1^{1/2} V_1^T \tag{5.14}$$

By comparing Eq. (5.10) and Eq. (5.14), $\tilde{\Theta} = U_1 S_1^{1/2}$ is identified as an estimate of Θ and $\tilde{X} = S_1^{1/2} V_1^T$ is an estimate of X. Θ consists of the state feedback matrices

$F(k)$ whose eigenvalues determine the instantaneous frequencies of the sinusoids. $F(k)$ can be estimated by two steps. First, $\tilde{\Theta}$ is partitioned into a number of small matrices in which the number of rows in each small matrix equals d, the mean value in the L time instants.

$$\tilde{\Theta}_k = rows\ from\ k\ to\ (d+k)\ of\ \tilde{\Theta}, k = 1, 2, 3, \cdots \tag{5.15}$$

Second, from Eq. (5.10), a relationship between $F(k)$ and the partitioned matrices $\tilde{\Theta}_k$ is observed as follows.

$$\tilde{\Theta}_k F(d+k) \simeq \tilde{\Theta}_{k+1}, k = 1, 2, 3, \cdots \tag{5.16}$$

or

$$\begin{aligned} \tilde{\Theta}_1 F(d+1) &= \tilde{\Theta}_2 \\ \tilde{\Theta}_2 F(d+2) &= \tilde{\Theta}_3 \\ \tilde{\Theta}_3 F(d+3) &= \tilde{\Theta}_4 \\ &\vdots \end{aligned} \tag{5.17}$$

The least square method can be used to solve for $F(d+k)$ because the system of linear equations in Eq. (5.16) is overdetermined [34]; and the instantaneous frequencies of the sinusoids at time $(d+k+1)$ are then determined by computing the angles of the eigenvalues of $F(d+k)$.

From the above, it is shown that based on the assumption that the sinusoidal frequencies are slowly varying with time such that they can be considered approximately constant over a small fraction of time interval, i.e. L time instants in this case, a Hankel matrix constructed directly from the data samples can be approximated by another matrix whose lower rank equals the number of dominant singular values given by the SVD. The instantaneous frequencies of the sinusoids are estimated by the related approach used for the stationary sine waves except that the

observability matrix Θ is partitioned into several smaller matrices. Those small matrices represents the approximately constant sinusoidal frequencies which are regarded as the instantaneous frequencies over that particular short time interval.

5.2 Suppression of Ocean Clutter Signals

The time-varying frequencies in the Khan [7] model for the "Bragg" phenomenon in radar-sensed ocean clutter can be estimated or tracked through the Hankel data matrix rank reduction method. If a signal's frequency can be tracked instantaneously, it will be possible to have the signal suppressed or filtered. Since the instantaneous frequencies of the sinusoids are obtained from the angles of the eigenvalues of $F(k)$, the eigenvalue corresponding to each sinusoid can be regarded as the power of the signal. Thus, a reverse process is developed in such a way that any singular signal, particularly the ocean clutter signal, can be suppressed without affecting the other signals if its associated eigenvalue is removed from $F(k)$. After a new $F(k)$ is calculated, a new partitioned $\tilde{\Theta}new_k$ and a new $\tilde{\Theta}new$ can be estimated accordingly. Consequently, a new Hankel matrix, $Hnew$, will be reconstructed from $\tilde{\Theta}new$. The derivation of the signal suppression process is described below.

The eigenvalue decomposition of the instantaneous feedback matrices $F(k)$ can be represented by

$$F(k)v(k) = \lambda(k)v(k) \tag{5.18}$$

where $\lambda(k)$ are the eigenvalues of $F(k)$ in the form of $diag[\lambda_1, \lambda_2, \lambda_3, \cdots, \lambda_{2r}]$; and $v(k)$ is the corresponding eigenvectors. So as to suppress the clutter signals, the eigenvalues of the signals whose angular positions on the unit circle determine the sinusoids' instantaneous frequencies are first identified by the "Bragg" frequencies and then are zeroed. The new matrix $F(k)$ is computed by the following equation.

$$Fnew(k) = (\lambda new(k)v(k))v'(k) \tag{5.19}$$

where $\lambda new(k)$ is the same as $\lambda(k)$ except that the eigenvalues of the clutter signal are zero. $v'(k)$ is the inverse of $v(k)$. Once the new $F(k)$'s are obtained,

it is possible to estimate the new partitioned matrices $\tilde{\Theta}new_k$ using the following relationship.

$$\tilde{\Theta}new_{k+1} = \tilde{\Theta}_k Fnew(d+k), \quad k = 1, 2, 3, \cdots \tag{5.20}$$

As a result, a new $\tilde{\Theta}new$ can be obtained by concatenating the $\tilde{\Theta}new_k$'s into one matrix, and a new estimated Hankel matrix can therefore be constructed by the relationship of

$$Hnew = \tilde{\Theta}newX \tag{5.21}$$

By inspection of the structure of the Hankel matrix, it will be possible to estimate a new time series data, $\tilde{y}(k)$, from the new Hankel matrix. For example,

$$\begin{aligned} \tilde{y}(1) &= H(1,1) \\ \tilde{y}(2) &= (H(1,2) + H(2,1))/2 \\ \tilde{y}(3) &= (H(1,3) + H(2,2) + H(3,1))/3 \\ &\vdots \end{aligned} \tag{5.22}$$

The new time series data is the one with the clutter components suppressed.

From the above, it has been shown that the first part of the proposed clutter suppression scheme employs the Hankel rank reduction method, a time-varying frequency tracking technique, to track the frequencies of all signals including the ocean clutter and the targets. After identifying the ocean clutter signals from their "Bragg" frequencies, a signal suppression process is derived to remove the signal power of the ocean clutter given as the eigenvalue of the $F(k)$ matrix instantaneously. A reverse but similar process used for estimating the instantaneous frequencies is developed to recreate another reduced rank Hankel matrix from which a data sequence containing only the target signal can be extracted.

Chapter 6

Computer Analysis and Simulation

The performance of the clutter suppression scheme presented in this thesis is tested on both the computer-synthesized and the real HF radar data. In both cases, the received signal from each ocean range cell contains only a single target in addition to the ocean clutter. The size of the range cells in this HF radar is 400 m.

6.1 Computer Simulations and Results

Recently, a HF groundwave radar, operating at a centre frequency of 6.75 MHz, has been built at Cape Race, Newfoundland, Canada. According to Eq. (2.2) and Eq. (2.1), the "Bragg" clutter signals would have Doppler frequencies at approximately ± 0.265 Hz and a characteristic propagation speed of about 5.9 metres per second (m/s). To simulate the ocean clutter signals, two narrowband frequency-modulated sinusoidal signals were synthesized and specified as follows:

$$s_1(t) = \exp[j\phi_1(t)] \tag{6.1}$$

$$s_2(t) = \exp[j\phi_2(t)] \tag{6.2}$$

where

$$\phi_1(t) = 2\pi f_1 t + B_1 \cos(2\pi f_{m1} t + \theta_1) \tag{6.3}$$

$$\phi_2(t) = 2\pi f_2 t + \theta_2 + B_2 \cos(2\pi f_{m2} t) \tag{6.4}$$

where f_1 and f_2 are the center frequencies of the "Bragg" clutter signals and are set to be 0.245 Hz and -0.275 Hz, respectively; B_1, f_{m1}, B_2 and f_{m2} are the parameters of the frequency modulation and their values are selected to be 0.625, 0.08, 0.775 and 0.065, respectively to attain a close approximation to the narrowband characteristic of the ocean clutter signals; θ_1 and θ_2 are some arbitrary phases used to differentiate these two similar signals. The amplitudes of both signals are assumed to be unity. The simulated "Bragg" frequencies are set to be slightly deviated from the theoretical values (± 0.265 Hz) because in reality, the ocean surface currents have effects on the "Bragg" frequencies and cause a small offset between the actual and the theoretical values. The frequencies of the simulated clutter signals were made to fluctuate within the range of ± 0.05 Hz about the center frequencies. This means that the ocean clutter signal would have maximum frequencies of 0.295 Hz and -0.225 Hz; and minimum frequencies of 0.195 Hz and -0.325 Hz, respectively. The instantaneous frequencies, f_{i1} and f_{i2}, of $s_1(t)$ and $s_2(t)$ are defined as the derivatives of their phases with respect to time and are as expressed below.

$$\begin{aligned} f_{i1}(t) &= \frac{d\phi_1(t)}{dt} \\ &= 2\pi f_1 - B_1 2\pi f_{m1} \sin(2\pi f_{m1} t + \theta_1) \end{aligned} \tag{6.5}$$

and

$$\begin{aligned} f_{i2}(t) &= \frac{d\phi_2(t)}{dt} \\ &= 2\pi f_2 - B_2 2\pi f_{m2} \sin(2\pi f_{m2} t) \end{aligned} \tag{6.6}$$

In discrete time representation,

$$s_1(k) = \exp[j\phi_1(k)]$$

$$
\begin{aligned}
s_2(k) &= \exp[j\phi_2(k)] \\
f_{i1}(k) &= (\phi_1(k) - \phi_1(k-1))/T_s \\
f_{i2}(k) &= (\phi_2(k) - \phi_2(k-1))/T_s
\end{aligned} \tag{6.7}
$$

where k refers to the kth sampling instant. A sampling rate of $T_s = 0.5$ second and a data length of 128 samples were used in the simulation. The computer program of the proposed clutter suppression scheme written in MATLAB language is shown in Appendix C. The inputs to the program are the number of columns in the Hankel matrix and the sampling time. The output of the program is the target signal with the ocean clutter suppressed. The program is written based on the specifications of the HF radar built at Cape Race. Some changes in the program's parameters such as the centre frequency of the radar signal may be needed if it is used on a different HF radar system.

6.1.1 Test I

In this test, the proposition that the Hankel matrix H could be approximated to a lower rank matrix by means of Singular Value Decomposition (SVD) was verified under various signal-to-noise ratios (SNR) where the Guassian white noise with zero mean was introduced. The selection of the Guassian white noise for the simulation is based on the Central Limit Theorem. Three SNR's were considered. They were SNR = ∞ (noiseless), SNR = 20 dB and SNR = 10 dB. First of all, a quick check was done to confirm that the rank of H is determined by the number of the principal singular values which correspond to the number of complex sinusoids whose angular frequencies are time invariant in the received signal in a noiseless condition. Let the received signal, $y(k)$, consist of two stationary sine waves with constant frequencies, f_1 and f_2.

$$
y(k) = \exp[j(2\pi f_1 k)] + \exp[j(2\pi f_2 k)], \quad k = 1, 2, \cdots, 128 \tag{6.8}
$$

Singular Value	SNR = ∞	SNR = 20 dB	SNR = 10 dB
σ_1	22.0124	22.0276	22.1969
σ_2	16.4261	16.4469	16.6740
σ_3	0	0.8030	3.8125

(a)

Singular Value	SNR = ∞	SNR = 20 dB	SNR = 10 dB
σ_1	27.6287	27.7624	27.8828
σ_2	21.8801	22.0022	22.1511
σ_3	0	0.7946	3.4650
σ_4	0	0.7522	3.2832
σ_5	0	0.7120	3.2391

(b)

Table 6.1: The singular values of H consisting of stationary sine waves at SNR = ∞, 20 dB and 10 dB: (a) $L = 3$, (b) $L = 5$

The singular values of H of two different sizes, in which the number of columns of H, L, equals 3 and 5 as examples, at three different noise levels, are shown in Table 6.1 (see Appendix B for the computation of the singular values of a matrix).

From Table 6.1, it is noticed that there are only two nonzero singular values corresponding to the number of complex sinusoids in the ideal situation where no noise is present, and the other singular values are zero regardless of the size of H. This indicates that H has a rank of 2. With noise introduced, the Hankel matrix H is perturbed. The two largest singular values represent most of the signal power while the remaining ones are no longer nonzero and represent the noise.

If the sinusoidal frequencies are time-varying, H will be full rank even without the presence of noise. The received signal now contains the two frequency-modulated signals, $s_1(k)$ and $s_2(k)$, as specified in Eq. (6.7). Table 6.2 contains the singular values of H at three different SNR's with examples of $L = 3$ and $L = 5$.

Singular Value	SNR = ∞	SNR = 20 dB	SNR = 10 dB
σ_1	21.9756	21.8466	22.0128
σ_2	16.3891	16.3180	16.5076
σ_3	1.2874	1.4936	5.0166

(a)

Singular Value	SNR = ∞	SNR = 20 dB	SNR = 10 dB
σ_1	27.1652	27.1028	27.9537
σ_2	21.8362	21.8028	22.5712
σ_3	4.9093	4.9540	6.2166
σ_4	1.5755	1.8088	3.7730
σ_5	0.1583	0.7901	3.2318

(b)

Table 6.2: The singular values of H consisting of time-varying sine waves at SNR = ∞, 20 dB and 10 dB: (a) $L = 3$, (b) $L = 5$

Again, all the singular values in Table 6.2 are nonzero and that indicates H being full rank. Although H is full rank, it is quite clear that there are still two dominant singular values corresponding to the sinusoids. As the noise level increases, the gap between σ_2 and σ_3 gets closer because more noise is distributed among those less dominant singular values. This effect can be seen in both Tables 6.1 and 6.2. At very low SNR, it is noticeable that the above proposition will produce quite significant errors. It will be difficult to distinguish between the signal and the noise subspaces because the singular values are not split into two distinctive groups. Thus, an acceptable and useful low rank approximation of H will depend on where the SNR threshold level is set. As far as the simulation is concerned, SNR = 10 dB is considered as the worst case. This 10 dB threshold level is quite representative of the real situations but it does not include some special cases such as when one of the "Bragg" peaks is driven into the noise floor by sustained winds along the beam. Further work is needed for those cases.

6.1.2 Test II

The estimation of the instantaneous frequencies of the sinusoids was evaluated in this test. A single sinusoid with time-varying frequency, $s_1(t)$, as given in Eq. (6.1), was first used to test the Hankel rank reduction method. Fig. 6.1 shows the actual and the estimated instantaneous frequencies of $s_1(t)$ in a noiseless environment. The form of the estimated instantaneous frequencies are mapped onto the actual one given by Eq. (6.5). The slight difference in their amplitudes can be accounted for by the assumption that the frequencies are considered approximately constant over a certain period of time. This assumption is valid only if the frequencies are changing significantly slowly with time. The clutter signals can be identified by their "Bragg" frequencies which would approximately agree with the average values of the instantaneous frequencies. Similarly, the average values of the close estimated instantaneous frequencies can be utilized to identify the clutter signals. Two noisy cases, at SNR = 20 dB and SNR = 10 dB, were then considered. The estimated instantaneous frequencies of $s_1(t)$ in both noisy environments are shown in Fig. 6.2 and Fig. 6.3. Although the amplitude of the estimated instantaneous frequencies in both noisy cases were distorted, their forms were preserved even in the worst case, i.e. SNR = 10 dB (see Fig. 6.3). An average value of the instantaneous frequencies near to the "Bragg" frequencies could be obtained. It should be pointed out that the original frequency in the above Figures is computed from Eq. (6.5).

6.1.3 Test III

In addition to the simulated clutter signals, a third sinusoidal signal, $s_3(t)$, regarded as a single target with a constant Doppler frequency of 0.5 Hz moving towards the radar site at a velocity of 11.1 m/s, was added. The number of data samples used in this test is also 128. Fig. 6.4 shows the power density spectrum

of the received signal that contains $s_1(k)$, $s_2(k)$ and $s_3(t)$. The power spectrum was computed by fast Fourier transform (FFT). To suppress the clutter signals, the instantaneous frequencies of the clutter signals were first tracked by using the Hankel reduction method and were then identified. Another reduced rank Hankel matrix with the frequency components of the clutter signals removed was constructed by the procedures discussed in section 5.2 and a new time series data was estimated. Fig. 6.5 compares the power spectra of the original received signal and the one with the clutter signals suppressed in a noiseless case. About 20 to 30 dB clutter level were suppressed. Subsequently, noise was taken into consideration in the testing process. The resultant power spectra of the signal before and after the clutter suppression process in the noisy cases at SNR = 20 dB and SNR = 10 dB are shown in Fig. 6.6 and Fig. 6.7, respectively. In both Figures, a level of 10 to 20 dB clutter was suppressed.

There is always a limit as to how close two frequencies can be so that they can be resolved by the frequency estimation method. In this clutter suppression scheme, the limit of the closeness between the Doppler frequency of the target and the "Bragg" frequencies of the ocean clutter where the target signal will not be affected during the clutter suppression process was examined. It is experimentally found that if the target's Doppler frequency has a space of less than 0.09 Hz from that of the ocean clutter, the scheme has difficulty in tracking the frequencies of the ocean clutter signals as well as the target signal. The experiment was conducted in such a way that the target's Doppler frequency was varied to be close to the "Bragg" frequencies until the scheme failed to track both frequencies properly. This experimentally found value, 0.09 Hz, is close to the modulation frequency, $f_{m1} = 0.08$ Hz. This suggests that if the target's Doppler frequency is very close to the second-order scattering peaks, which can be interpreted as the contribution from the modulation frequency in the clutter signal, then the suppression process

will be affected.

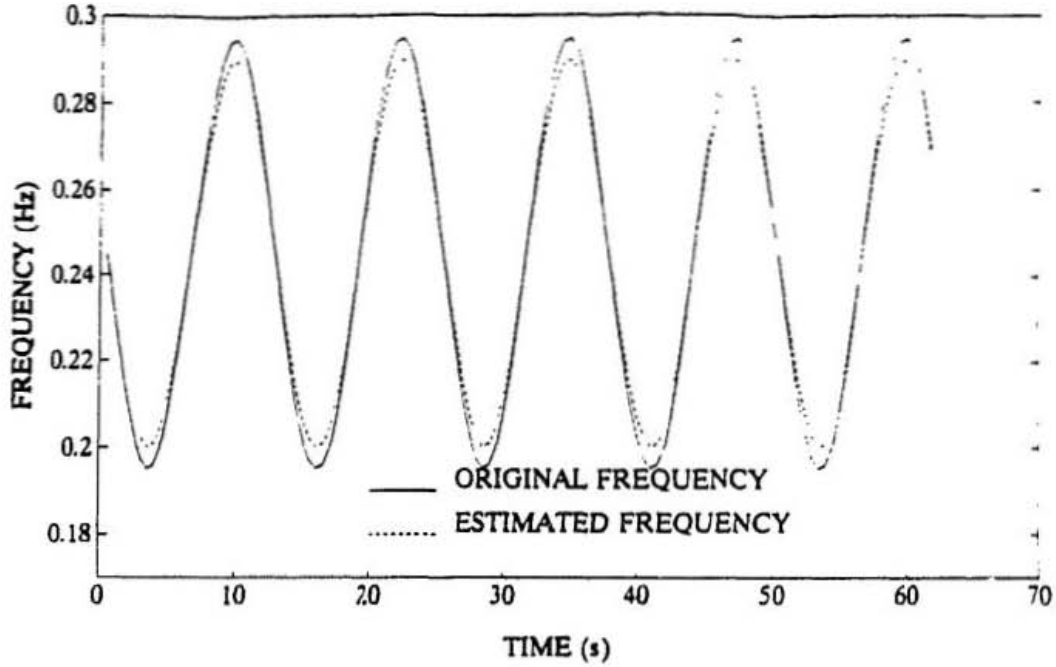

Figure 6.1: Instantaneous frequencies of $s_1(t)$ in noiseless case

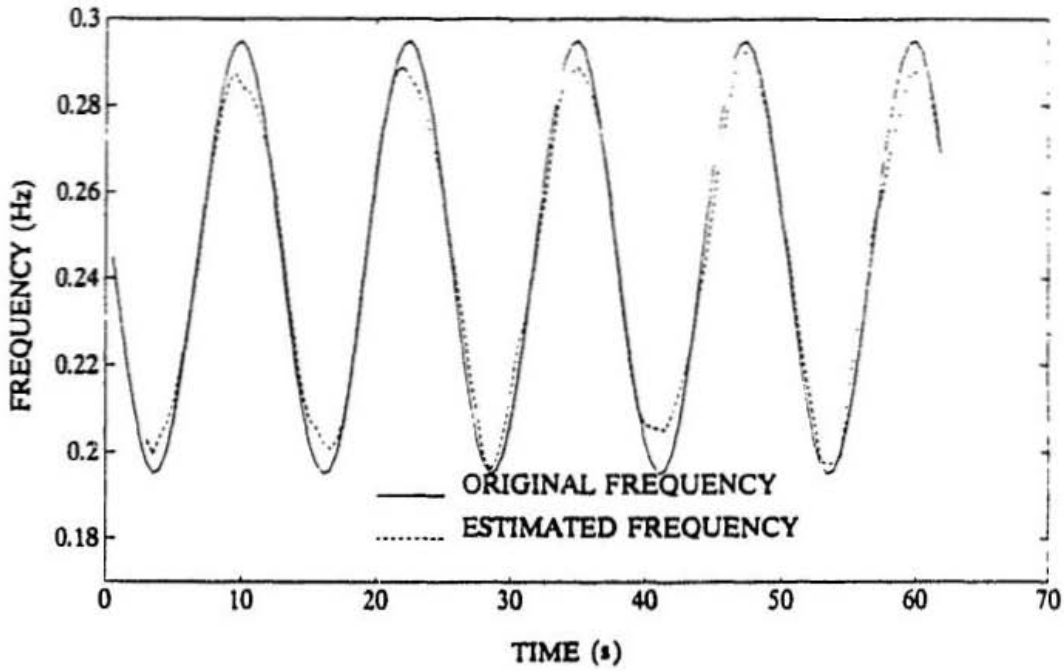

Figure 6.2: Instantaneous frequencies of $s_1(t)$ at SNR = 20 dB

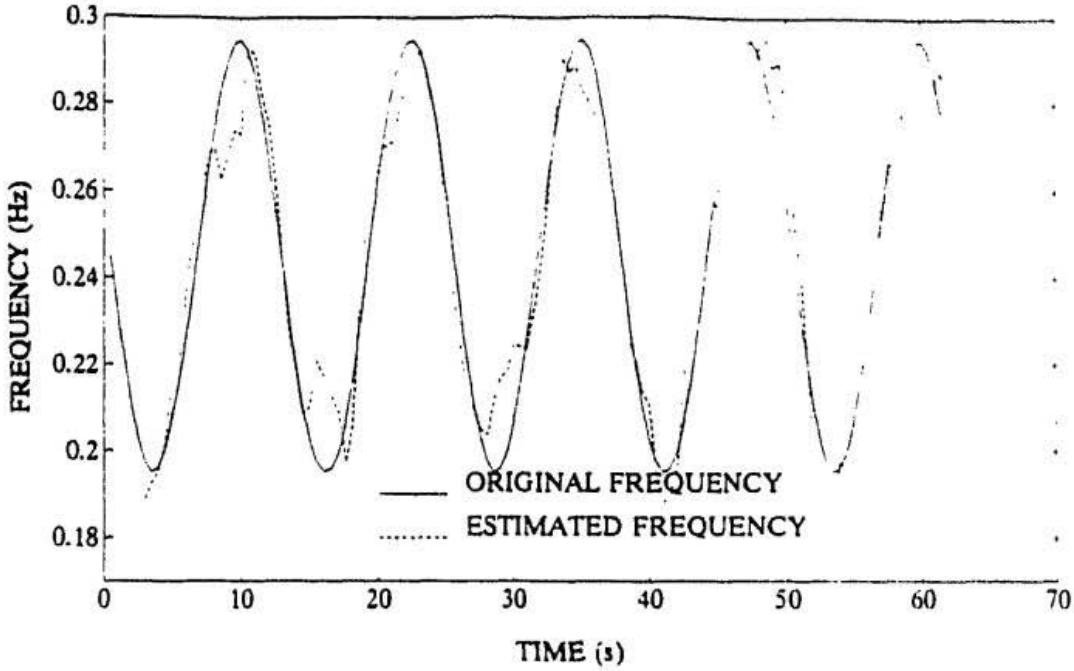

Figure 6.3: Instantaneous frequencies of $s_1(t)$ at SNR = 10 dB

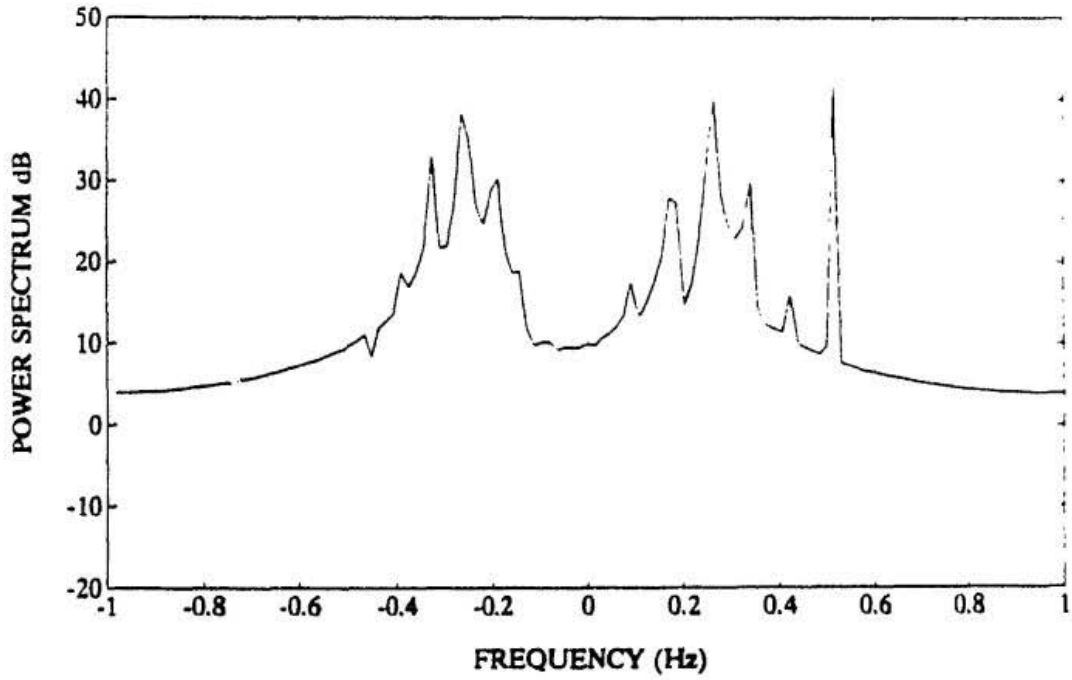

Figure 6.4: Power spectrum of $s_1(t) + s_2(t) + s_3(t)$

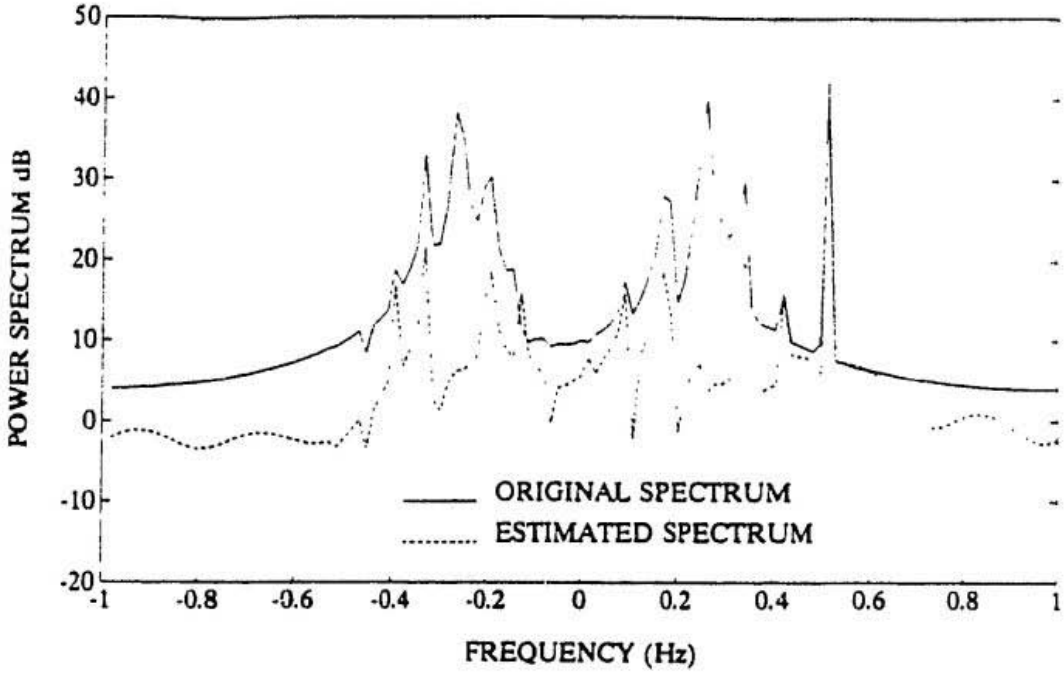

Figure 6.5: Suppression of ocean clutter in noiseless case

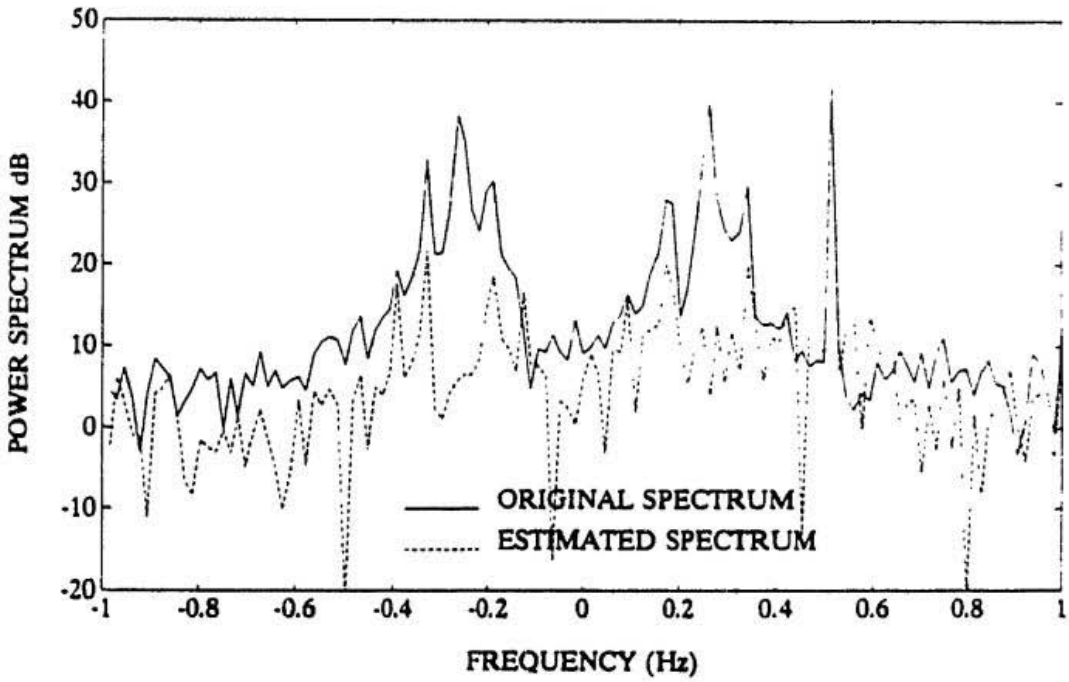

Figure 6.6: Suppression of ocean clutter at SNR = 20 dB

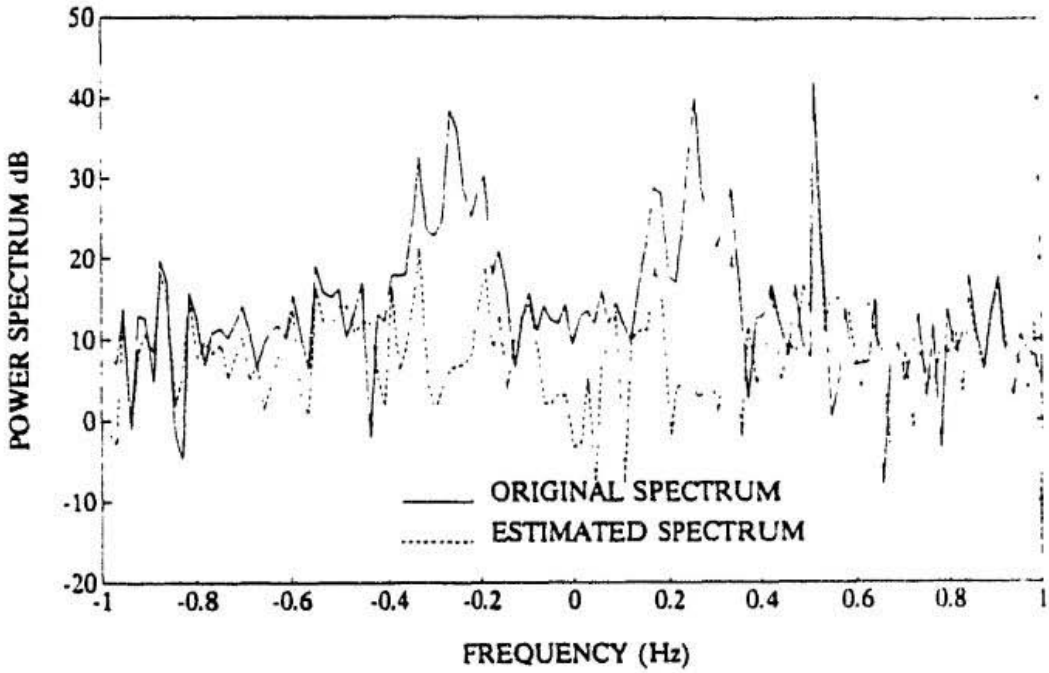

Figure 6.7: Suppression of ocean clutter at SNR = 10 dB

6.2 Real HF Radar Data Testing

Computer simulations have shown that a substantial level of the clutter signals can be suppressed by the proposed clutter suppression scheme. Now, real HF radar data will be used to examine the scheme's performance. A single ship which was moving at various velocities away from the radar site was detected. The ship's movement was continuously monitored by the radar. The echoes from the ocean consisted of three sinusoidal signals - one corresponding to the ship and the other two corresponding to the ocean clutter signals. The signal received from each range cell has 512 data samples at a sweeping rate of 0.601 second. The data samples are complex-valued. During the testing process, the 512 samples were divided into 4 segments which represent four different periods of the recorded time so that the movement of the target within each range cell could be examined along the time of observation. Therefore, there were 128 samples used in each test run. It is preferable to have the whole data record divided into more shorter segments so that the target's movement can be better monitored. However, too short data record may not provide adequate Doppler resolution for target discrimination. In this test, a data record of 128 samples was found to be short enough to provide sufficient Doppler resolution.

Two test trials were conducted to track the locations of the ship at different ranges. Also, owing to the fact that the longer the distance, the higher the propagation loss will be, different reflection signal strengths result. Therefore, the capability of the clutter suppression scheme to deal with two different target signal strengths were tested in those two trials. The Doppler spectrum from each data segment of the range cells was obtained simply by using a FFT, and it was used to detect the ship and to estimate its radial velocity. The tests described in the following sections compare the signals before and after the clutter suppression

process in the frequency domain and the time domain at different ranges. In the frequency domain, the energy of the reflected signal from the ship will be shown as the power spectrum whereas the time series of the ship signal will be expressed by the value of its real part (note that the radar data is complex-valued). The real part and the imaginary part of the ship signal are similar except for the phase shift, and the time series behaviour of the signal can be sufficiently shown by the values of its real part alone. In each test case, data from three adjacent range cells were investigated simultaneously because it would help locate the correct position of the target by looking at the relative magnitudes of the return energy of the target among those adjacent range cells. In reality, the clutter suppression process is continuous; but this is not an on-line testing. Three range cells are selected only for the purpose of testing.

6.2.1 Test Case I

At time 15:18:05, the ship was observed at the ranges of 70.4 km, 70.8 km and 71.2 km by means of Doppler detection. Fig. 6.8 (a) to (d) show the Doppler spectra of four different segments of the data record before and after the clutter suppression process at the range of 70.4 km. In Fig. 6.8 (a), three peaks are noticed. The one in the middle represents the reflection signal from the ship, and the other two are from the ocean clutter with a characteristic propagation speed of about 5.96 m/s or a Doppler frequency of about $\pm$ 0.265 Hz. This result agrees with that in the simulation. The ship has a negative radial velocity of about 3 m/s as inferred from the Doppler spectra. The negative sign indicates that the ship was moving away from the radar site. It is noted that not only the first-order but also the second-order scattering from the ocean surface were suppressed. This result confirmed that the ocean clutter can be closely modelled by two narrowband frequency-modulated sinusoidal signals. Among the four power spectra in Fig. 6.8, a progressive decrease

in the magnitudes of the target's energy was observed whereas the magnitude of the clutter's energy stayed almost the same throughout the whole data length. The target signal appeared to have magnitudes of about 1 dB, -7 dB, -10 dB and -12 dB in those four segments, respectively. This scenario showed that the target was moving towards farther range cells. Moreover, the average radial velocity of the target among those four segments was slightly different.

The data from the range of 70.8 km was tested next. The resultant power spectra of the four data segments with and without the clutter signals are depicted in Fig. 6.9 (a) to (d). The magnitudes of the target's energy in all four segments exhibited a relatively higher level than those at range 70.4 km. This implies that the target was likely at range 70.8 km rather than at range 70.4 km during some times of observation. The movement of the target could be described by the magnitudes of its return energy. The magnitude of the target's return energy in the second segment (see Fig. 6.9 (b)) displayed a maximum in relation to the other three. It means that the target was at the range of 70.8 km around sometime during the second quarter of the recorded time.

A similar test was run on the data from the range of 71.2 km. A progressive increase in the magnitudes of the target's return energy was shown among the power spectra of the four data segments as in Fig. 6.10 (a) to (d). A maximum magnitude appeared in the last one segment (Fig. 6.10 (d)). The plots demonstrated that the target was moving into range 71.2 km during the last quarter of the recorded time. A substantial level of clutter suppression is noticed among these three tests, and is approximately quantified in Table 6.3. An average relative level of 30 dB clutter suppression is obtained.

The real part of the time series of the raw radar data including the target and the clutter signals collected from range 70.4 km is shown in Fig. 6.11 (a). A fine sine wave representing the target signal extracted from the raw radar data is shown

	Data Segment							
	1:128		129:256		257:384		385:512	
Range (km)	$-f_{oc}$	$+f_{oc}$	$-f_{oc}$	$+f_{oc}$	$-f_{oc}$	$+f_{oc}$	$-f_{oc}$	$+f_{oc}$
70.4	20	30	30	40	35	40	40	45
70.8	25	30	20	30	20	25	25	35
71.2	25	40	25	30	25	30	25	30

Table 6.3: A summary of the relative quantification of the clutter suppression (in dB) in the range cells: 70.4 km, 70.8 km and 71.2 km at four different periods of the observation time (where $\pm f_{oc}$ are the "Bragg" frequencies)

in Fig. 6.11 (b). A progressive decrease in the magnitude of the target's return energy is also observed in that Figure. Fig. 6.12 (a) and (b) compare the time series of the target signal with and without the ocean clutter at the range of 70.8 km. At this range cell, the sine wave of the return signal from the target, as shown in Fig. 6.12 (b), appeared to be stronger as compared to that at range 70.4 km and persisted for a quite long period of time. The comparison between the time series of the target signal with and without the ocean clutter at range 71.2 km are depicted in Fig. 6.13 (a) and (b). The sine wave of the target in Fig. 6.13 (b) showed a progressive increase in its amplitude and had a maximum at nearly the last quarter of the recorded time. Comparing the time series of the target signal among those three range cells leads to the conclusion that the ship was at the range of 70.8 km during most of the recorded time and was leaving the range cell of 70.8 km and heading towards the range cell of 71.2 km during the last quarter of the time. The interpretation of the plots of the ship's movement bears a good agreement with the available but limited ground-truthing data [35].

In this test case, a good quality target signal was successfully extracted from the received radar data. Table 6.4 presents a summary of the relative magnitudes of the return energy of the ship's signal in the above three range cells at different periods of the observation time.

	Data Segment			
Range (km)	1:128	129:256	257:384	385:512
70.4	1	-7	-10	-12
70.8	4	5	-1	3
71.2	-12	-2	2	6

Table 6.4: A summary of the relative magnitudes of the return energy from the ship (in dB) in the range cells: 70.4 km, 70.8 km and 71.2 km at four different periods of the observation time

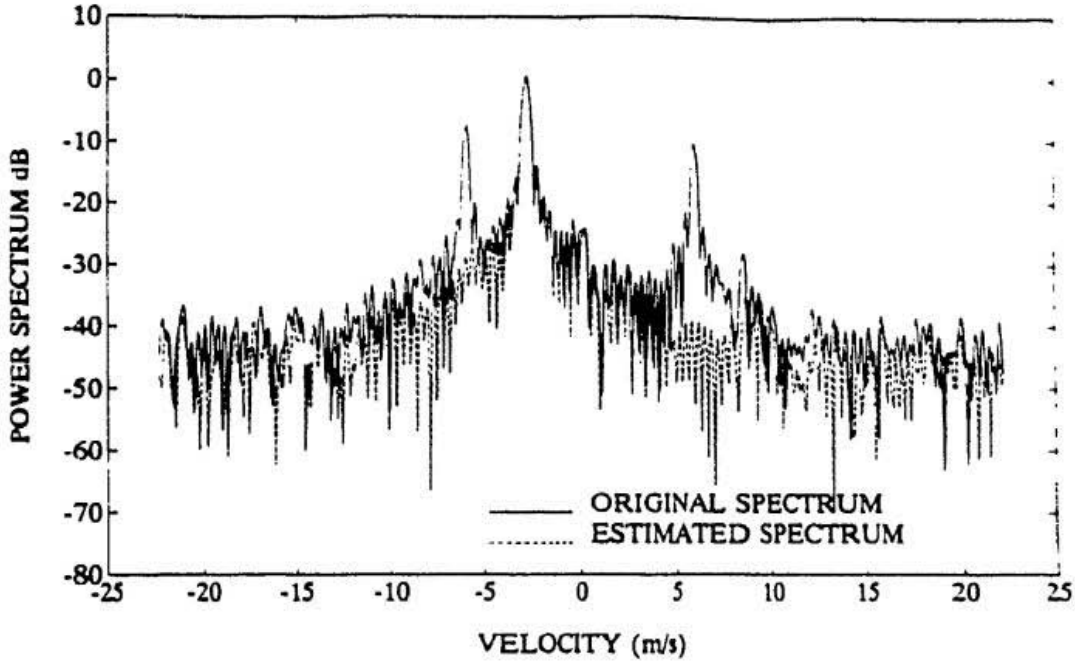

(a)

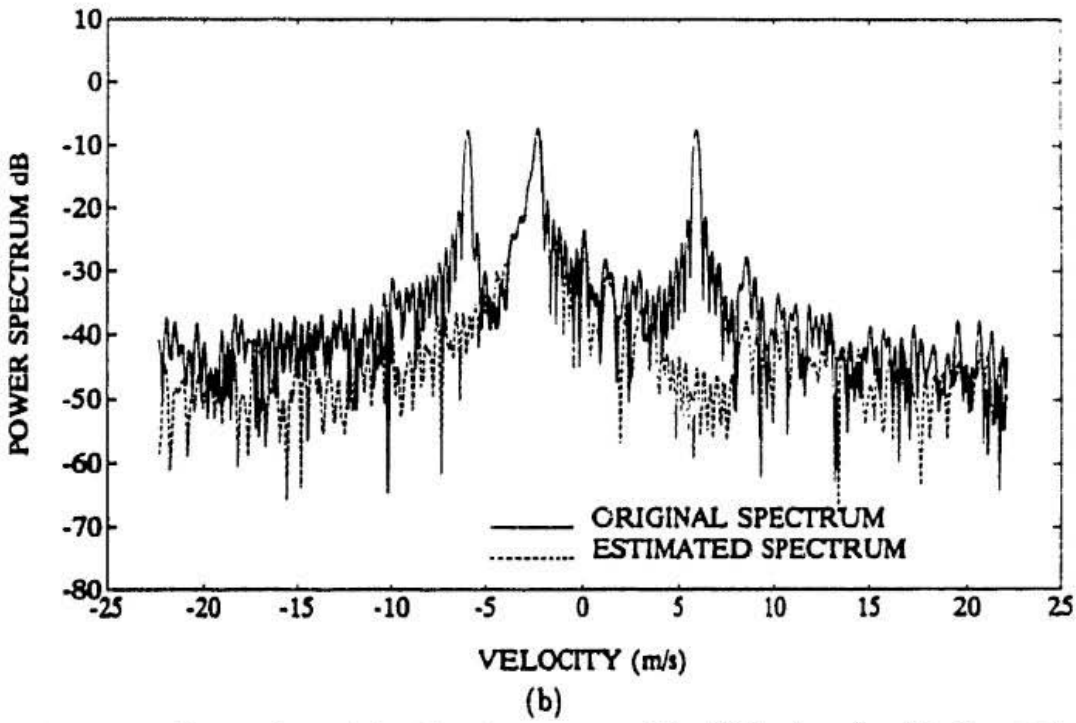

(b)

Figure 6.8: Comparison of the Doppler spectra of the HF radar signal before and after the clutter suppression process at range of 70.4 km: (a) data sample length = 128 (1:128); (b) (129:256); (c) (257:384); (d) (385:512)

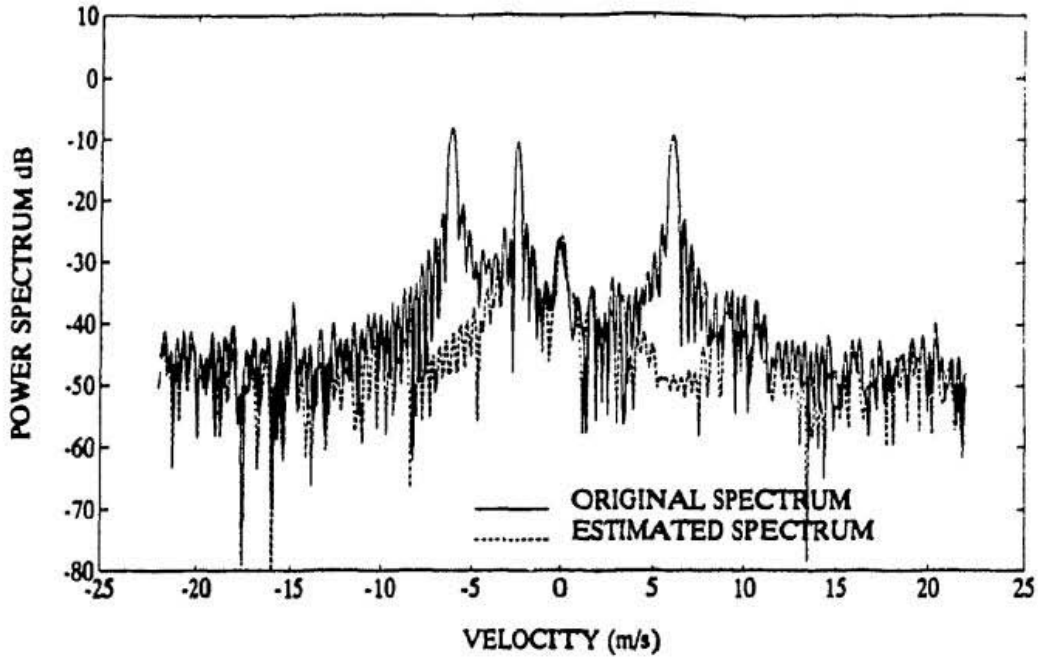

(c)

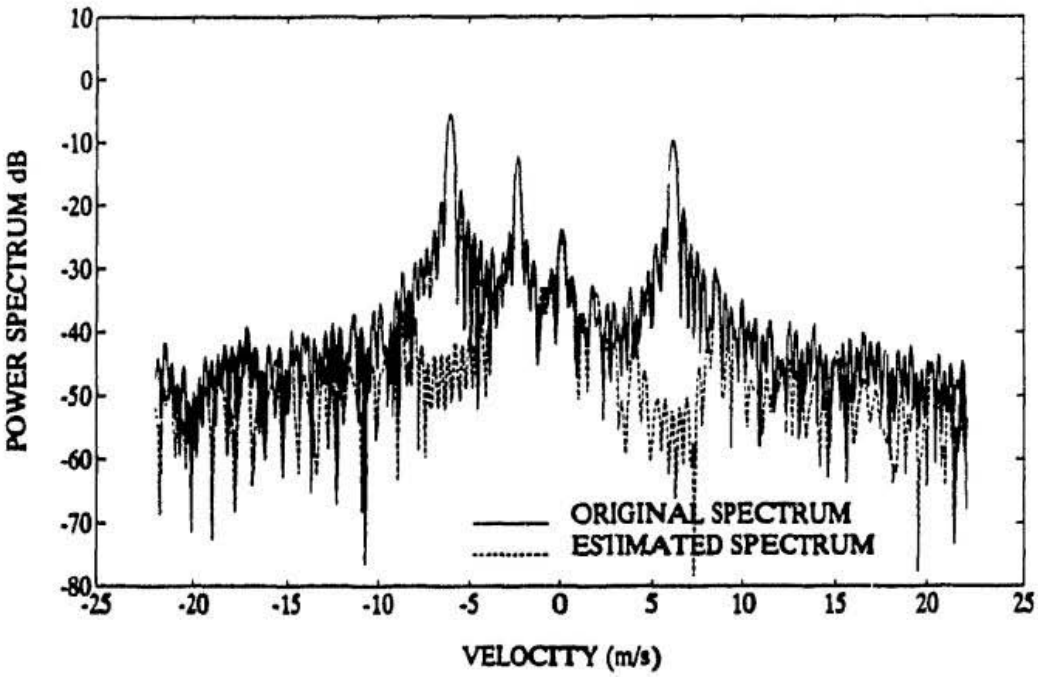

(d)

Figure 6.8 (cont'd)

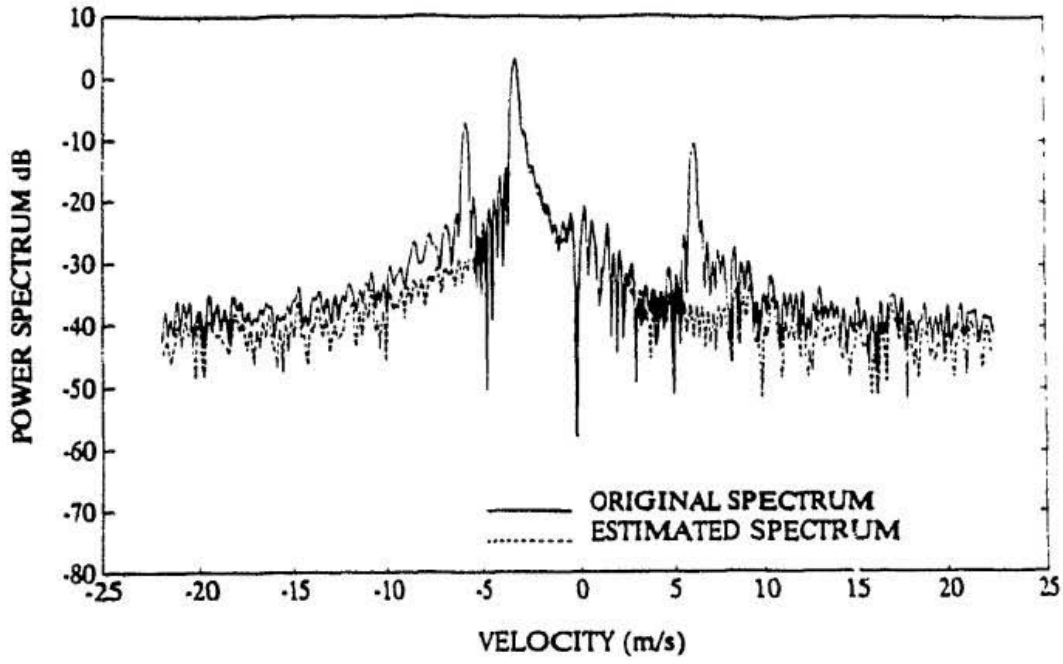

(a)

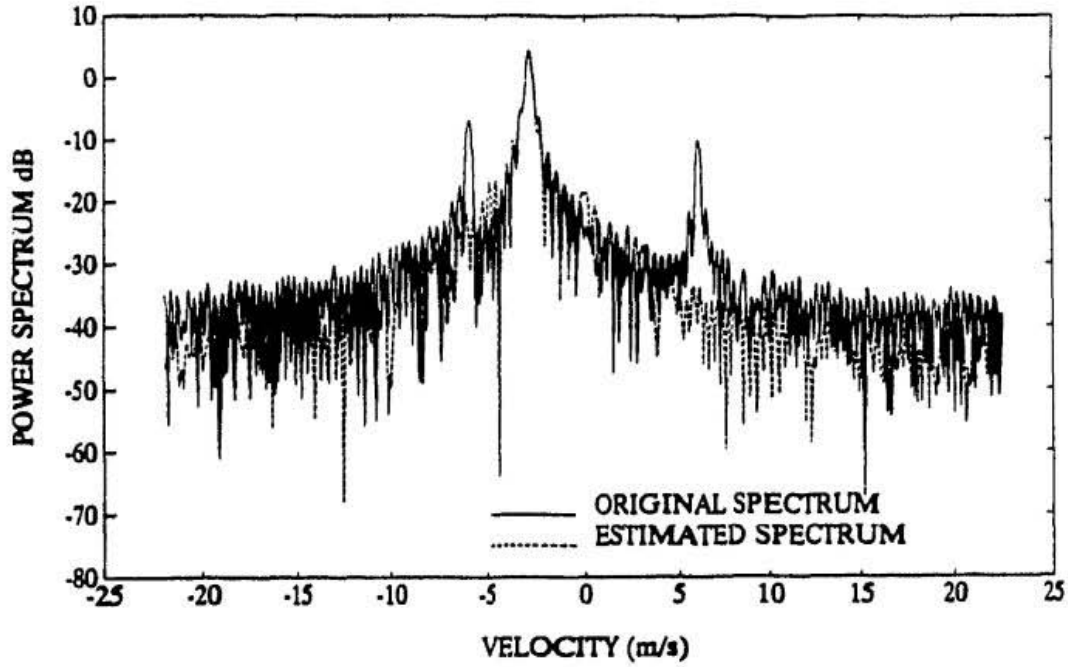

(b)

Figure 6.9: Comparison of the Doppler spectra of the HF radar signal before and after the clutter suppression process at range of 70.8 km: (a) data sample length = 128 (1:128); (b) (129:256); (c) (257:384); (d) (385:512)

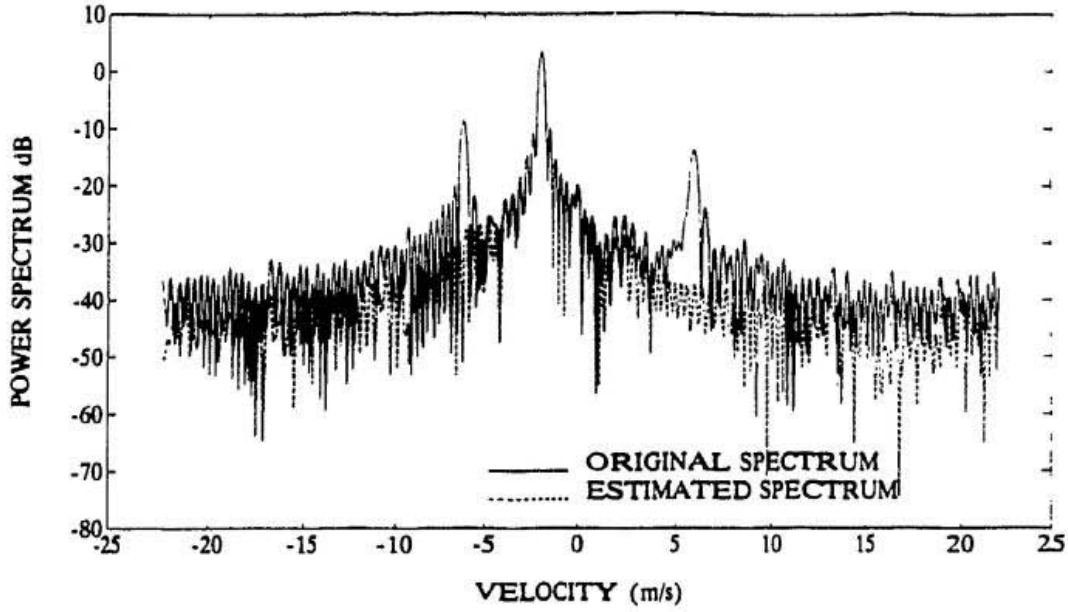

(c)

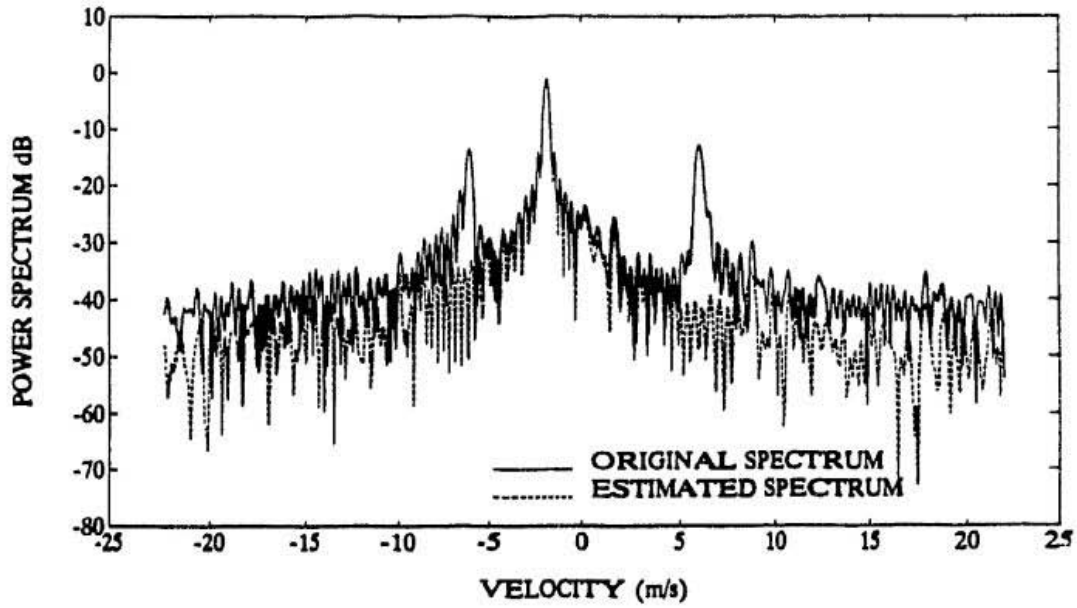

(d)

Figure 6.9 (cont'd)

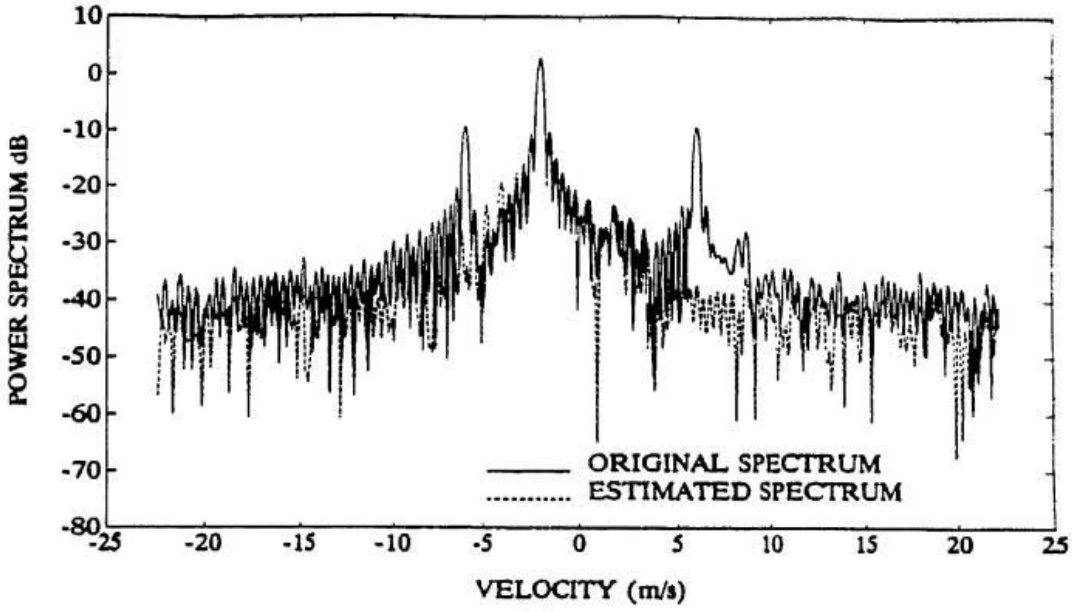

(c)

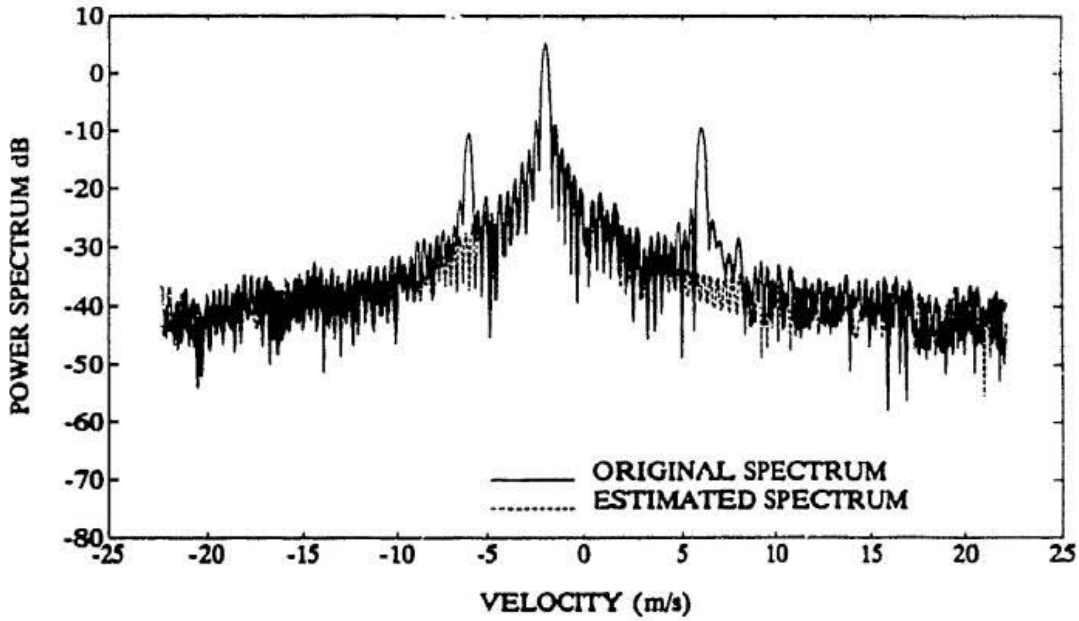

(d)

Figure 6.10 (cont'd)

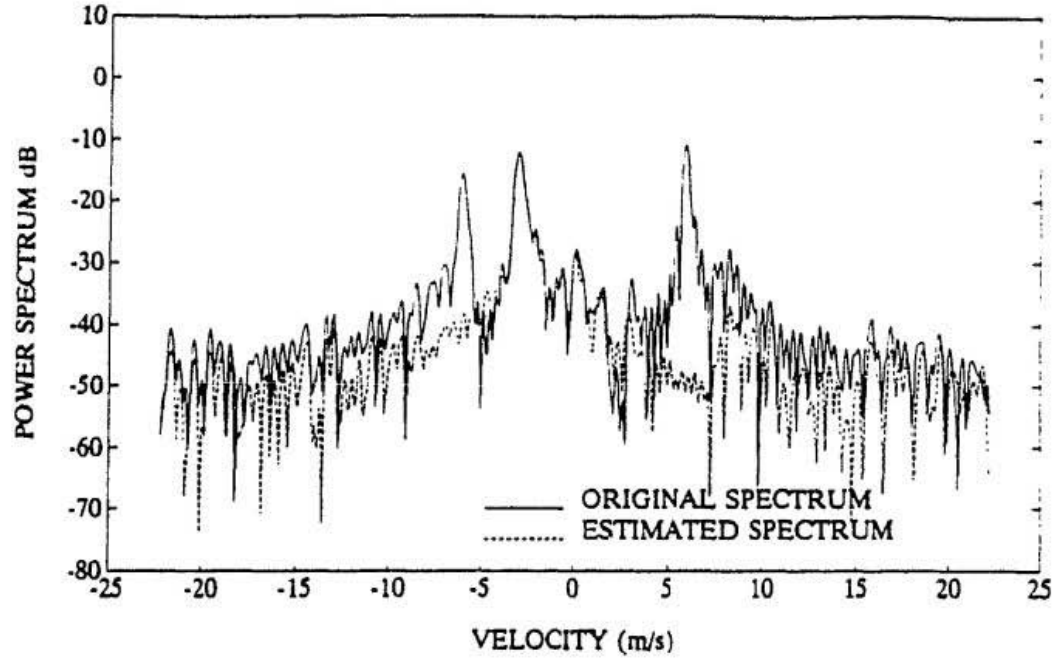

(a)

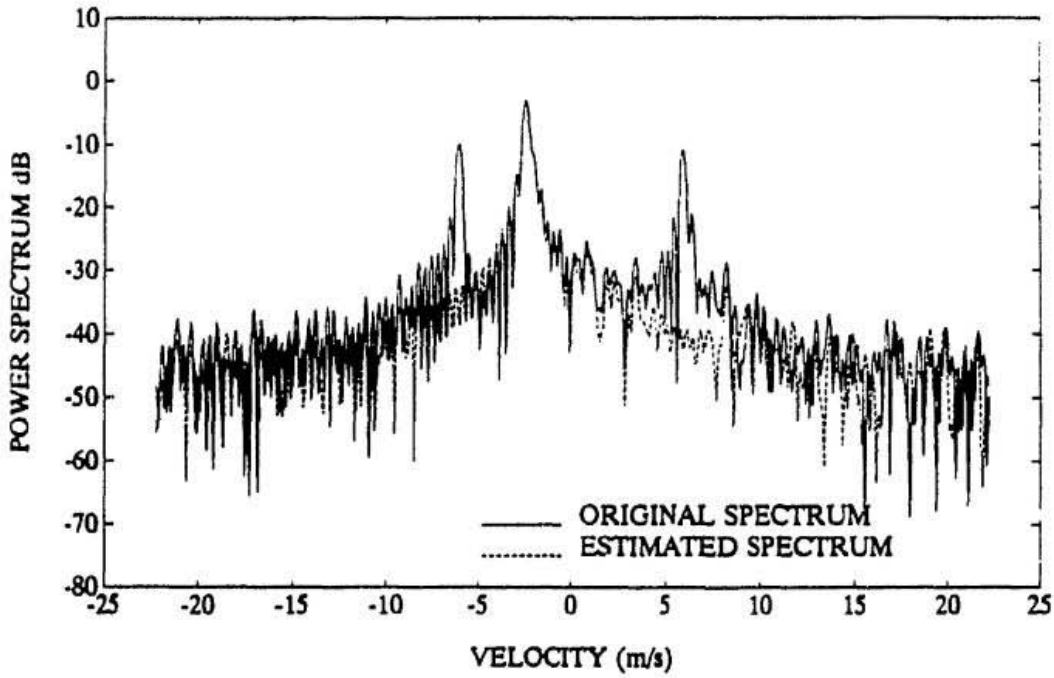

(b)

Figure 6.10: Comparison of the Doppler spectra of the HF radar signal before and after the clutter suppression process at range of 71.2 km: (a) data sample length = 128 (1:128); (b) (129:256); (c) (257:384); (d) (385:512)

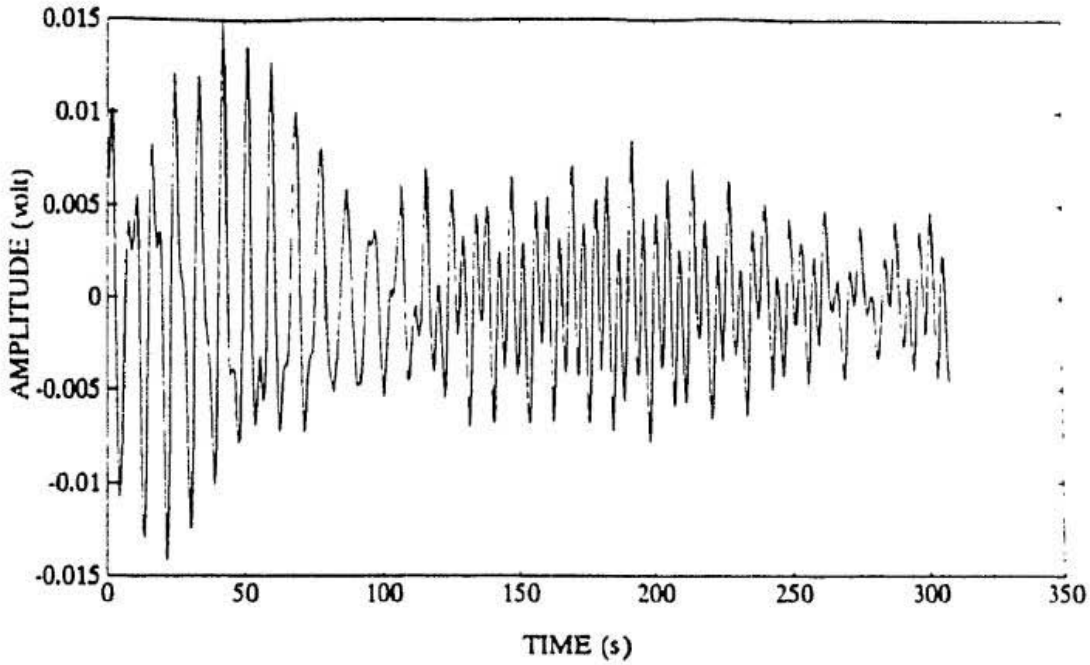

(a)

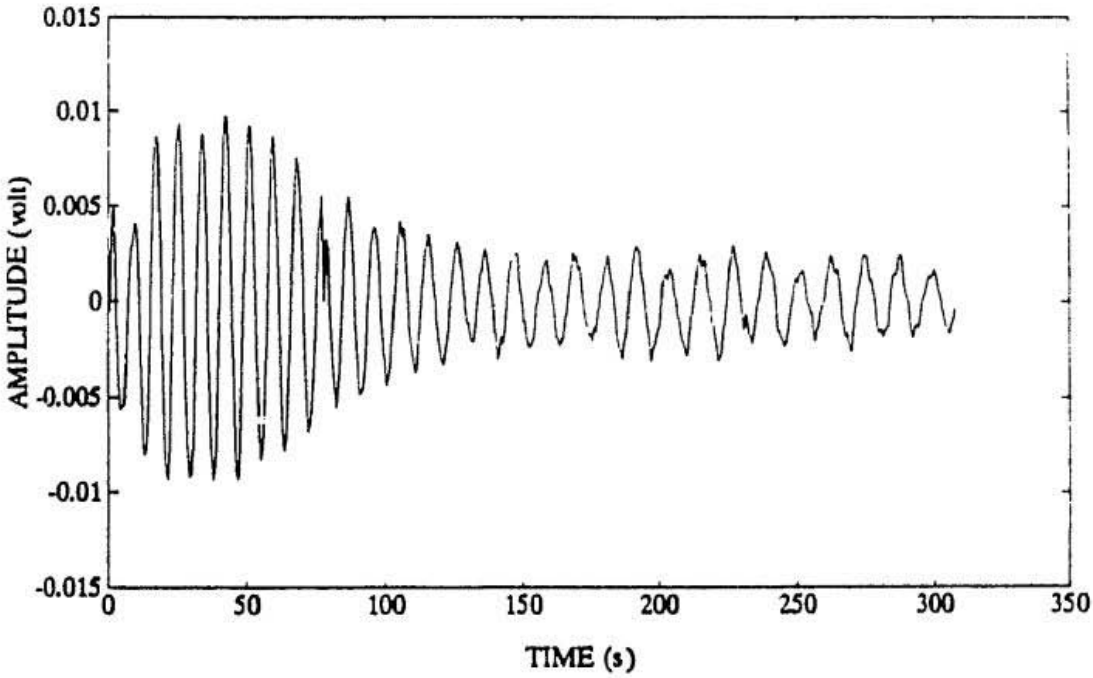

(b)

Figure 6.11: Comparison of the time series of the ship signal at range of 70.4 km: (a) original HF radar signal; (b) ship signal after suppression of ocean clutter

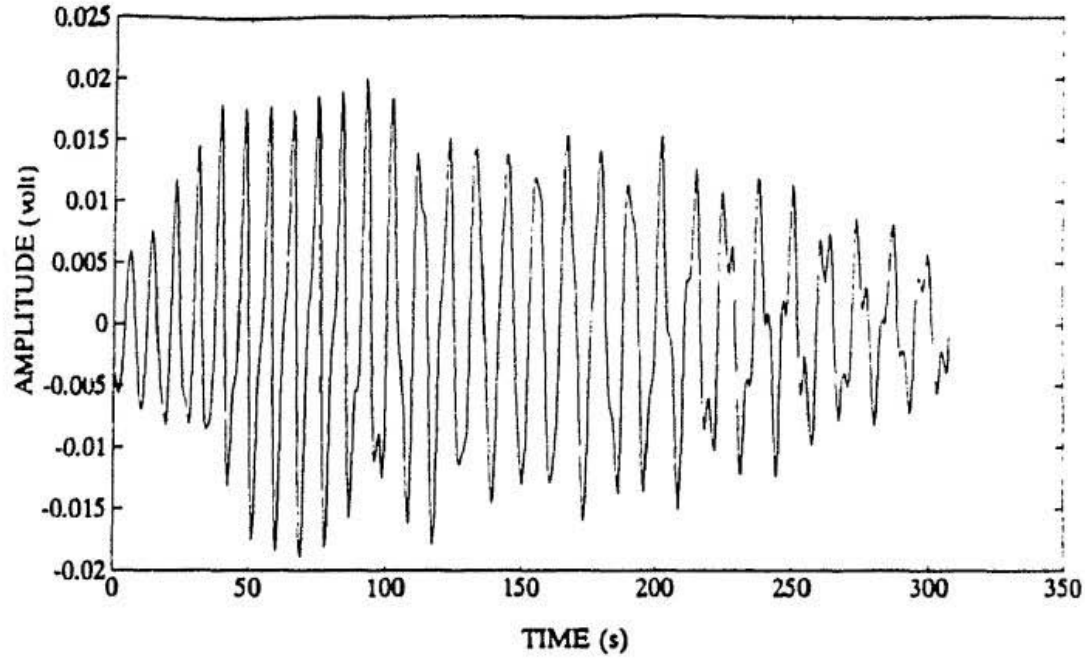

(a)

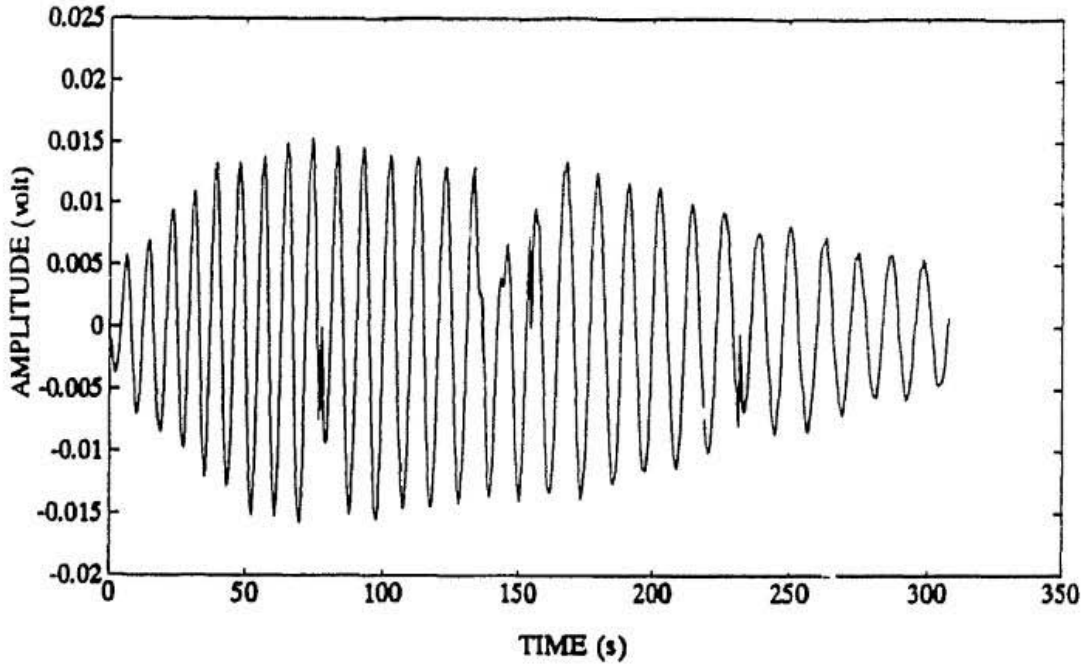

(b)

Figure 6.12: Comparison of the time series of the ship signal at range of 70.8 km: (a) original HF radar signal; (b) ship signal after suppression of ocean clutter

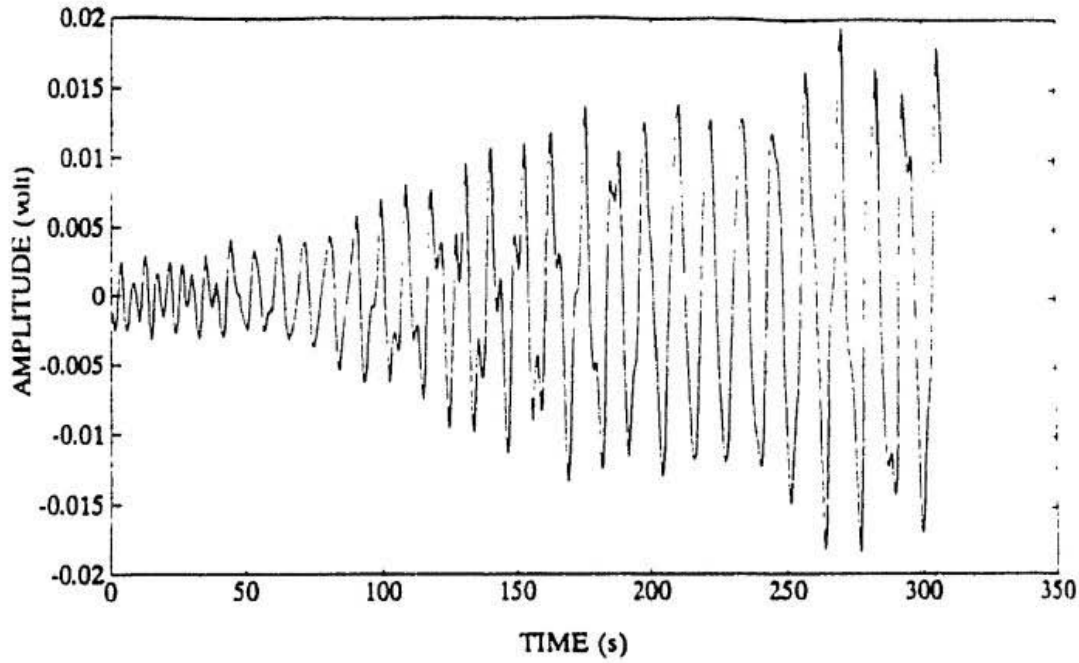

(a)

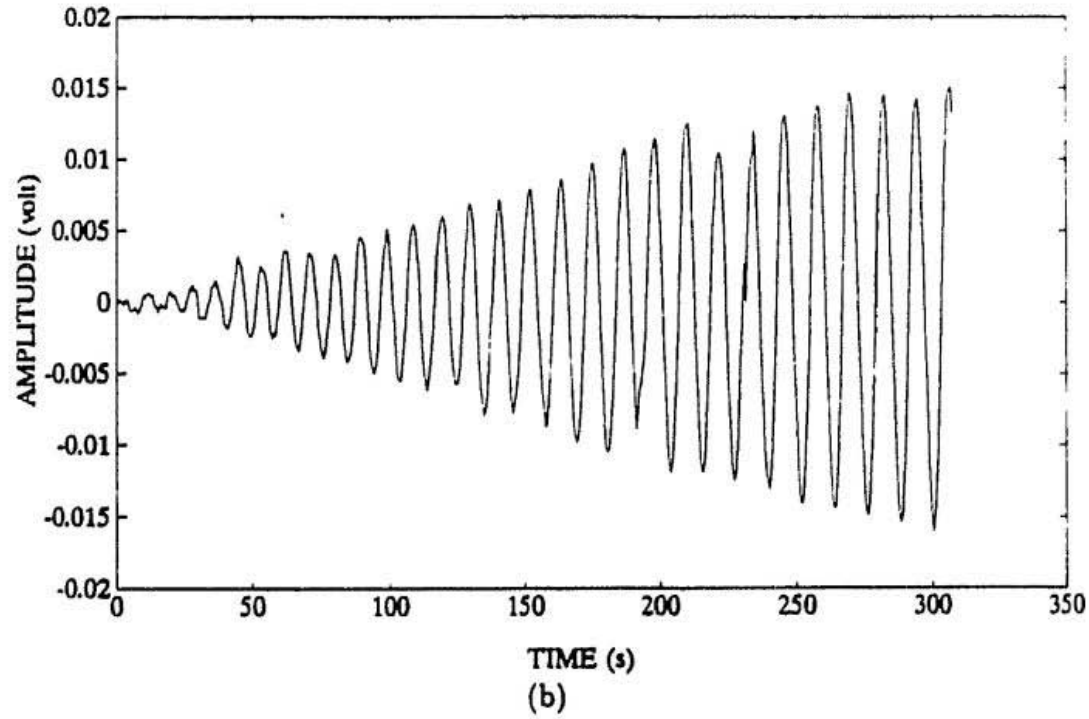

(b)

Figure 6.13: Comparison of the time series of the ship signal at range of 71.2 km: (a) original HF radar signal; (b) ship signal after suppression of ocean clutter

6.2.2 Test Case II

At time 16:24:56, the ship was detected at the ranges of 88.4 km, 88.8 km and 89.2 km. As the ship was at farther distances, its return signal was expected to be weaker. At the range of 88.4 km, the ship had a negative radial velocity of about 7.5 m/s. Since the ship was moving at a faster speed than in the previous case, a fairly quick progressive fading of the ship target's signal was observed in the Doppler spectra as shown in Fig. 6.14 (a) to (d). In Fig. 6.14 (a), three dominant peaks are noticed. The two peaks at velocities of about $\pm$ 5.9 m/s represent the return signals from the ocean waves. The third one at velocity of about -7.5 m/s indicates backscatter from the ship. The magnitude of the target return energy is smaller overall compared to the previous cases. The data from the next range cell, i.e. 88.8 km, in Fig. 6.15 (a) to (d) presents similar Doppler spectra but with stronger signal energy. Fig. 6.15 (a) displays a maximum magnitude of the target signal's energy while Fig. 6.15 (d) shows no target signal. The target observed in the last range cell, 89.2 km, exhibits the strongest signal level as compared to those in the other two cells. This can be seen from the Doppler spectra in Fig. 6.16 (a) to (d).

The power spectra of the data record provide a means of analyzing the movement of a target. A similar analysis can be done by looking at the time series of the target signal. Also the time series will provide a better indication of the ship's location during the time of observation. Since there is not much target signal in the data record from the range of 88.4 km, only a very short duration of sine wave is seen in Fig. 6.17 (b) where Fig. 6.17 (a) is the time series of the original data. The time series of the target signal at the range of 88.8 km shown in Fig. 6.18 (b) gives a better sine wave as compared to that at range 88.4 km, and the original time series is shown in Fig. 6.18 (a). According to the ship's speed, it would

	Data Segment							
	1:128		129:256		257:384		385:512	
Range (km)	$-f_{oc}$	$+f_{oc}$	$-f_{oc}$	$+f_{oc}$	$-f_{oc}$	$+f_{oc}$	$-f_{oc}$	$+f_{oc}$
88.4	20	30	25	35	20	40	25	40
88.8	25	35	30	35	30	50	40	40
89.2	25	30	25	40	35	40	40	40

Table 6.5: A summary of the relative quantification of the clutter suppression (in dB) in the range cells: 88.4 km, 88.8 km and 89.2 km at four different periods of the observation time (where $\pm f_{oc}$ are the "Bragg" frequencies)

take about 53.3 seconds for the ship to travel across a range cell of width 400 m. The time series of the ship signal at range 89.2 km in Fig. 6.19 (b) shows a quite steady sine wave, without much amplitude variation, for 50 to 60 seconds and a rather complex time series that contains the ocean clutter and the target signals is illustrated in Fig. 6.19 (a). This shows that the time series of the target signal can be used as an alternative to analyze the target's movement. The correct position of the ship is found to be at the range of 89.2 km during the time of observation. Again, the ground-truthing data agrees with the results inferred from the plots.

In this test case, although the return signal of the ship appeared to be weaker because of the farther distance when compared to the previous cases, the clutter suppression scheme worked well and extracted a good quality target signal from the received data. Moreover, the ocean clutter was suppressed again by an average relative level of 33 dB as observed from Table 6.5. Table 6.6 contains a summary of the relative magnitudes of the return energy from the ship in the above three range cells.

6.3 Discussion

From both simulations and real HF data testing, it is demonstrated that the proposed clutter suppression scheme is capable of tracking the frequencies of the ocean

	Data Segment			
Range (km)	1:128	129:256	257:384	385:512
88.4	-22	-28	-30	-29
88.8	-12	-24	-26	-35
89.2	-2	-15	-26	-26

Table 6.6: A summary of the relative magnitudes of the return energy from the ship (in dB) in the range cells: 88.4 km, 88.8 km and 89.2 km at four different periods of the observation time

clutter signals and the target signal and then selectively suppressing the ocean clutter. Good quality target signal is extracted from the dominant ocean clutter environment. Moreover, the time-varying model of the ocean clutter is verified.

As compared to other adaptive clutter suppression techniques, this technique seems to be simpler in terms of operational steps. In other techniques, it is necessary to select a kind of adaptation algorithm and an appropriate convergence factor. Also, it is quite common that other techniques only model the clutter signals. In this technique, the clutter signals and the target signal are modelled simultaneously in terms of their frequencies. No adaptation algorithm or any convergence factor is required in this technique. However, the choice of the number of columns in the Hankel matrix depends upon several factors such as the rate of change in the frequency, the number of sinusoids present in the received data and the amplitude of the sinusoids. Due to the non-stationarity of the ocean clutter, there is no unique number of columns suitable for all the situations. During the real data testing, the choice of the number of columns varied from 7 to 11. The technique does have a limition of resolving the frequencies of two very closely-spaced sinusoids. A possible solution to overcome this limitation is suggested in Chapter 7. Last, the SVD utilized in this technique enhances the signal-to-noise ratio. This effect can be seen in the power spectrum plots of the ship signal when

compared to those of the raw HF data.

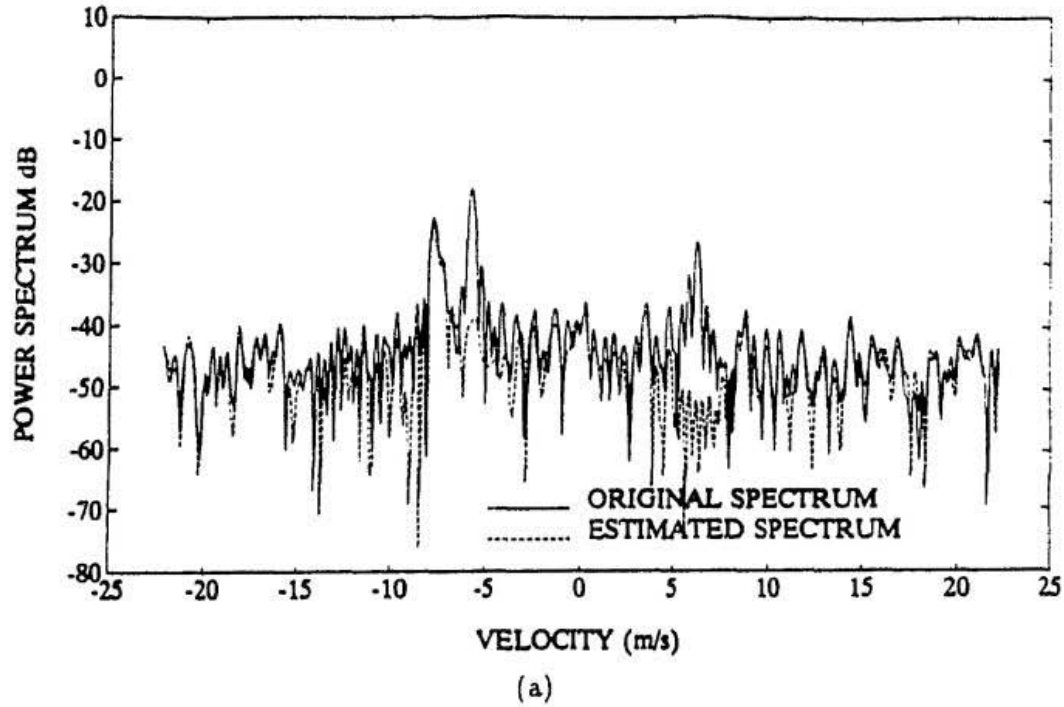

(a)

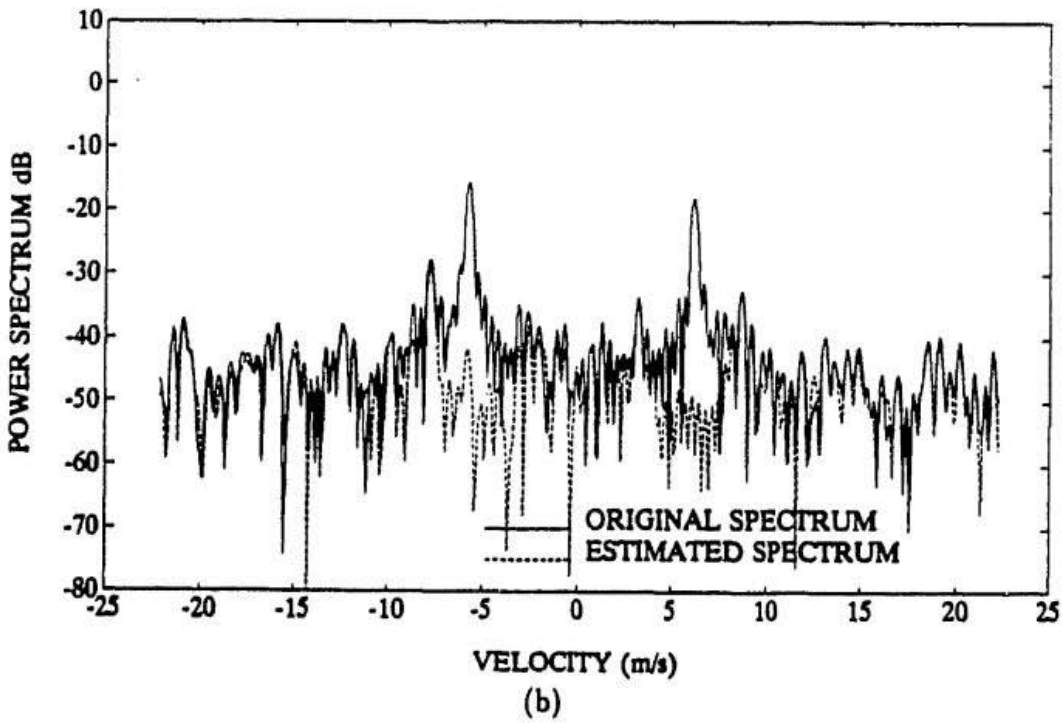

(b)

Figure 6.14: Comparison of the Doppler spectra of the HF radar signal before and after the clutter suppression process at range of 88.4 km: (a) data sample length = 128 (1:128); (b) (129:256); (c) (257:384); (d) (385:512)

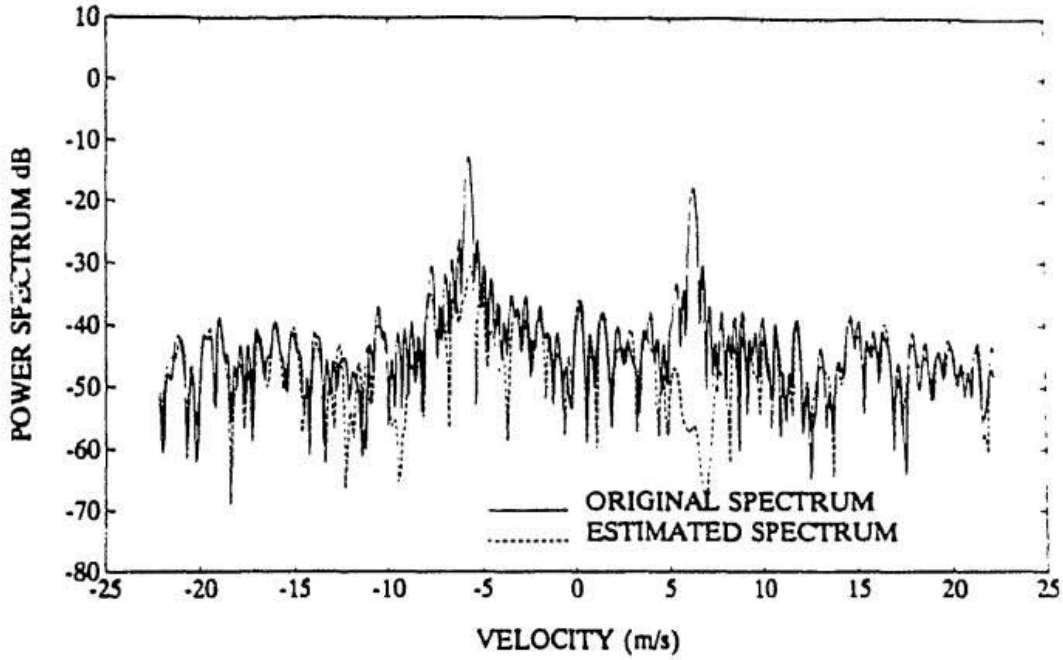

(c)

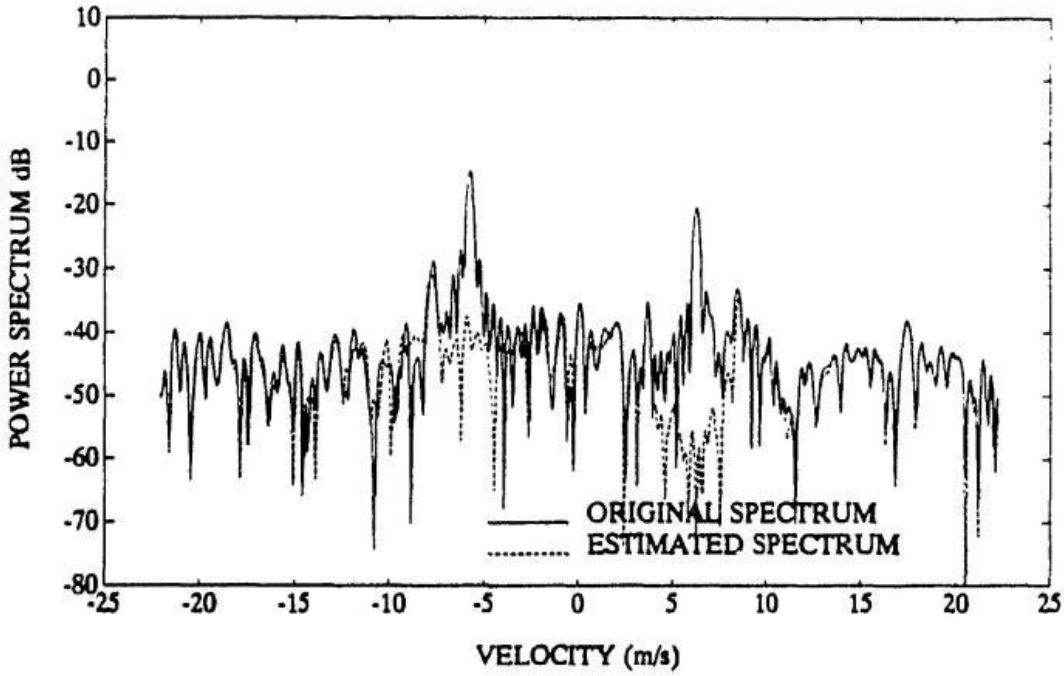

(d)

Figure 6.14 (cont'd)

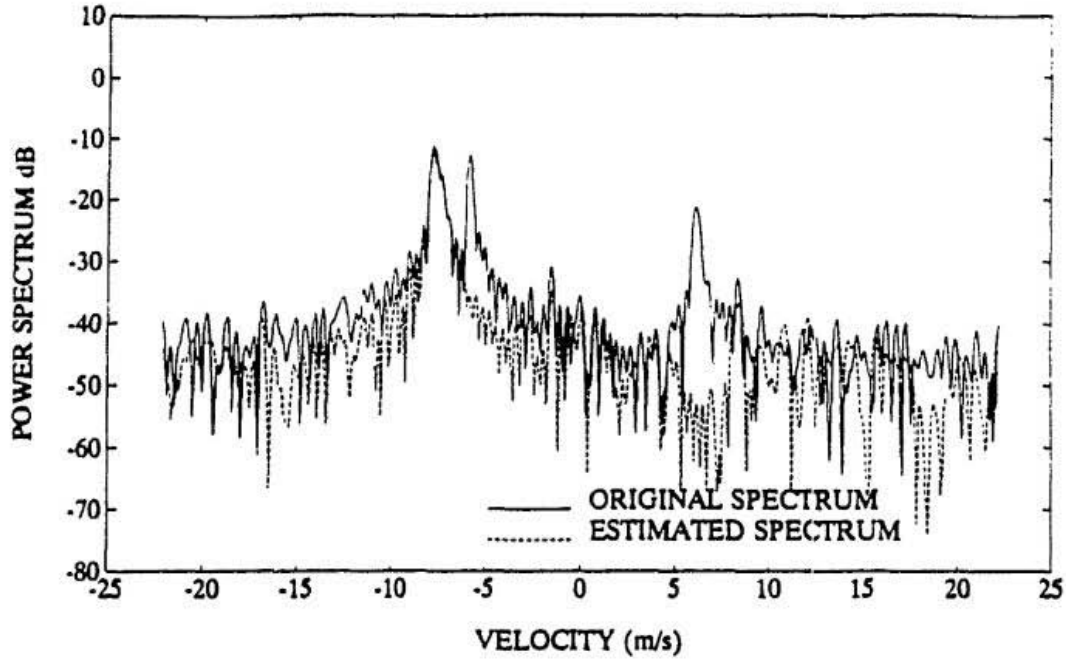

(a)

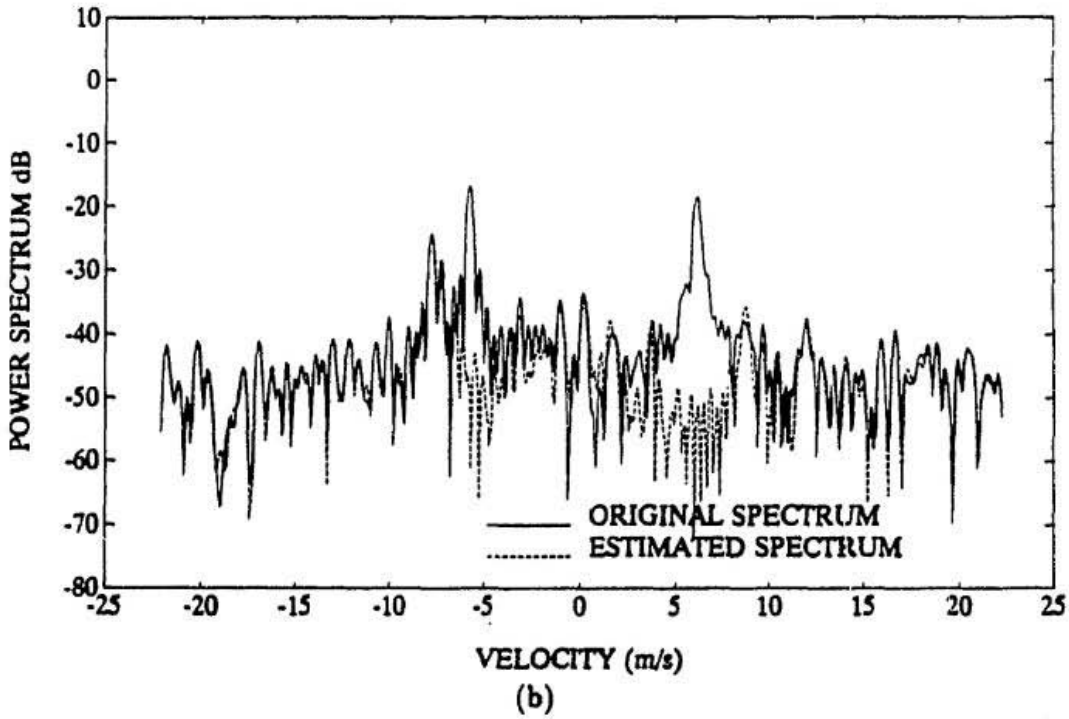

(b)

Figure 6.15: Comparison of the Doppler spectra of the HF radar signal before and after the clutter suppression process at range of 88.8 km: (a) data sample length = 128 (1:128); (b) (129:256); (c) (257:384); (d) (385:512)

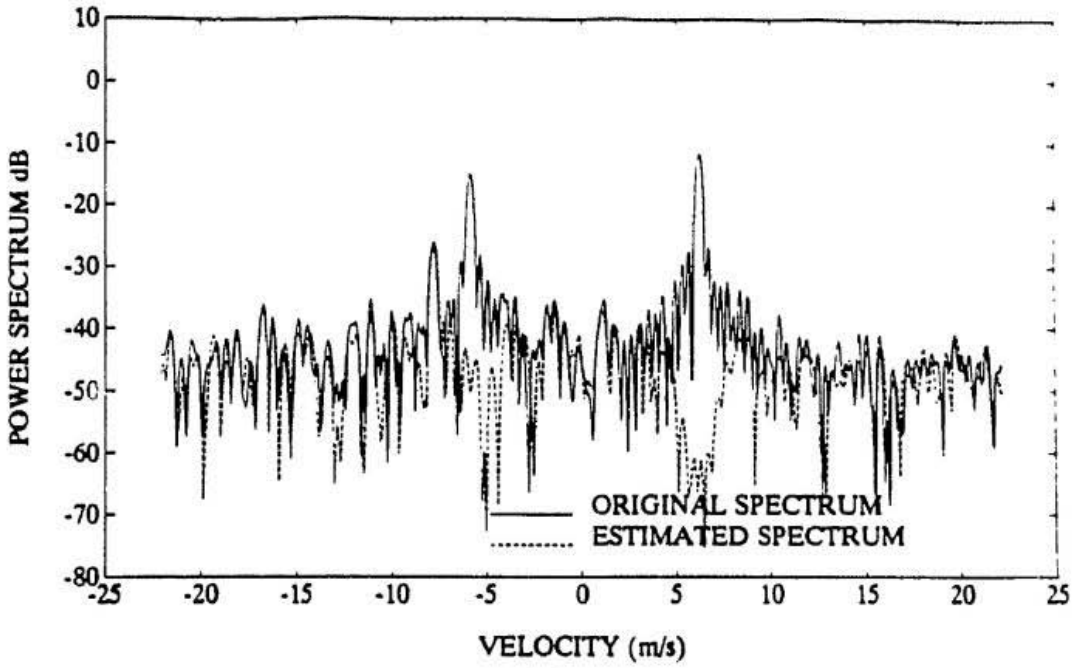

(c)

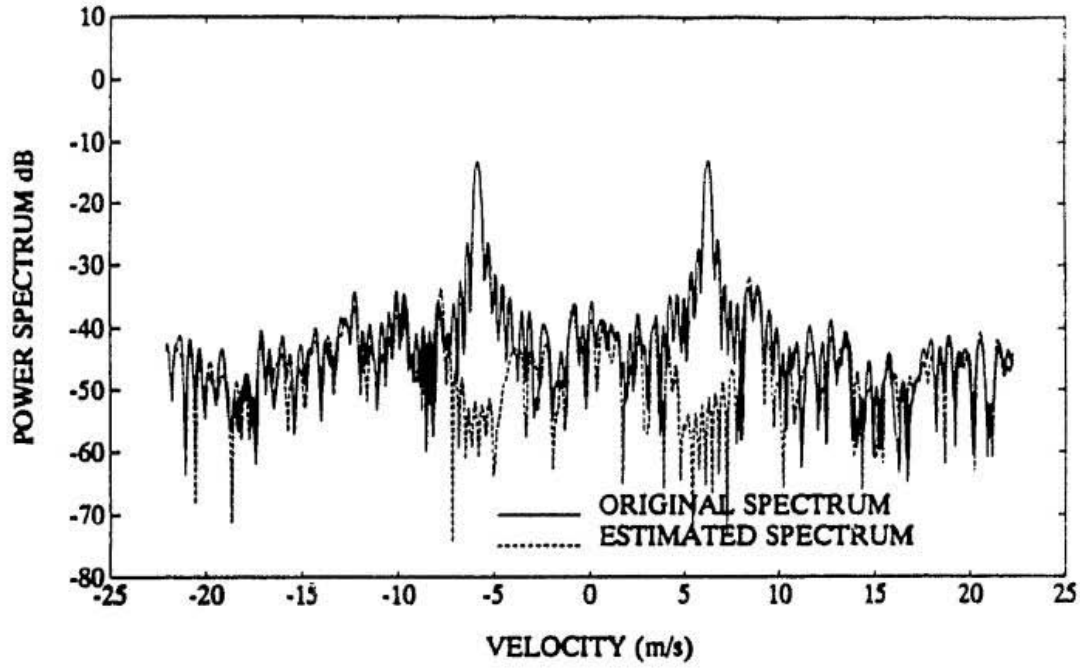

(d)

Figure 6.15 (cont'd)

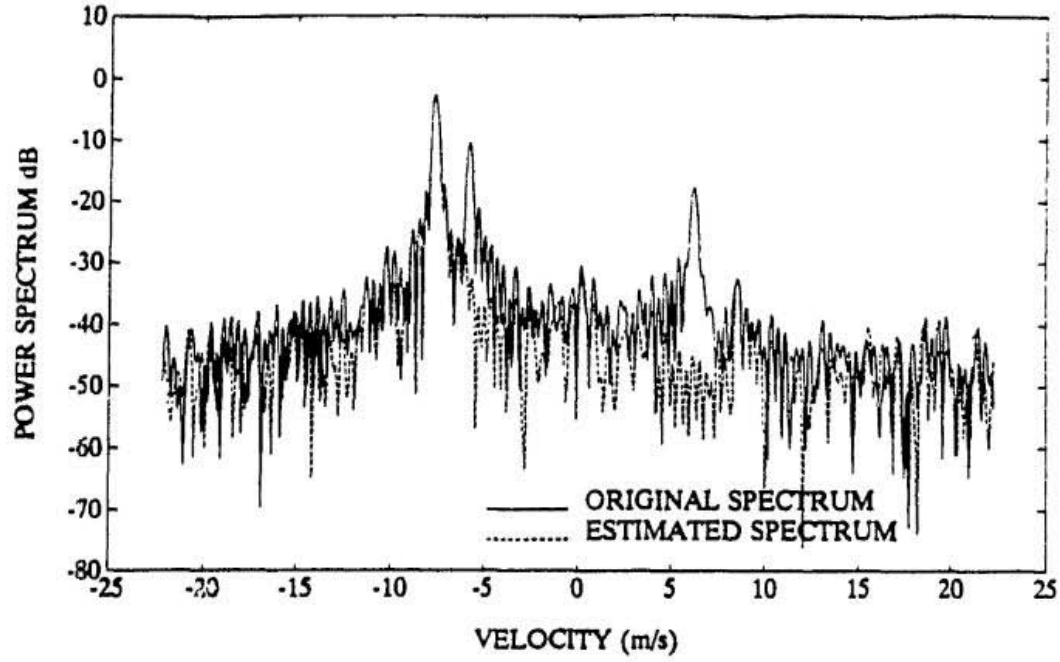

(a)

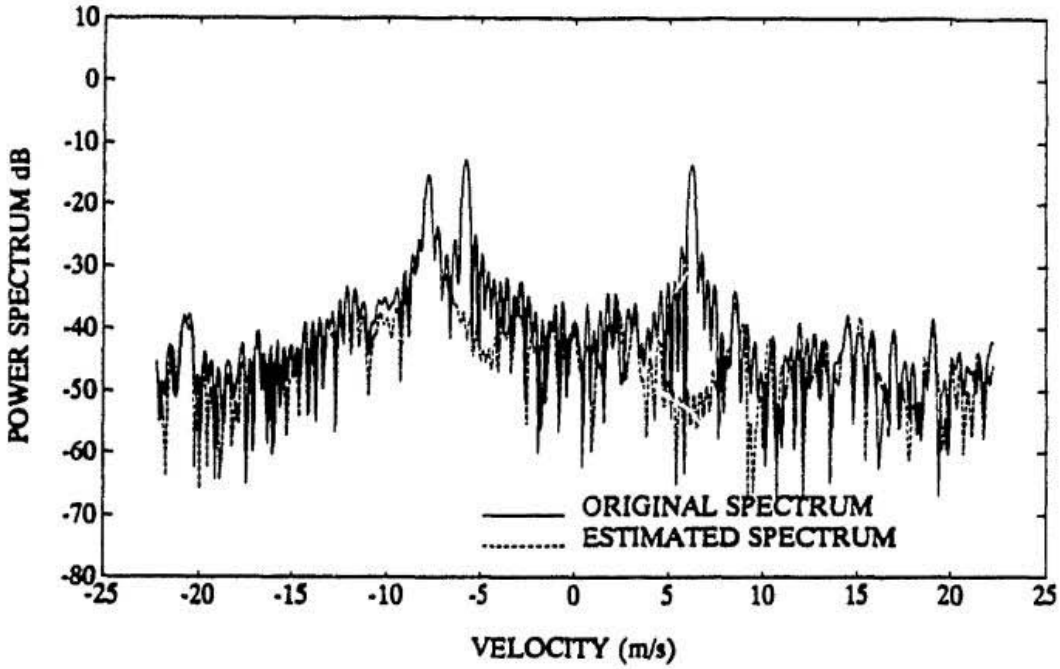

(b)

Figure 6.16: Comparison of the Doppler spectra of the HF radar signal before and after the clutter suppression process at range of 89.2 km: (a) data sample length = 128 (1:128); (b) (129:256); (c) (257:384); (d) (385:512)

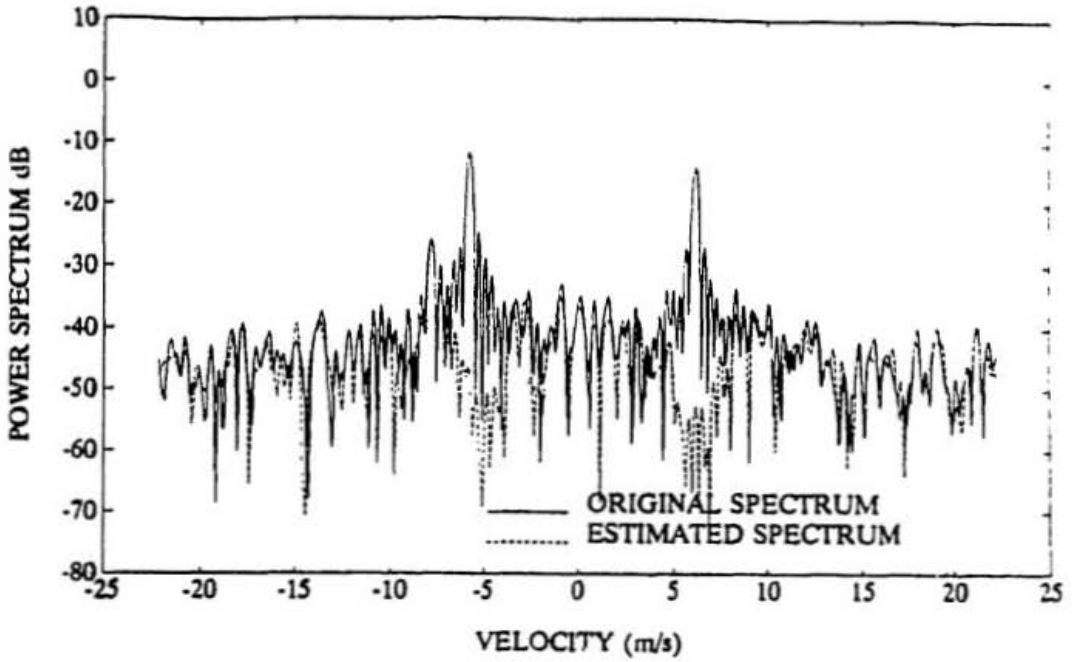

(c)

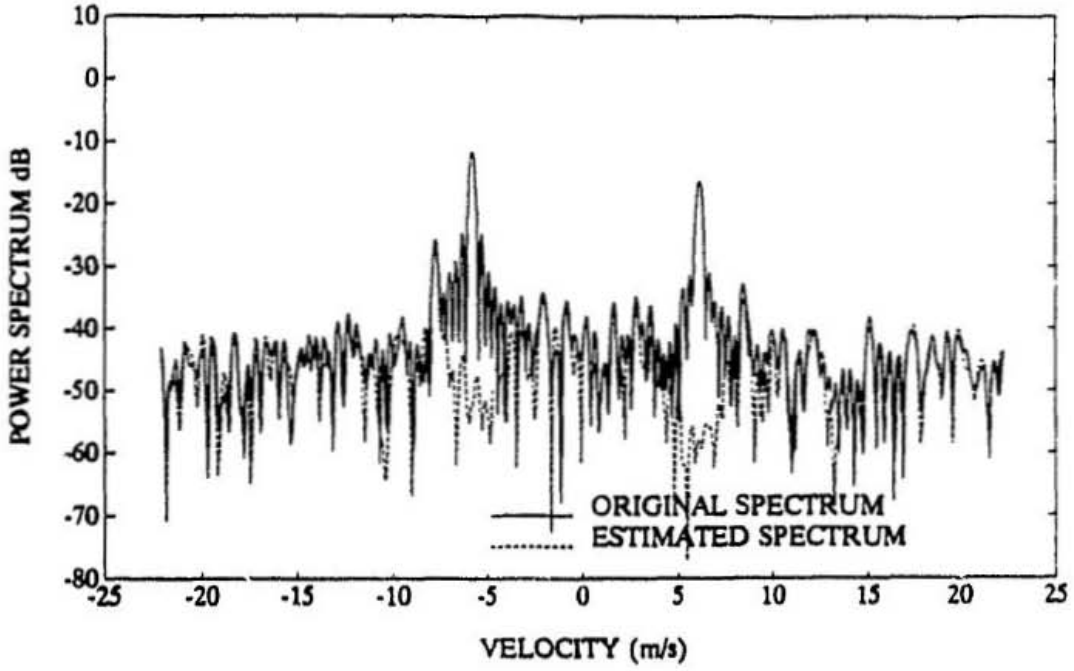

(d)

Figure 6.16 (cont'd)

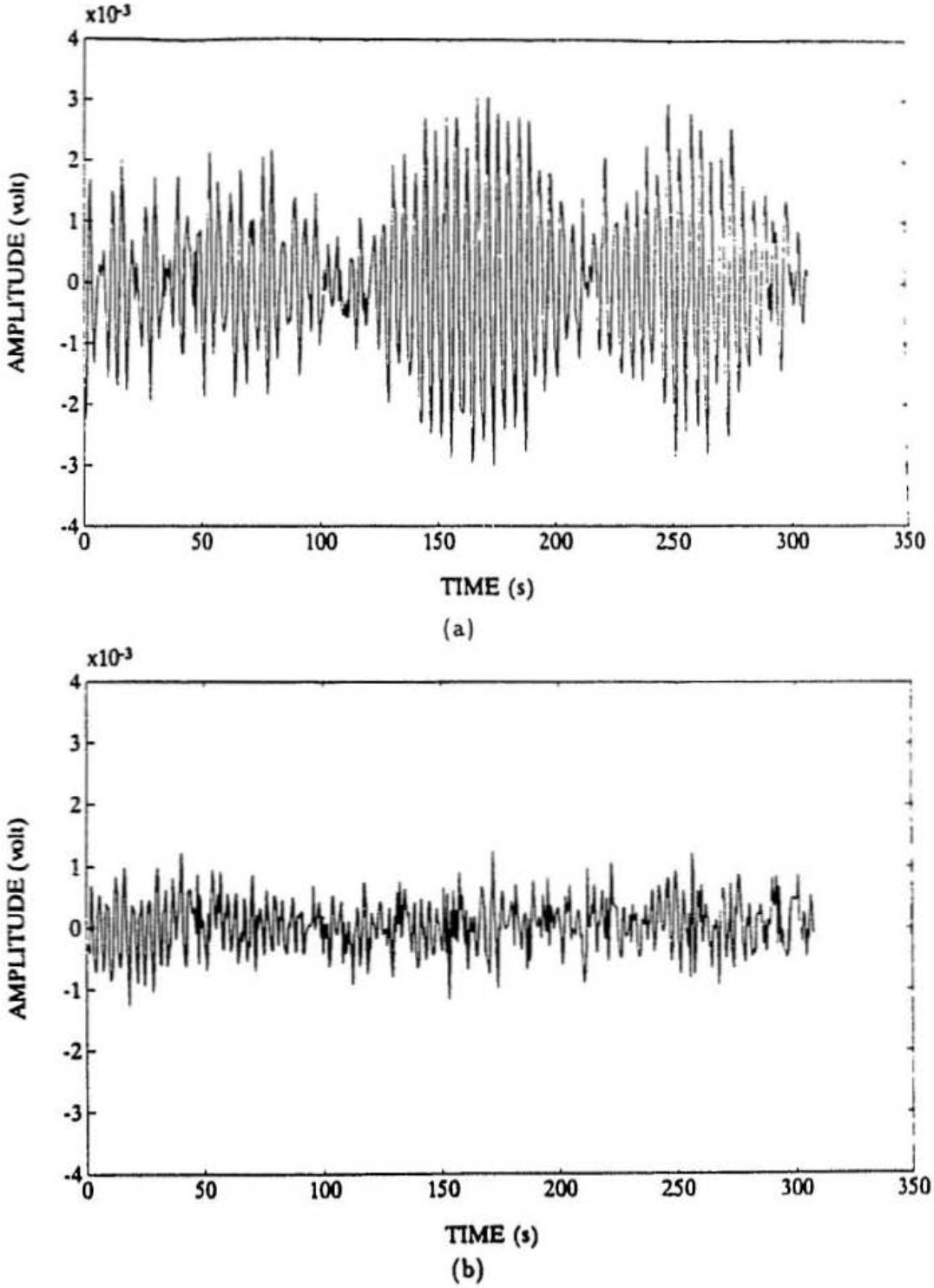

Figure 6.17: Comparison of the time series of the ship signal at range of 88.4 km: (a) original HF radar signal; (b) ship signal after suppression of ocean clutter

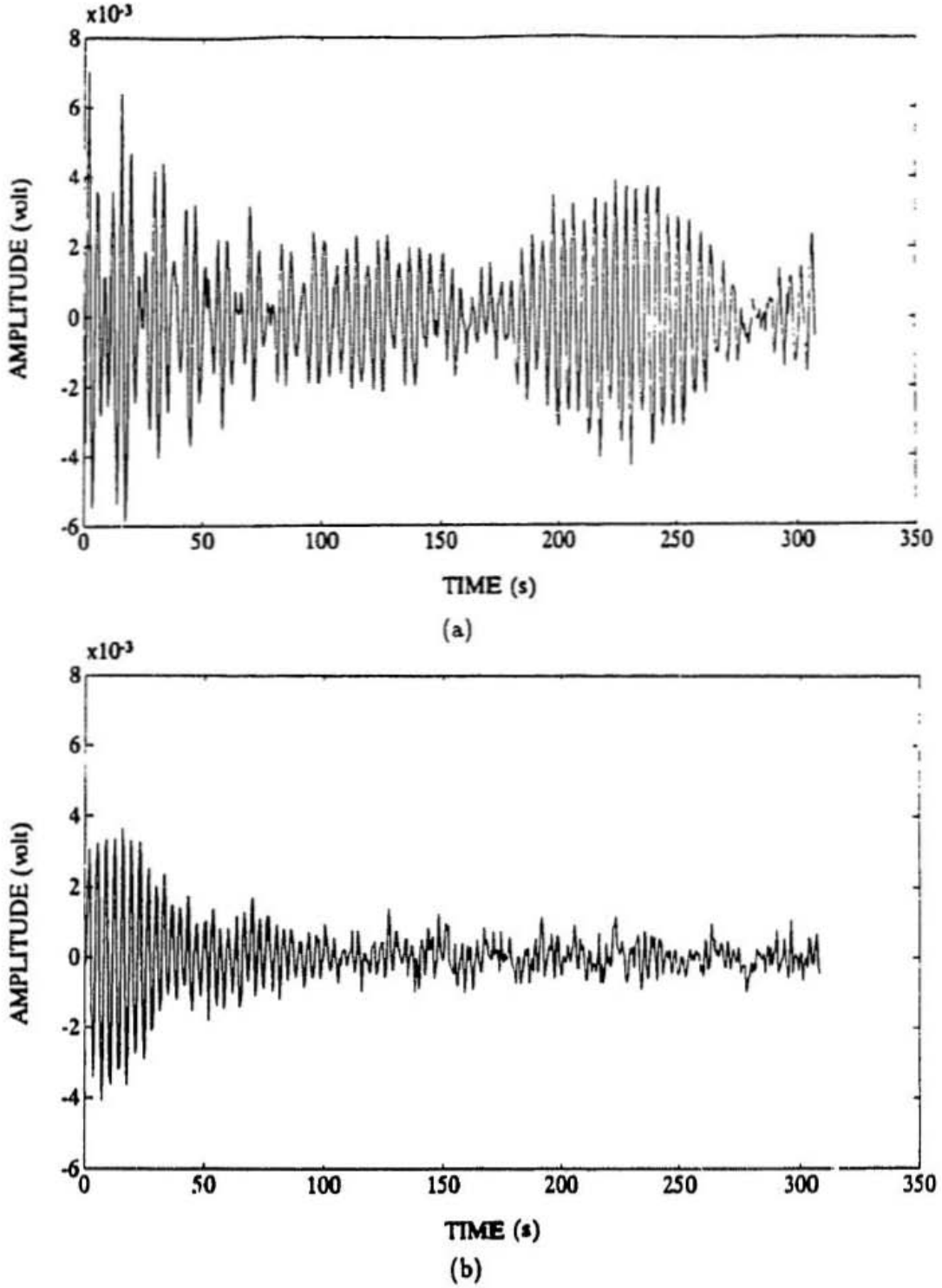

Figure 6.18: Comparison of the time series of the ship signal at range of 88.8 km: (a) original HF radar signal; (b) ship signal after suppression of ocean clutter

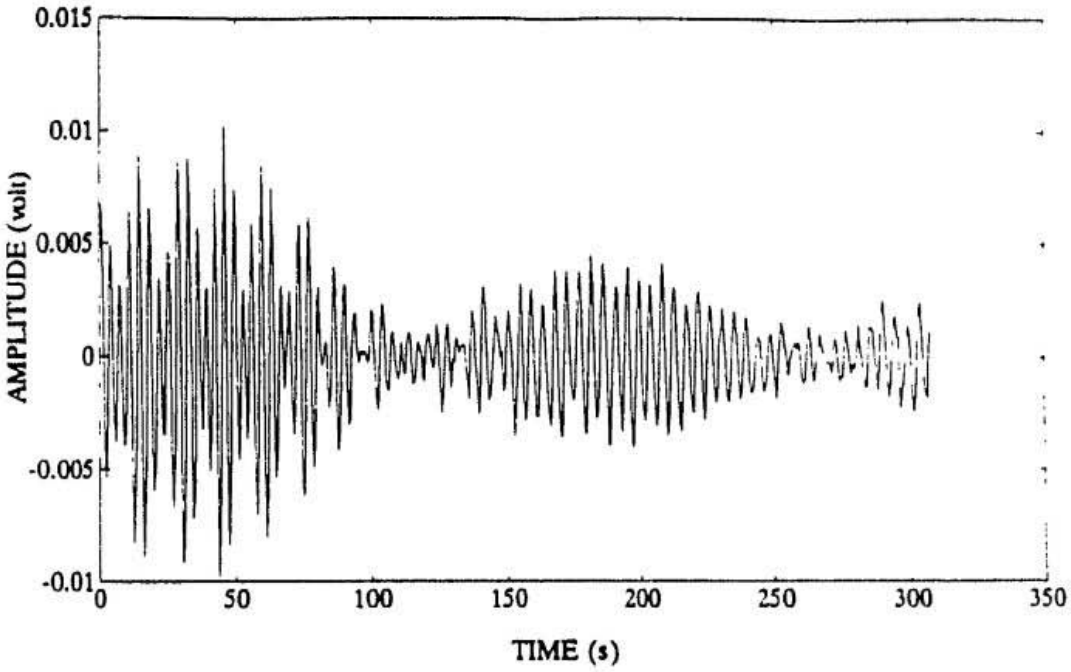

(a)

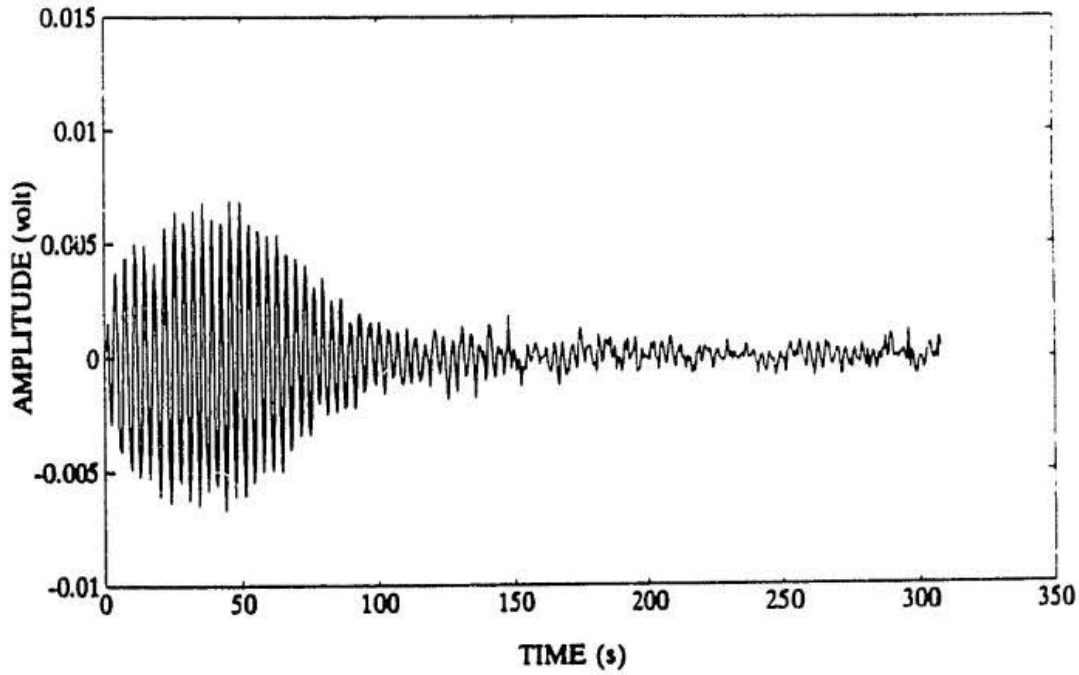

(b)

Figure 6.19: Comparison of the time series of the ship signal at range of 89.2 km: (a) original HF radar signal; (b) ship signal after suppression of ocean clutter

Chapter 7

Conclusions and Recommendations

A clutter suppression technique for high frequency (HF) radar has been considered. The radar clutter here refers to the HF scattering from the ocean surface, namely ocean clutter. The approach taken by the technique proposed is based on the recognition of the inherent time-varying behaviour in ocean clutter. It has been shown that ocean clutter can be adequately modelled as two narrow-band angle-modulated signals. A time-varying signal processing method, Hankel rank reduction, was then implemented to track the instantaneous frequencies of the clutter signals. Two simulated ocean clutter signals were generated to examine the tracking capability of the method. Under different signal-to-noise-ratios (SNR's), a close estimate of the instantaneous frequencies of the clutter signals was obtained. The average values of the instantaneous frequencies are close to the "Bragg" frequencies. Moreover, it has been demonstrated that a Hankel matrix formed directly from time series data, composed of a finite number of sinusoids, can be approximated by a reduced rank matrix characterized by the finite number of principal singular values obtained from the SVD. This approximation is held even when the sinusoidal frequencies are varying slowly with time. The sinusoidal frequencies are estimated from those principal singular values.

The clutter signals are suppressed by removing their corresponding frequency components from the reduced rank Hankel matrix. As a result, another reduced rank Hankel matrix is created from which a new time series is extracted. The estimated time series will contain only the target signal and noise of a level insufficient to disturb target identification. In addition to the two simulated clutter signals, a target signal was generated to test the suppression performance of the proposed technique. This was further examined using the real HF data. The results from both cases revealed that the ocean clutter signals and the target signal could be tracked properly in terms of their frequencies. Also, a substantial level of ocean clutter, in the range of 20 to 50 dB, could be suppressed, permitting the extraction of a good quality target signal. Unlike some other adaptive clutter suppression schemes, this proposed technique can model the ocean clutter signals and the target signal simultaneously without any adaptation algorithm and convergence factor, and is simple to use. No prior information on the ocean clutter is required.

Estimation of the frequencies of two very closely spaced sinusoids used to be a difficult problem in signal processing. In this technique, it was experimentally found that, if the expected Doppler frequency of a target had a space less than 0.09 Hz from the "Bragg" scattering frequencies, the scheme had difficulty in tracking both the ocean clutter and the target. However, the worst situation could happen when the target signal is masked by the ocean clutter where the Doppler frequency of the target coincides with that of the ocean clutter. One solution can prevent this situation from happening. As stated in Eq. (2.1) and Eq. (2.2), both the Doppler frequency of a target signal and the "Bragg" frequency of the ocean clutter are different functions of radar centre frequency. Thus, by periodically altering the radar centre frequency, the target and the ocean clutter can be separated in terms of their Doppler frequencies, and estimating the frequencies of two extremely close

sinusoids would be unnecessary.

The proposed clutter suppression scheme is developed to formulate a general algorithm to selectively suppress the ocean clutter. The program of the scheme is written in MATLAB language because it is easy to use and many well developed routines are available. The scheme is not fully implemented yet. The following recommendations are suggested to improve the scheme's performance and compatibility.

- The Hankel rank reduction method works based on the condition that the sinusoidal frequency has to be varying slowly with time. Further work is needed to monitor the rate of change in frequency so as to assure that the method gives good estimates of the frequencies.

- The flexibility of the scheme applicable to range cells of any size can be enhanced by further work on determining the exact number of sinusoids (targets) in each range cell. This will be necessary for automatic processing operation.

- The routine used in MATLAB to solve the SVD problem is general. In terms of implementation, the running time of the program can be improved using some specific fast routines to solve the SVD problem and some high level programming languages.

References

[1] D.D. Crombie, "Doppler Spectrum of Sea Echo at 13.56 Mc/s," *Nature*, Vol. 175, 1955, pp. 681-682.

[2] M. I. Skolnik, *Introduction to Radar Systems*, McGraw Hill, New York, 1980, chap. 14.

[3] D. E. Barrick, "First-order Theory and Analysis of MF/HF/VHF Scatter from the Sea," *IEEE Transactions on Antennas and Propagation*, Vol. AP-20, no.1, Jan. 1972, pp. 2-10.

[4] D. E. Barrick, "Remote Sensing of Sea State by Radar," in *Remote Sensing of Troposphere*, ed., V. E. Derr, GPO, Washington, DC, 1972, chap. 12.

[5] S. K. Srivastava, "Scattering of High Frequency Electromagnetic Waves from an Ocean Surface: An Alternate Approach Incorporating a Dipole Source," *Ph. D. dissertation*, Memorial University of Newfoundland, St. John's, Newfoundland, Canada (available from Canadian Thesis on Microform Service, National Library of Canada, 395 Wellington street, Ottawa, Ont. K1A 0N4, Canada), 1984.

[6] J. Walsh, R. Howell and B. Dawe, "Model Development for Evaluation Studies of Groundwave Radar," Contracted Report for Dept. of National Defence, Canada, No. W7714-8-5655/01-55, SSC File No. 05255-7714-8-5655, Novmber, 1990.

[7] R. H. Khan, "Ocean-Clutter Model for High-Frequency Radar," *IEEE Journal of Oceanic Engineering*, Vol. 16, no.2, April 1991, pp. 181-188.

[8] B. L. Lewis, F. F. Kretsumer, Jr., and W. W. Shelton, *Aspects of Radar Signal Processing*, Aritech House Inc., Norwood, MA., 1986, chap. 4.

[9] C. Gibson, and S. Haykin, "Radar Performance Studies of Adaptive Lattice Clutter-Suppression Filters," *IEE Proceedings*, Vol. 130, Part F, no. 5, August 1983, pp. 357-367.

[10] X. Hou, "The Maximum Entropy Method to Applied Radar Adaptive Clutter Power Elimination," in *Proceedings of the 1984 International Symposium on Noise and Clutter Rejection in Radars and Imaging Sensors*, Oct. 22-24 1984, Tokyo, Japan, pp. 312-324.

[11] Q-T Zhang, and S. Haykin, "Radar Clutter Suppression Schemes," *Electronic Letters*, Vol. 20, no. 24, Nov. 1984, pp. 1007-1008.

[12] C. L. DiMonte, and K. S. Arun, "Tracking the Frequencies of Superimposed Time-Varying Harmonics," in *Proceedings of ICASSP 90*, Albuquerque, NM., April 1990, pp. 2539-2542.

[13] B.J Dawe, R.H. Khan, J. Walsh, and J.R. Benoit, "A Long Range Groundwave Radar System for Offshore Surveillance," in *Proceedings of the 12th Canadian Symposium on Remote Sensing (IGARSS '89)*, Vancouver, B.C., July 1989, pp. 2950-2952.

[14] J.M. Headrick, and M.I. Skolnik, "Over-the-horizon Radar in the HF Band," *Proceedings of the IEEE*, Vol. 62, no. 6, June 1974, pp. 664-672.

[15] L. R. Wyatt, "Progress in the Interpretation of HF Sea Echo: HF Radar as a Remote Sensing Tool," *IEE Proceedings*, Vol. 137, Part F, no. 2, April 1990, pp. 139-147.

[16] R. H. Khan, and D. K. Mitchell, "Waveform Analysis for High-frequency FMICW Radar," *IEE Proceedings*, Vol. 138, Part F, no. 5, October 1991, pp. 411-419.

[17] J. R. Barnum, "Ship Detection with High Resolution HF Skywave Radar," *IEEE Journal of Oceanic Engineering*, Vol. OE-11, no. 2, April 1986, pp. 196-209.

[18] E. D. R. Shearman, G. D. Burrows, and M. D. Moorhead, "An FMICW Ground-wave Radar for Remote Sensing of Ocean Waves and Currents," *IEE Conference Radar*, 1987, pp. 598-605.

[19] J. Walsh, B. J. Dawe, and S. K. Srivastava, "Remote Sensing of Icebergs by Ground-wave Doppler Radar," *IEEE Journal of Oceanic Engineering*, Vol. OE-11, no. 2, April 1986, pp. 276-284.

[20] D. E. Barrick, "Theory of HF and VHF Propagation across the Rough Sea," *Radio Science*, Vol. 6, June 1971, pp. 517-533.

[21] J. Walsh, "On the Theory of Electromagnetic Propagation across a Rough Sea and Calculations in the VHF Region," Dept. Supply and Services, Defence Res. Establ. Atlantic (DREA) (available from Ocean Eng. Inform. Centre, Rep. no. N00232, Memorial Univ. of NF, St. John's, NF).

[22] S. O. Rice, "Reflection of Electromagnetic Waves from a Slightly Rough Surface," in *Theory of Electromagnetic Waves*, ed., M. Kline, Interscience, New York, 1951, pp. 351-378.

[23] L. J. Griffiths, "Rapid Measurement of Digital Instantaneous Frequency," *IEEE Transactions on Acoustic, Speech, and Signal Processing*, Vol. ASSP-23, no. 2, April 1975, pp. 207-222.

[24] R. D. DeGroat, and R. A. Roberts, "A Family of Rank-One Subspace Updating Methods," in *SVD and Signal Processing: Algorithm, Applications and Architectures*, ed., E. F. Deprettere, Elsevier Science Publishers, B. V. North Holland, 1988, pp. 277-300.

[25] S. M. Kay, and S. L. Marple Jr., "Spectrum Analysis - A Modern Perpective", *Proceedings of the IEEE*, Vol. 69, no. 11, Nov. 1981, pp. 1380-1419.

[26] S. Haykin, *Adaptive Filter Theory*, Prentice-Hall, Englewood Cliffs, New Jersey, 1986, chap. 4.

[27] F. B. Hilderbrand, *Introduction to Numerical Analysis*, McGraw-Hill, New York, 1956, chap. 9.

[28] D. W. Tufts, and R. Kumaresan, "Estimation of Frequencies of Multiple Sinusoids: Making Linear Prediction Perform Like Maximum Likelihood," *Proceedings of the IEEE*, Vol. 70, no. 9, Sept. 1982, pp. 975-989.

[29] R. Kumaresan, "On the Zeros of the Linear Prediction-error Filter for Deterministic Signals," *IEEE Transactions on Acoustic, Speech, and Signal Processing*, Vol. ASSP-31, no. 1, Feb. 1983, pp. 217-220.

[30] S. Y. Kung, K. S. Arun, and D. V. Bhasber Rao, "State-space and Singular-value Decomposition Based Approximation Methods for the Harmonics Retrieval Problem," *Journal of Optical Society of America*, Vol. 73, no. 12, Dec. 1983, pp. 1799-1811.

[31] A. D. Poularikas, and S. Seely, *Signals and Systems*, PWS Publishers, Boston, 1985, chap. 12.

[32] C. Eckart, and G. Young, "The Approximation of One Matrix By Another of Lower Rank," *Psychometrika*, Vol. 1, no. 3, Sept. 1936, pp. 211-218.

[33] D. W. Tufts, and R. Kumaresan, "Singular Value Decompostion and Improved Frequency Estimation Using Linear Prediction," *IEEE Transactions on Acoustic, Speech, and Signal Processing*, Vol. ASSP-30, no. 4, August 1982 pp. 671-675.

[34] G. H. Golub, and C. F. Van Loan, *Matrix Computations*, The Johns Hopkins University Press, Baltimore, MD., 1983, chap. 5.

[35] R. H. Khan, "HF Radar Trials with HMCS Nipigon," *Northern Radar Technical Report*, St. John's, Newfoundland, Canada, January. 1991.

Appendix A

Doppler Effect

Consider a radar with a frequency of $f = 1/T_0$, where T_0 is the period of the transmitted wave, and a target moving at a constant radial speed, v, towards the radar site. At time $t = t_0$, the target is at range $R = R_0$. It is assumed that at that time a peak or crest of the wave is emerging from the radar's antenna. At time $t = t_0 + T_0$, the next crest of the wave (point B in Figure A.1) is emerging at this time. Let the target's range be $R = R_1$. The time, Δt, necessary for point A on the wave to travel from the radar to the target is

$$\Delta t = \frac{(R_0 - v\Delta t)}{c} \tag{A.1}$$

or

$$\Delta t = \frac{R_0}{c + v} \tag{A.2}$$

where c is the speed of the light. The time necessary for point A to return to the radar is again Δt. Thus point A returns to the radar at time,

$$t_1 = t_0 + \frac{2R_0}{c + v} \tag{A.3}$$

Similarly, point B returns to the radar at time,

$$t_2 = t_0 + T_0 + \frac{2R_1}{c + v} \tag{A.4}$$

The period of the received wave, T_0', is $t_2 - t_1$ or

$$T_0' = T_0 - \frac{2(R_0 - R_1)}{c + v} \tag{A.5}$$

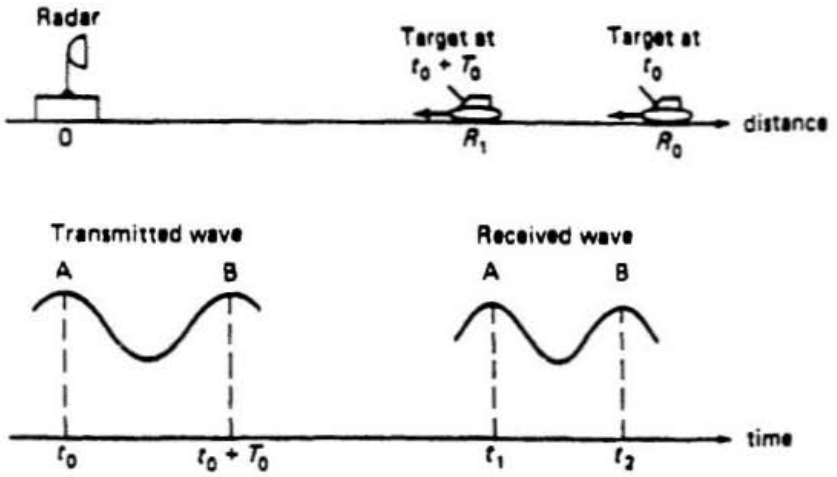

Figure A.1: Target geometry and transmitted and received waveforms for Doppler effect derivation (J. L. Eaves and E. K. Reedy: Principles of Modern Radar, 1987)

Since $vT_0 = R_0 - R_1$

$$\begin{aligned} T_0' &= T_0 - \frac{2vT_0}{c+v} \\ &= T_0 \frac{1 - v/c}{1 + v/c} \end{aligned} \tag{A.6}$$

in terms of the received frequency,

$$\begin{aligned} f' &= \frac{1}{T_0'} \\ &= f \frac{1 + v/c}{1 - v/c} \end{aligned} \tag{A.7}$$

For most cases of interest, $v/c \ll 1$; and $1/(1-x) = 1 + x + x^2 + \cdots$ if $x \ll 1$.

Thus

$$\begin{aligned} f' &\simeq f(1 + v/c)(1 + v/c + v^2/c^2 + \cdots) \\ &= f(1 + 2v/c + 2v^2/c^2 + \cdots) \\ &\simeq f(1 + 2v/c) \\ &= f + 2v/\lambda \end{aligned} \tag{A.8}$$

Therefore, the received wave has been shifted in frequency from the transmitted wave by the amount of $f_d = 2v/\lambda$. f_d is the Doppler frequency shift.

Appendix B

Eigenvalues, Eigenvectors and Singular Value Decomposition of a Matrix

B.1 Eigenvalues and Eigenvectors of a Matrix

Given an n-by-n matrix A,

$$A = \begin{bmatrix} a_{11} & a_{12} & \cdots & a_{1n} \\ a_{21} & a_{22} & \cdots & a_{2n} \\ . & . & & . \\ . & . & & . \\ a_{n1} & a_{n2} & \cdots & a_{nn} \end{bmatrix} \tag{B.1}$$

By a linear transformation,

$$Ax = \lambda x \tag{B.2}$$

where A is a known real square matrix of order n-by-n; x is an unknown column vector and λ is a scalar parameter. Since λ is a constant, the vector x has special significance in which it is left invariant in direction by the transformation A. To show this, Eq. (B.2) is rewritten as

$$\begin{aligned} (Ax - \lambda x) &= 0 \\ (A - \lambda I)x &= 0 \end{aligned} \tag{B.3}$$

where I is the n-by-n identity matrix. Equation (B.3) has a nontrival solution x if and only if

$$\det|A - \lambda I| = 0 \tag{B.4}$$

Equation (B.4) can be written explicitly as

$$\det|A - \lambda I| = \begin{vmatrix} a_{11} - \lambda & a_{12} & \cdots & a_{1n} \\ a_{21} & a_{22} - \lambda & \cdots & a_{2n} \\ . & . & & . \\ . & . & & . \\ a_{n1} & a_{n2} & \cdots & a_{nn} - \lambda \end{vmatrix} = 0 \tag{B.5}$$

or

$$\lambda^n - (a_{11} + a_{22} + \cdots + a_{nn})\lambda^{n-1} + \cdots + (-1)^n|A| = 0 \tag{B.6}$$

where $|A|$ is the determinant of A. Equation (B.6) is called the characteristic equation of the matrix A. The roots of Eq. (B.6) are called the eigenvalues of matrix A. Corresponding to each eigenvalue, there exists a nonzero column vector x that satisfies Eq. (B.3). x_i is the eigenvector (column) corresponding to the eigenvalue λ_i. An eigenvalue may have many eigenvectors but an eigenvector can correspond to only one eigenvalue.

B.2 Singular Value Decomposition of a Matrix

Given an m-by-n matrix B where $m > n$. B can be represented in the form of

$$B = USV^T \tag{B.7}$$

where $S = diag[\sigma_1, \sigma_2, \cdots, \sigma_n]$ and in the order of $\sigma_1 \geq \sigma_2 \geq \cdots \geq \sigma_n$; and U and V are unitary. Equation (B.7) is referred to as the Singular Value Decomposition (SVD) of the martix B. Then

$$V^T(B^TB)V = S^2 \quad \in \Re^{n \times n} \tag{B.8}$$

and

$$U^T(BB^T)U = S^2 \quad \in \Re^{m \times m} \tag{B.9}$$

where the columns of U (V, respectively) are viewed as vectors that constitute an orthonormal eigenbasis of BB^T in $\Re^{m\times m}$ (of B^TB in $\Re^{n\times n}$, respectively). Thus, a SVD of the matrix B can be obtained by solving the eigenvalue-eigenvector problem for the matrices BB^T and B^TB, whose eigenvalues are in $S^2 = diag[\sigma_1^2, \sigma_2^2, \cdots, \sigma_n^2]$.

Appendix C

The Computer Program of the Clutter Suppression Scheme

```
%%%%%%%%%%%%%%%%%%%%%%%%%%%%%%%%%%%%%%%%%
%%%% The Clutter Suppression Scheme %%%%
%%%%%%%%%%%%%%%%%%%%%%%%%%%%%%%%%%%%%%%%%

%% Load the input data
%load y;
y = x0002(1:128);

%% Construct the Hankel matrix "H"
input('The number of columns in the Hankel matrix: ')
L = ans;
N = length(y);           % the data length of y
R = N-L+1;               % number of rows in the Hankel matrix
H = [];
for i = 1:R,
  for j = 1:L,
    H(i,j) = y(i+j-1);
  end
end

%% Rank reduction and estimation of the observability matrix
%% "theta" and state vector matrix "X"
M = 3;                   % number of complex sinusoids in y
[U,S,V] = svd(H);        % Singular Value Decomposition of "H"
THETA = U*sqrt(S);
theta(1:R,1:M) = THETA(1:R,1:M);
X = (inv(sqrt(S)'*sqrt(S))*sqrt(S)'*S)*V';

%% Compute the time-dependent state matrix "F" from the
%% observability matrix "theta", and then estimate the
%% instantaneous frequencies from the angles of the eigenvalues
%% of "F"

input('The sampling time: ')
ts = ans;
d = fix((L+1)/2);        % mean value of each row in "H"
ne = N-L-d;              % number of estimates
for k = 1:ne,
   theta1(1:d+1,1:M) = theta(k:d+k,1:M);
   theta2(1:d+1,1:M) = theta(k+1:d+k+1,1:M);
   F = inv(theta1'*theta1)*theta1'*theta2;

   % eigenvectors and eigenvalues of "F"
   [evtr,eval] = eig(F);

   %Estimate instantaneous frequency in Hertz (Hz)
   w1(k) = angle(eval(1,1))/(2*pi*ts);
   w2(k) = angle(eval(2,2))/(2*pi*ts);
   w3(k) = angle(eval(3,3))/(2*pi*ts);
end
```

```
%% Suppress the clutter signals
mw1 = mean(w1);          % average value of the instantaneous
mw2 = mean(w2);          % frequencies
mw3 = mean(w3);
theta_new = THETA;       % initialization of the new observability
                         % matrix "theta_new"
for k = 1:ne,
   theta1(1:d+1,1:M) = theta(k:d+k,1:M);
   theta2(1:d+1,1:M) = theta(k+1:d+k+1,1:M);
   F = inv(theta1'*theta1)*theta1'*theta2;
   [evtr,eval] = eig(F);
   eval_new = eval;

   % identify the clutter signals by the "Bragg" frequencies
   if (mw1>=.2601 & mw1<=.2699) | (mw1>=-.2699 & mw1<=-.2601),
      eval_new(1,1) = 0.0;
   end
   if (mw2>=.2601 & mw2<=.2699) | (mw2>=-.2699 & mw2<=-.2601),
      eval_new(2,2) = 0.0;
   end
   if (mw3>=.2601 & mw3<=.2699) | (mw3>=-.2699 & mw3<=-.2601),
      eval_new(3,3) = 0.0;
   end

   % estimate new "F" and "theta"
   F_new = (evtr*eval_new)*inv(evtr);
   theta2_new = theta1*F_new;
   theta_new(k+1:d+k+1,1:M) = theta2_new(1:d+1,1:M);
end

%% Construct a new Hankel matrix "H_new"
H_new = theta_new*X;

%% Extract a new time series data from "H_new"
p = 0;
for l = 1:N,
   y_new(l) = 0;
   if l < L,
      c1 = l;
      for ro = 1:l,
         y_new(l) = H_new(ro,c1)+y_new(l);
         c1 = c1-1;
      end
      y_new(l) = y_new(l)/l;
   elseif l >= L & l <= N-L+1,
      for ro = 1:L,
         y_new(l) = H_new(ro+p,L-ro+1)+y_new(l);
      end
      p = p+1;
      y_new(l) = y_new(l)/L;
   elseif l > N-L+1
      c1 = L;
      for ro = l-L+1:N-L+1,
         y_new(l) = H_new(ro,c1)+y_new(l);
         c1 = c1-1;
      end
      y_new(l) = y_new(l)/(N-l+1);
   end
end
```

```
%% Plot the power spectrum of "y" and "y_new"
N1 = 512;                  % number of zero padding
Y = fft(y,N1);
Y = fftshift(Y);
My = Y.*conj(Y);
Y_new = fft(y_new,N1);
Y_new = fftshift(Y_new);
My_new = Y_new.*conj(Y_new);
f = 2*(-(N1/2-1):(N1/2))/N1;
Vel = (1/2)*f*(3*10^(8))/(6.75*10^(6));  % radial velocity
for pos = 200:250,         % place figure legends
    tx1(pos) = -70;
    tx2(pos) = -75;
end
pos = 200:250;
My_dB = 10*log10(My);
My_new_dB = 10*log10(My_new);
axis([-25 25 -80 10]);
plot(Vel,My_dB,Vel,My_new_dB,Vel(pos),tx1(pos),'-',Vel(pos),tx2(pos),'--'
text(Vel(250),tx1(250),'  ORIGINAL SPECTRUM');
text(Vel(250),tx2(250),'  ESTIMATED SPECTRUM')
xlabel('VELOCITY (m/s)'),ylabel('POWER SPECTRUM dB')
axis;
```